FILE COPY

ANALYSIS OF SACRAMENTO RIVER BEND FLOWS, AND DEVELOPMENT OF A NEW METHOD FOR BANK PROTECTION

by

A. Jacob Odgaard and John F. Kennedy

Sponsored by
U.S. Army Corps of Engineers
Sacramento District
Sacramento, California
and
U.S. Army Corps of Engineers
Waterways Experiment Station
Vicksburg, Mississippi

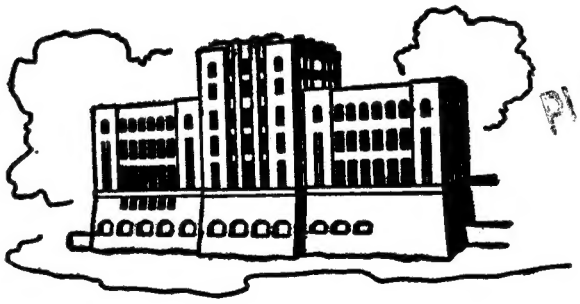

PLEASE DO NOT REMOVE

IIHR Report No. 241
Iowa Institute of Hydraulic Research
The University of Iowa
Iowa City, Iowa 52242
May 1982

REPORT DOCUMENTATION PAGE	1. REPORT NO. No. 241	2.	3. Recipient's Accession No.
4. Title and Subtitle: ANALYSIS OF SACRAMENTO RIVER BEND FLOWS, AND DEVELOPMENT OF A NEW METHOD FOR BANK PROTECTION			5. Report Date: May, 1982 6.
7. Author(s): A. Jacob Odgaard & John F. Kennedy			8. Performing Organization Rept. No. 241
9. Performing Organization Name and Address: Iowa Institute of Hydraulic Research, The University of Iowa, Iowa City, Iowa 52242			10. Project/Task/Work Unit No. 11. Contract(C) or Grant(G) No. (C) DACW05-80-C-0083 (G) DACW39-80-C-0129
12. Sponsoring Organization Name and Address: U.S. Army Corps of Engineers, Sacramento Dist., Sacramento, Calif.; U.S. Army Corps of Engineers, Waterways Experiment Station, Vicksburg, Mississippi			13. Type of Report & Period Covered 14.

15. Supplementary Notes

16. Abstract (Limit: 200 words)

This study includes an investigation of analytical models for the description of flow and bed characteristics in a bend of the Sacramento River, California; and a study of a proposed new technique for bank protection.

Existing models for the prediction of the steady-state transverse bed profile in channel bends are reviewed; and alternative models are developed and validated. The new models predict the transverse bed slope to vary linearly with d/r (the ratio of depth, d, to radius of curvature, r) and almost linearly with the sediment-particle Froude number. Equations for the transverse variation of depth-averaged velocity and mean-grain size also are developed, which, together with the equations for the transverse variation of depth, can provide a guide to the depth of bed erosion and depth-averaged velocity near the outer banks of river bends.

It is shown, theoretically and by a physical model, that short, vertical, submerged vanes installed at incidence to the channel axis in the outer half of a river-bend channel significantly reduce the secondary currents and the attendant undermining and high-velocity attack of the outer bank. The effect of the vanes on the secondary flow is estimated by a simple torque calculation using the Kutta-Joukowski theorem. A design relation for the vane spacing is derived by equating the torque, about the channel centroid, produced by the flow curvature to that resulting from the lateral force exerted on the vanes. The relation is verified in an idealized, physical model of the mentioned bend of the Sacramento River, Calif.

17. Document Analysis a. Descriptors

River bend flows; Bank protection; Sediment transport

b. Identifiers/Open-Ended Terms

c. COSATI Field/Group

Availability Statement: Release Unlimited	19. Security Class (This Report): Unclassified	21. No. of Pages: 85
	20. Security Class (This Page)	22. Price

(See ANSI-Z39.18) See Instructions on Reverse

OPTIONAL FORM 272 (4-77) (Formerly NTIS-35) Department of Commerce

ANALYSIS OF SACRAMENTO RIVER BEND FLOWS, AND DEVELOPMENT OF A NEW METHOD FOR BANK PROTECTION

by

A. Jacob Odgaard and John F. Kennedy

Sponsored by
U.S. Army Corps of Engineers
Sacramento District
Sacramento, California
and
U.S. Army Corps of Engineers
Waterways Experiment Station
Vicksburg, Mississippi

IIHR Report No. 241
Iowa Institute of Hydraulic Research
The University of Iowa
Iowa City, Iowa 52242
May 1982

LIST OF SYMBOLS

a = distance above river bed to sampler intake nozzle when suspended-sediment sampler is at the lowest vertical position

A = cross-sectional area of channel

C = point-integrated local suspended-sediment concentration

$\bar{C}$ = mean suspended-sediment concentration averaged over depth

d = local flow depth

$\bar{d}$ = mean flow depth (A/W)

D_{50} = median size of bed sediment

$\bar{D}_{50}$ = mean median size of bed sediment

D_g = geometric mean size of bed sediment

q = water discharge per unit width (Q/W)

Q = water discharge

q_B = bed-load discharge per unit width (Q_B/W)

q_i = water discharge for i-th subsection of transect

q_s = suspended-load discharge per unit width (Q_s/W)

Q_B = bed-load discharge

Q_s = suspended-load discharge

Q_T = total sediment discharge (Q_B+Q_s)

q_{Bi} = bed-load discharge for i-th subsection of transect

q_{si} = suspended-load discharge for i-th subsection of transect

$\bar{q}$ = water discharge per unit width (q_i/W_i)

$\bar{q}_B$ = bed-load discharge per unit width (q_{Bi}/W_i)

$\bar{q}_s$ = suspended-load discharge per unit width (q_{si}/W_i)

S = slope of energy gradient

T = surface water temperature

u = local flow velocity

U = mean flow velocity (Q/A)

$\bar{u}$ = mean flow velocity at vertical

u_* = shear velocity

w = fall velocity of sediment particle

W = channel width

W_i = width of i-th subsection of transect

y = distance above river bed

z = Rouse number ($w/\beta\kappa u_*$)

Z = distance from right bank

β = ratio of ε_s to ε_m ($\varepsilon_s/\varepsilon_m$)

ε_m = diffusion coefficient for momentum

ε_s = diffusion coefficient for sediment

κ = Kármán constant

σ_g = geometric standard deviation of particle size

ABSTRACT

This study includes an investigation of analytical models for the description of flow and bed characteristics in a bend of the Sacramento River, California; and a study of a proposed new technique for bank protection.

Existing models for the prediction of the steady-state transverse bed profile in channel bends are reviewed; and alternative models are developed and validated. The new models predict the transverse bed slope to vary linearly with d/r (the ratio of depth, d, to radius of curvature, r) and almost linearly with the sediment-particle Froude number. Equations for the transverse variation of depth-averaged velocity and mean-grain size also are developed, which, together with the equations for the transverse variation of depth, can provide a guide to the depth of bed erosion and depth-averaged velocity near the outer banks of river bends.

It is shown, theoretically and by a physical model, that short, vertical, submerged vanes installed at incidence to the channel axis in the outer half of a river-bend channel significantly reduce the secondary currents and the attendant undermining and high-velocity attack of the outer bank. The effect of the vanes on the secondary flow is estimated by a simple torque calculation using the Kutta-Joukowski theorem. A design relation for the vane spacing is derived by equating the torque, about the channel centroid, produced by the flow curvature to that resulting from the lateral force exerted on the vanes. The relation is verified in an idealized, physical model of the mentioned bend of the Sacramento River, California.

ACKNOWLEDGEMENTS

This investigation was sponsored by the U.S. Army Corps of Engineers' Sacramento District, California, under Contract No. DACW05-80-C-0083; and Waterways Experiment Station, under Contract No. DACW39-80-C-0129. Grateful acknowledgement is expressed to Mr. Dallas Childers of the U.S. Geological Survey for collection of the field data and to Messrs. David Gundlach, Ed Sing, and Bud Pahl of the COE Sacramento District for their assistance in coordinating various aspects of the study.

TABLE OF CONTENTS

LIST OF SYMBOLS

A	projected surface area of sediment particle;
b	width of channel;
a_1, a_2	distances;
C	Chezy's coefficient;
c	constant;
c_1	lift force coefficient for sediment particle;
c_2	constant;
c_D	drag coefficient;
c_L	lift force coefficient for vane;
D	particle diameter;
D_{50}	mean sediment diameter;
d	flow depth;
d_c	flow depth at channel-center line;
F	Froude number = $V/\sqrt{gd}$;
F_D	particle Froude number = $V/\{[(\rho_s - \rho)/\rho]gD\}^{1/2}$;
F_d	longitudinal drag component;
F_ℓ	lift force;
F_r	radial drag component;
f	friction factor;
f'	flat-bed friction factor;
f_v	forced vortex distribution;
g	acceleration of gravity;
H	height of vane;
K	ratio of transverse bed slope to d/r;
L	length of vane;
M, N, N_f	functions of friction factors;

N_V number of vanes;

n, n', n_f velocity-profile exponents;

p pressure;

p' bed-layer porosity;

R_* boundary Reynolds number = $V_* D/\nu$;

r radius of curvature; radial coordinate;

r_c mean channel radius;

S longitudinal channel slope;

S_T transverse bed slope;

s distance in streamwise direction;

V flow velocity;

V_* shear velocity = $\sqrt{\tau_o/\rho}$;

$\overline{V}$ depth-averaged flow velocity;

$\forall$ particle volume;

W_s particle submerged weight;

y distance upward from stream bed;

α projected area-volume ratio for particle normalized by that for sphere;

α' angle of incidence of vane;

β transverse inclination;

β' ratio of actual to theoretical value of c_L ($\beta' \simeq 0.9$);

δ deviation angle;

κ von Karman's constant;

ξ dimensionless height = y/d;

θ Shields' parameter = $\tau_{cr}/[(\rho_s - \rho)g\, D_{cr}]$;

μ dynamic friction coefficient;

ν kinematic viscosity;

ρ	fluid density;
ρ_s	particle density;
τ	shear stress;
ϕ	bend angle
ϕ'	angle of repose of submerged sediment;
Φ	friction angle; and
Γ	circulation.

Subscripts

a	cross-sectional average;
c	center line;
cr	critical
f	related to Darcy-Weisbach's flat-bed friction factor;
i	innermost;
o	bottom, outermost;
r	radial direction; and
s	sediment.

LIST OF TABLES

LIST OF FIGURES

ANALYSIS OF SACRAMENTO RIVER BEND FLOWS, AND DEVELOPMENT OF A NEW METHOD FOR BANK PROTECTION

I. INTRODUCTION

This report presents the results of: (1) an investigation of analytical models for the description of flow and bed characteristics in a bend of the Sacramento River, California; and (2) a study of a proposed new technique for bank protection. The investigation was commissioned by the U.S. Army Corps of Engineers, Sacramento District, CA (Contract No. DACW05-80-C-0083), and has been carried out in accordance with the proposal submitted to the U.S. Army Corps of Engineers by IIHR in December 1979. The construction of and testing in a physical model of mentioned bend of the Sacramento River was commissioned by the U.S. Army Corps of Engineers, Waterways Experiment Station, MI (Contract No. DACW39-80-C-0129).

The bend selected for this study is located between Sacramento River miles 187.5 and 189.5, which is just above Ord Ferry. The data were obtained by the U.S. Geological Survey in April and May 1979, and March 1980.

Bank erosion is believed to be caused primarily by flow-induced boundary-shear stresses. Because the depth-averaged velocity tends to increase toward the outer bank of a river-bend cross section, these shear stresses are higher at the concave bank than in the central and convex-bank portions. The higher velocities at the outer bank, in turn, are due to greater water depth there. In an attempt to provide a means of predicting potential areas of bank erosion, this study has investigated several mathematical models (and developed new ones) for predicting the near-bank velocity. Since the velocity distribution is intimately related to the depth distribution, much emphasis has been put on finding reliable bed-topography and depth predictors. The effectiveness of short, vertical, submerged vanes as a means of bank protection also has been evaluated, both theoretically and in a physical model of the river bend.

II. VALIDATION OF MATHEMATICAL MODEL

A. Summary of Existing Theories

Among the available theories describing the flow-bed interaction in alluvial-channel bends are those by van Bendegom (1947), NEDECO (1959), Yen (1967), El-Khudairy (1970), Ikeda (1974), Allen (1970), Engelund (1974a), Kikkawa, Ikeda, and Kitagawa (1976), Zimmermann and Kennedy (1978), and Falcon (1979). All of these theories are for bends with fixed banks and constant discharges. They are based on the assumption that the mobile bed will eventually assume a lateral slope such that the net force on a moving grain at the bed will be zero in the radial direction. The equilibrium lateral bed slope calculated is that for which the radial-plane components, parallel to the bed, of the fluid drag, F_r, and the particle submerged weight, W_s, are equal (Figure 1):

$$F_r = W_s \sin \beta \tag{1}$$

in which $\sin \beta$ = radial (transverse slope of the bed surface. It is principally in the calculation of F_r that the theories differ.

van Bendegom (1947) determined F_r by balancing the forces acting on an elemental fluid volume traveling at steady state through the bend. He considered the forces due to the longitudinal and transverse slopes of the water surface, and the centrifugal force. By assuming that: (1) the shear stress behaves according to Prandtl's mixing length hypothesis; (2) the direction of the shear stress corresponds to that of the velocity vector; (3) the radial and vertical components of the velocity vector are small compared with the longitudinal component; and (4) the longitudinal velocity profile is described by the Manning-Strickler power law he obtained

$$\sin \beta = K \frac{d}{r} \tag{2}$$

in which d = local depth of flow; r = local radius of channel curvature; and $K = 0.0585 F_D^2$. F_D is the particle Froude number defined as

$$F_D = \frac{\bar{V}}{\sqrt{gD(\rho_s - \rho)/\rho}} \tag{3}$$

in which ρ and ρ_s = density of the fluid and sediment, respectively; $\bar{V}$ = depth-averaged mean velocity; D = mean particle diameter; and g = acceleration of gravity. van Bendegom's results were later used by NEDECO (1959) with sin β replaced by the derivative d(d)/dr to yield a differential equation which was solved to obtain an expression for the radial profile of the bed.

Yen (1967), in his analysis , related F_r in Eq. 1 to the radial component of the flow velocity, and obtained a relationship between sin β and the maximum radial velocity. El-Khudairy's (1970) and Ikeda's (1974) analyses are very similar to the analysis by Yen (1967), except that the radial velocities used in the calculation of F_r were computed from Rozovskii's (1961) velocity-distribution formulas. Allen (1970), who was unaware of van Bendegom's results, used a force balance similar to that of van Bendegom (1947). He obtained a relation between: (1) transverse slope, sin β ; (2) deviation angle, δ , between the direction of the longitudinal drag, F_d, and the direction of the mean flow; (3) bed shear stress, τ_o; and (4) mean particle diameter, D.

Engelund (1974a) and Kikkawa, Ikeda, and Kitagawa (1976) assumed that the longitudinal drag F_d, on a sediment particle is balanced by the friction force on the particle from the channel bed. While Engelund (1974a) related F_r and F_d by the deviation angle, δ, using his (1974b) experimental finding that tan δ = 7d/r, Kikkawa, Ikeda, and Kitagawa (1976) related F_r and F_d by assuming that the ratio between them equals the ratio between the radial, V_r, and longitudinal, V_o, velocity components of the flow at bed level. V_o was determined from a relationship between F_d and V_o, using a drag coefficient; V_r was determined by solving the radial momentum equation using a simplified stream-function formulation, constant eddy viscosity, and a logarithmic profile for the mean flow velocity (modified by the forced-vortex distribution). Both Engelund (1974a) and Kikkawa et al. (1976) obtained Eq. 2; however, K is essentially a constant in Engelund's analysis, while it is a function of F_D and the Darcy-Weisbach friction factor, f, in the formulation of Kikkawa et al. Engelund's (1974a) findings were used by Engelund (1974a) and Gottlieb (1976) to calculate the bed topography of a curved channel with given discharge and grain size. Engelund (1976) later showed that the transverse bed slope increases when the suspended sediment load increases.

Zimmermann and Kennedy (1978) related F_r in Eq. 1 directly to stream-flow characteristics by equating the moment, about the channel axis, of the radial boundary shear stress (averaged around the wetted perimeter) to the moment produced by the nonuniformity (over depth) of the centrifugal force. The balance is a simplified expression for the conservation of the flux of moment of momentum. Falcon's (1979) approach is an extension of Zimmermann and Kennedy's (1978). Falcon assumed that F_r is determined from a relationship equating the centrifugal force on a unit volume, $\rho V^2/r$, to the radial pressure gradient, $\partial p/\partial r$, and the vertical gradient of the radial shear stress, $\partial \tau_r/\partial y$:

$$\rho \frac{V^2}{r} = \frac{\partial p}{\partial r} - \frac{\partial \tau_r}{\partial y} \tag{4}$$

in which p = pressure; y = vertical distance from river bed; and τ_r = radial shear stress. The pressure gradient was determined by equating the integral over depth of the moment of $\partial p/\partial r$ with respect to a longitudinal axis, to the integral over depth of the moment of the centrifugal force about the same axis. Using the power law,

$$V = \frac{n+1}{n} \left(\frac{y}{d}\right)^{1/n} \overline{V} \tag{5}$$

in which n = dimensionless factor (which will be termed the velocity-profile exponent), the radial shear stress, τ_r, is determined as a function of y by integration. He then obtained the radial drag, F_r, by multiplying the radial shear stress at the bed by the projected surface area of a sediment particle, A:

$$F_r = \rho A \overline{V}^2 N \frac{d}{r} \tag{6}$$

in which

$$N = \frac{n+1}{n(n+2)} \tag{7}$$

According to Zimmermann and Kennedy (1978), n^2 equals the inverse of the overall friction factor, f. In Falcon's (1979) analysis, n is determined from the longitudinal slope, S, of the water surface, using the Darcy-Weisbach

formula modified by Falcon (1979). Both Zimmermann and Kennedy (1978) and Falcon (1979) obtained Eq. 2, with

$$K = cNF_D^2 \tag{8}$$

In Zimmermann and Kennedy's analysis, the value of c is one third that in Falcon's analysis, because Falcon neglected the moment contribution of vertical shear stresses.

Table 1 is a summary of key relations in the reviewed models.

B. Alternative Approaches

1. Odgaard's Approach - The preceding models are based on the assumption that the equilibrium bed profile is determined by particles in downstream motion and radial static equilibrium. Considering that many natural river beds (including those of the Sacramento River) consist of nonuniform sediments, and often have an armoring of coarser sediments at the bed surface, there can be a significant difference between the grain-size distribution of the bed-load discharge and that of the bed-surface material. The following approach (Odgaard, 1981) is an attempt to relate the radial bed slope to bed-surface characteristics rather than to bed-load characteristics. Since armoring is believed to be a process that intervenes to bring the bed into equilibrium such that no net sediment deposition or erosion occurs, armoring is considered to be an incipient-motion problem. Therefore, for an armored bed, the slope may be determined by sediment particles whose motion is impending rather than by particles that are in motion. This approach is basically a critical-shear-stress analysis, somewhat similar to that of White (1940) and Shields (1936).

It is assumed that, in the state of equilibrium, the sediment particles constituting the bed surface are statically stable in both the radial direction and the longitudinal direction (the mean flow direction), but at incipient motion in the longitudinal direction. That is, the size of the bed-forming particles is such that the particles are just about to move in the longitudinal direction by rolling about their points of support. Figure 2 shows the vertical longitudinal-plane force diagram for one such particle. Equating moments of the gravity (W_s), lift (F_ℓ), and drag (F_d) forces about the support point yields

$$F_d = c_2 W_s \tag{9}$$

in which

$$c_2 = \frac{(a_1/a_2)\tan \phi'}{1 + c_1 (a_1/a_2)\tan \phi'} \tag{10}$$

a_1 and a_2 are the distances shown in Figure 2; c_1 = the lift/drag ratio, F_ℓ/F_d; and ϕ' = the angle of repose of the submerged sediment. Shields (1936) and White (1940) reduced Eq. 9 to the following equation for the critical shear stress, τ_{cr}:

$$\tau_{cr} = \theta\ (\rho_s - \rho) g\ D_{cr} \tag{11}$$

in which ρ_s = density of the sediment particles; g = acceleration of gravity; ρ = density of water; D_{cr} = the diameter of the particle whose motion is impending; and θ = a dimensionless factor, which, according to Shields (1936), is a function of a critical boundary Reynolds number. From Eqs. 9, 10, and 11 it is seen that

$$\theta = \alpha \frac{(a_1/a_2)\tan \phi'}{1 + c_1(a_1/a_2)\tan \phi'} \tag{12}$$

in which α = ratio of projected surface are to volume for a sediment particle divided by that for a sphere. Shields' experimental results, which appeared as a plot of $\tau_{cr}/[(\rho_s - \rho) g\ D_{cr}]$ versus the critical boundary Reynolds number, were approximated by a curve (the Shields curve) by Rouse (1939). The curve is included in many books on sediment transport (e.g., Vanoni, 1970). Shield's curve is valid only for flat beds; therefore, τ_{cr} in Eq. 11 is the critical flat-bed shear stress. This shear stress may also be related to a critical mean-flow velocity, $\overline{V}_{cr}$, by means of the Darcy-Weisbach friction factor, f' (flat-bed friction factor):

$$\tau_{cr} = \frac{f'}{8} \rho\ \overline{V}_{cr}^{\,2} \tag{13}$$

Introduction of $f' = 8\ \kappa^2 n'^{-2}$ (obtained by comparing the power law, Eq. 5, with the logarithmic relation for the velocity profile; Zimmermann and Kennedy, 1978) yields

$$\tau_{cr} = \frac{\kappa^2}{n'^2} \rho \, \overline{V}_{cr}^2 \tag{14}$$

If the grain-shear stress, τ', exceeds τ_{cr}, sediment transport will occur. However, substantial evidence is available (Luque, 1974; Engelund and Fredsøe, 1976) indicating that the immobile bed will continue to be acted upon by τ_{cr}, while the residual part, $\tau'-\tau_{cr}$, is carried as drag on the moving bed particles and only indirectly is transferred to the bed by occasional encounters. If the mean velocity is $\overline{V}$, for a grain shear stress τ', the Darcy-Weisbach relation reads

$$\tau' = \frac{\kappa^2}{n'^2} \rho \, \overline{V}^2 \tag{15}$$

and the relationship between τ_{cr} and $\overline{V}$ may be written

$$\tau_{cr} = \frac{\kappa^2}{n_f^2} \rho \, \overline{V}^2 \tag{16}$$

in which

$$n_f^2 = n'^2 \frac{\tau'}{\tau_{cr}} = n'^2 \frac{\overline{V}^2}{\overline{V}_{cr}^2} \tag{17}$$

Equating Eqs. 11 and 16 yields

$$\overline{V}^2 = \frac{\theta}{\kappa^2} n_f^2 \frac{\rho_s - \rho}{\rho} g \, D_{cr} \tag{18}$$

or

$$n_f = \kappa \, F_{Dcr} \, \theta^{-1/2} \tag{19}$$

in which F_{Dcr} is the particle Froude number based on D_{cr}; that is,

$$F_{Dcr} = \frac{\overline{V}}{\sqrt{\frac{\rho_s - \rho}{\rho} g \, D_{cr}}} \tag{20}$$

Falcon (1979) and Zimmermann and Kennedy (1978) in their calculation of the transverse bed slope assumed that the entire fluid stress is transmitted

directly through the bed-load layer to the immobile bed. In the present alternative approach, the radial shear-stress component acting on the particles of the bed surface is the radial component of the critical shear stress $\tau_{cr,r}$, rather than τ_r. Therefore, the radial force balance is

$$A\tau_{cr,r} = W_s \sin \beta \tag{21}$$

in which $W_s = (\rho_s - \rho)\, g\, \forall$, $\forall$ = volume of sediment particle. In view of Eq. 16 it is reasonable to assume that $\tau_{cr,r}$ is the radial bed-shear stress necessary to generate a torque that balances the torque generated by a power-law velocity profile of the form

$$V = \frac{n_f+1}{n_f} \left(\frac{y}{d}\right)^{1/n_f} \overline{V} \tag{22}$$

which, if $\overline{V} = \overline{V}_{cr}$, is the velocity profile above a flat bed just before the onset of sediment motion. According to Falcon (1979), the radial bed-shear stress is then given by

$$\tau_{cr,r} = \rho N_f \overline{V}^2 \frac{d}{r} \tag{23}$$

in which

$$N_f = \frac{n_f+1}{n_f(n_f+2)} \tag{24}$$

Substituting Eq. 23 into Eq. 21 yields

$$\sin \beta = K \frac{d}{r} \tag{25}$$

where

$$K = \frac{3\alpha}{2} N_f F_{Dcr}^2 \tag{26}$$

This relationship is similar in form to Falcon's relationship for K. However, Falcon's K is a function of the overall bed resistance and the size of the bed-load particles, while the present K-value (Eq. 26) is a function of the bed resistance given by Eq. 19 and the size of the bed-surface particles. Because N_f is nearly equal to n_f^{-1} and n_f, in turn, is proportional to F_{Dcr}

(Eq. 19), Eq. 26 predicts a nearly linear variation of K with F_{Dcr}. In Falcon's (1979), Zimmermann and Kennedy's (1978), and van Bendegom's (1947) models, K is proportional to F_D^2.

2. Falcon and Kennedy's Approach - Very recently, Falcon and Kennedy (1982) proposed another approach for bed-profile modelling. They used the concept of bed-layer thickness originally proposed by Karim (1981) to establish an alternative radial force balance to Eq. 1. Considering, instead of the single particle in Figure 1, a volume of bed-layer particles of thickness y_b, Falcon and Kennedy proposed the following radial force balance

$$\tau_r = (\rho_s - \rho)(1-p')y_b \, g \sin \beta \tag{27}$$

in which p' = bed-layer porosity. Substituting into this equation: (1) Karim's (1981) formula for the bed-layer thickness

$$y_b = D_{50} \, V_*/V_{*c} \tag{28}$$

where

$$V_* = \overline{V}\sqrt{f/8} \tag{29}$$

and

$$V_{*c} = \sqrt{\frac{\rho_s - \rho}{\rho} g \, D_{50} \, \theta} \tag{30}$$

and (2) Falcon's (1978) Eq. 6 using $n = 1/\sqrt{f}$ and $\tau_r = F_r/A$, Falcon and Kennedy obtained Eq. 2 with K determined by

$$K = \frac{\sqrt{8\theta}}{1-p'} \frac{1 + \sqrt{f}}{1 + 2\sqrt{f}} F_D \tag{31}$$

The term in Eq. 31 involving f is nearly constant; therefore, Eq. 31 predicts nearly linear variation of K with F_D.

C. Comparison of Predictive Capabilities

It is seen that all of the analytical models that relate the local transverse bed slope to mean-flow characteristics predict the local transverse slope to be proportional to the radio between depth, d, and radius of curvature, r:

$$\frac{d(d)}{dr} = K \frac{d}{r} \tag{32}$$

in which $S_T = d(d)/dr$ at the centerline.

1. Comparison with Laboratory Data - Initially, the performance of the models was tested by means of Zimmermann and Kennedy's (1978) experimental results. Figure 3 (a,b,c,d, and e) shows a comparison of measured and predicted slopes, the ordinate being the measured values of $S_T(d_c/r_c)$ and the abscissa values determined by the formula for K, using measured values of d, D, and $\overline{V}$.

Figure 3(a) shows the performance of the van Bendegom model (1947). The agreement between measured slopes and slopes predicted by this model (calibrated by a factor of 3.55) is quite good at smaller values of S_T. Systematic deviation of the measured values of S_T from the predicted is seen to occur at the larger slopes.

As seen in Figure 3(b), the correlation between observed slopes, and slopes predicted by Engelund's (1974a) model, is fairly small. Since the dynamic friction coefficient, μ, is more or less constant. Engelund's model almost always predicts the same value of $S_T/(d_c/r_c)$.

To apply Kikkawa et al.'s (1976) model, the function M (Table 1) must be evaluated at the centerline of the channel. Using: (1) A value of one for the forced vortex distribution (which is the value to be expected at the centerline); (2) $V_*/\overline{V} = \sqrt{f/8} = 1/(n\sqrt{8})$; and (3) a sheltering factor of 0.592, their K-value is reduced to F_D (1.628-0.912/n). The value of n for each experiment was determined experimentally by Zimmermann and Kennedy, using the side-wall correction procedure of Vanoni and Brooks (Vanoni, 1976). As seen in Figure 3(c), the agreement between observed slopes and slopes predicted by Kikkawa, et al.'s model (calibrated by a factor of 0.76) is very good. Figure 3(d) compares the observed slopes and the slopes predicted by Zimmermann and

Kennedy's/Falcon's model. The agreement is seen to be somewhat smaller than when Kikkawa, et al.'s model is applied.

To apply Odgaard's (1981) model, n_f must be evaluated using Eq. 19. The value of Re_* is found to be approximately four in Zimmermann and Kennedy's (1978) Runs 1-1 through 3-12, and approximately nine for the remaining runs. According to Shields' curve, these values of Re_* correspond to values of θ of 0.04 and 0.03, respectively. As shown in Figure 3(e), the agreement between observed slopes and slopes predicted by Odgaard's model is good. Odgaard's model was applied without introduction of a calibration factor.

Figure 3(f) shows that Falcon and Kennedy's (1982) model also conforms very well to Zimmermann and Kennedy's data. The slope of the straight line through the points gives a value of porosity p' of 0.43 if Shield's limiting value of $\theta = 0.06$ is adopted.

2. Comparison with Field Data - The ultimate test of a model's predictive capability is against field data. The data obtained by the U.S. Geological Survey, Sacramento, from the bend of the Sacramento River between river miles 187.5 and 189.5 were used to verify the different models. Figure 4 shows a schematic plan view of the study reach. Six cross sections of the bend were surveyed in April and May 1979, and again in March 1980 to measure channel geometry and flow characteristics for two different flow rates. Detailed velocity measurements, bed-material samples, and depth soundings were taken across each section. The direction and magnitude of the flow velocity were measured over 4 to 10 verticals across each section, using Price and Ott flow meters in the 1979 surveys, and a Marsh-McBirney flow meter in the 1980 surveys. In each vertical the velocity, V, was measured at 1- to 2-foot depth intervals; the recording time was 2 to 5 minutes at each point of the vertical. Based on these measurements, a depth-averaged velocity, $\overline{V}$, was determined by dividing the known (gaged) flow rate by the measured cross-sectional area. The bed samples were taken by a "digging sampler" (USBM-54), which samples to a depth of 2 to 3 inches below the bed surface. Figures A-1 through A-10 in Appendix show log-log plots of $V/\overline{V}$ versus $\xi = y/d$ for each vertical. The velocity-profile exponents, n, were determined from these plots by measuring the slope of the best fitting line. Figures A-11 through A-25 in Appendix show plots of local and overall grain-size distributions. (Figures

A-24 and A-25 show composite grain-size distributions from an additional field survey in July 1980). The results are summarized on the drawings of the cross sections in Figures 5 through 14, and in Table 2. Two sets of n-values are listed in Table 2. The values in Column 10 were determined on the basis of the longitudinal slope, S, of the water surface, using the Darcy-Weisbach formula modified by Falcon (1979). The procedure for the determination of n is described by Falcon (1979). The slope of the water surface was measured and found to be about 0.0003. Brice (1977) also reports that the average slope of the bed between river miles 190 and 185 is approximately 0.0003. The n-values in Column 11 are cross-sectional averages of values determined from the individual velocity profiles as described above. These n-values are seen to be significantly higher than those indicated by the drop of the water-surface elevation through the bend. That the n-values in Column 11 are more realistic characteristics of the bed friction than the values in Column 10 is also indicated in Figure 15, which shows a plot of radial velocity components, V_r, versus depth below the water surface. The plot is based on 210 velocity measurements in the bend at high flow (discharges between 24,000 cfs and 28,400 cfs). Measurements very close to the banks were omitted. Each point in the plot is the average value of the radial velocity components over an interval of 10% of the water depth. For example, the value of 6.9 for $V_r r_c/(\overline{V}_a\, d_a)$ at $\xi = 0.9$ is the arithmetic average of 28 measurements of $V_r r_c/(\overline{V}_a d_a)$ within the range $0.85 < \xi \leq 0.95$. The radial velocity components were determined by multiplying the point velocities by sine of the angle between the depth-averaged flow direction and the flow direction measured at each point in the profile. The points in Figures 15 are seen to conform very well to the curve shown, which is the radial velocity distribution calculated from Falcon's (1979) theory using n = 8.5. The average value of n in Column 11 (omitting Section 1) also is 8.5. Consequently, frictional characteristics and the secondary current in this bend may not be estimated reliably from the longitudinal slope of the water surface. The results presented in Figure 15 support Falcon's (1979) theory and the analytical approach used in this study.

Column 9 in Table 2 shows the transverse bed slopes, S_T. These were measured at the channel centerline, but they appeared to be practically constant across most of the sections. Figure 16 (a,b,c,d,e, and f) shows a comparison of measured and predicted slopes. The ordinate is the measured

value of $S_T/(d_a/r_c)$, and the abscissa is the value calculated by the formula for K, using measured cross-sectional-average values of velocity, mean particle diameter, and channel slope; that is, V_a, D_{50}, and S, respectively. As will be seen in Figure 16 (c,e, and f), the models by Kikkawa et al. (calibrated by a factor of 2.0), Odgaard (calibrated by a factor of 2.43), and Falcon and Kennedy (calibrated by a factor of 2.7) give good agreement between measured and predicted slopes. The agreement is also good at smaller values of S_T when Zimmermann and Kennedy's (calibrated by a factor of 5.1), and Falcon's model (calibrated by a factor of 1.7), is used, as will be seen in Figure 16(d), and when van Bendegom's or Engelund's model is used, as will be seen in Figures 16(a) and 16(b), respectively; systematic deviation of the measured values of S_T from the predicted is seen to occur at the larger slopes. Although Falcon (1979) recommends using D_{95} for the calculation of F_D, Falcon's model was found to give better agreement between measured and predicted slopes when D_{50} was used. In Odgaard's model, N_{fa} (the cross-sectional average value of N_f) was calculated by Eqs. 24 and 19, using $\theta = 0.06$, $\kappa = 0.4$, and the measured values of F_D for F_{Dcr}.

So far, the comparison of the models has been made on the basis of their capability of predicting the transverse bed slope at the centerline of the cross sections. A strict evaluation of the models should also include a comparison of the complete solutions in the form recommended by the respective authors. Engelund (1974), Kikkawa, Ikeda, and Kitagawa (1976), and Falcon (1979) recommend using their integrated solutions, while Zimmermann and Kennedy (1978) and Odgaard (1981) recommend using constant slopes across the sections. However, it is easily verified that the trend seen in Figure 16 remains unchanged whether integrated solutions or constant slopes are used with the present data. In all models, the key parameter is the grain size, whether it be that of the bed load or that of the bed surface. As will be seen in Table 2, the variation of D_{50} throughout the bend is very significant. No technique or model is yet available that can simulate a variation like that in a given bend from the flow and channel data. Instead, a rough estimate of D_{50} may be obtained on the basis of a combination of a Manning-Strickler type of equation and Eq. 19. Figure 17 shows a plot of n_{fa} (cross-sectional average value of n_f) versus relative depth, d_a/D_{50}. n_f was calculated by Eq. 19 using $\kappa = 0.4$, $\theta = 0.06$, and measured values of $\bar{V}$ and D_{50}. It is seen that a straight line of slope 1:4.6 gives a reasonably

accurate description of the correlation between n_{fa} and d_a/D_{50}. The line is given by the equation.

$$n_{fa} = 1.42 \ (d_a/D_{50})^{0.22} \tag{34}$$

Substituting Eq. 34 into Eq. 19 yields

$$D_{50} = 0.76 \ d_a \ F^{3.5} \tag{35}$$

in which F is the Froude number, defined as

$$F = \frac{V_a}{\sqrt{gd_a}} \tag{36}$$

In Figure 18, the measured correlation between relative roughness and Froude number is compared with that given by Eq. 35. The agreement is seen to be satisfactory. Note, however, that Eq. 35 is based on only data from the Sacramento River study bend.

The procedure for application of Odgaard's (1981) model is summarized as follows: Given the cross-sectional average values of depth, d_a, and velocity, V_a, the cross-sectional average value of D_{50} may be estimated using Eq. 35. (Eq. 35 is tentative and may apply only to the Sacramento River data). The cross-sectional average values of n_f and N_f may then be determined by Eqs. 19 and 24, respectively. The transverse bed slope, sin β, is then obtained by substituting n_{fa}, N_{fa}, and r_c into Eqs. 25 and 26. Based on the Sacramento River bend data, K in Eq. 25 should be multiplied by a calibration factor of 2.43.

The differential equation for the transverse bed slope, which is obtained by replacing sin β in Eq. 25 by d(d)/dr, is not readily solved since both n_f and F_{Dcr} are functions of mean velocity and grain size, both of which vary in a yet unknown manner across the channel sections. However, field data indicate that a reasonable first approximation may be obtained by considering sin β to be constant across a section. In that case, the transverse depth variation is described by the equation

$$\frac{d}{d_c} = 1 + K \left(\frac{r}{r_c} - 1\right) \tag{37}$$

D. Velocity and Grain-Size Predictor

It is reasonable to assume that: (1) the local depth-averaged velocity, $\overline{V}$, is related to the local longitudinal slope, S, by the Darcy-Weisbach equation:

$$\overline{V} = n\sqrt{8gSd} \tag{38}$$

and (2) S varies as

$$S = S_c \frac{r_c}{r} \tag{39}$$

in which S_c, r_c = centerline values of S and r, respectively. Therefore, the variation of the mean velocity across the channel can be expressed

$$\frac{\overline{V}}{\overline{V}_c} = \frac{n}{n_c} \left(\frac{d}{d_c}\right)^{1/2} \left(\frac{r_c}{r}\right)^{1/2} \tag{40}$$

in which $\overline{V}_c$, d_c, n_c = centerline values of $\overline{V}$,d, and n, respectively. Thus, if n is constant across a given section, that is, if $n = n_c$, the mean velocity will vary with d/r to the power 0.5. However, according to the analysis by Anderson et al (1970) n cannot be considered to be constant. They found that the Manning number for an alluvial channel varies with mean grain size to the 1/6-power. Henderson (1966) reports that a 1/6-power relationship also was observed by Strickler in this work on gravel-bed streams. This implies that n varies with relative depth, d/D, to the power 1/6:

$$n \sim \left(\frac{d}{D}\right)^{1/6} \tag{41}$$

and Eq. 40 is reduced to

$$\frac{\overline{V}}{\overline{V}_c} = \left(\frac{D_c}{D}\right)^{1/6} \left(\frac{d}{d_c}\right)^{2/3} \left(\frac{r_c}{r}\right)^{1/2} \tag{42}$$

As can be seen in Figure 19, Eq. 41 is supported by the results from the Sacramento River bend study. Eq. 42 shows that if $D = D_c$, that is, if the bed sediment is uniform and the grain-size distribution is the same across the width of the channel, the mean velocity, $\overline{V}$, varies with depth, d, to the power of 2/3.

If a large variety of grain sizes is available in the river bed, grain sorting seems to take place. As is illustrated very clearly in Figures 20 and 21 (from Bluck, 1971, and Bridge and Jarvis, 1976), the sediment near the inner bank in the downstream parts of the bends tends to be finer than that in the deeper parts along the outer bank. The same trend was observed in the downstream parts of the Sacramento River study bend. Figures 5 through 14, from the Sacramento River bend, show that the mean grain size can vary by a factor of more than ten across a given section. The variation of D across a section can be estimated analytically as follows: Eqs. 19 and 40 can be combined to yield

$$\frac{n_f}{n_{f_c}} = \frac{n}{n_c} \left(\frac{d}{d_c}\right)^{1/2} \left(\frac{r_c}{r}\right)^{1/2} \left(\frac{D_c}{D}\right)^{1/2} \left(\frac{\theta_c}{\theta}\right)^{1/2} \tag{43}$$

in which n_{fc} and θ_c are centerline values of n_f and θ, respectively. Substituting Eq. 43 into Eqs. 25 and 26 with $N_f \approx n_f^{-1}$, and using Eqs. 40 and 41, yields

$$\frac{S_T}{S_{Tc}} = \left(\frac{d}{d_c}\right)^{5/3} \left(\frac{r_c}{r}\right)^{3/2} \left(\frac{D_c}{D}\right)^{2/3} \left(\frac{\theta}{\theta_c}\right)^{1/2} \tag{44}$$

in which S_{Tc} = the centerline value of S_T. The data from the Sacramento River bend, and from several other bends with nonuniform bed sediments, indicate that the transverse bed slope may be considered to be constant across the major part of the cross section. From Eq. 44 it is seen that in order for this to be the case, the grain-size variation is governed by

$$\frac{D}{D_c} = \left(\frac{d}{d_c}\right)^{5/2} \left(\frac{r_c}{r}\right)^{9/4} \left(\frac{\theta}{\theta_c}\right)^{3/4} \tag{45}$$

Substituting Eq. 45 into Eq. 42 then yields

$$\frac{\overline{V}}{\overline{V}_c} = \left(\frac{d}{d_c}\right)^{1/4} \left(\frac{r_c}{r}\right)^{1/8} \left(\frac{\theta_c}{\theta}\right)^{1/8} \tag{46}$$

The Shields' parameter, θ, cannot be assumed to be a constant across a section. The data delineating Shields' curve were obtained from experiments in flumes with fully developed turbulence and artificially flattened beds of uniform, noncohesive sediments. The θ-values were determined from the values of the shear stress for zero sediment discharge obtained by extrapolating a

graph of observed sediment discharge versus shear stress. In a river, the flow conditions are very different from those in the flume experiments. Ripples and dunes, formed as a result of sediment movement, cause the value of θ to be different from that given by the Shields' curve (Shields, 1936; White, 1940; Einstein and Barbarossa, 1952; and Sundborg, 1956), and so does nonuniformity of the bed sediment. The latter may be inferred from the data by Rakoczi (1975), who, in three series of experiments, determined the critical shear stress for different fractions of a nonuniform sediment mixture. Figure 22 shows a plot of his measured critical shear stresses, nondimensionalized by $(\rho_s-\rho)g\ D_{50}$, versus D_{50}. Each point is based on five tests with a given grain-size distribution. The results seem to indicate that for a nonuniform (non-armored) sediment bed, the Shields' parameter decreases with increasing mean-grain size. The trend in Figure 22 may be explained in part by Eq. 12 which shows that θ decreases with increasing angle of repose, ϕ'. According to Simons and Senturk (1977), ϕ' for coarse sediment decreases with increasing grain size within the grain-size range from 0.5 mm to 3.6 mm. The decrease reported by them may be described approximately by the power function

$$\tan \phi' \simeq \text{const.} \times D^{-m} \tag{47}$$

in which $m \simeq 0.3$ and $D < 3.6$ mm. Substituting Eq. 47 into Eq. 12 and assuming that $c_1 \simeq 0$ yields

$$\theta \sim D^{-m} \tag{48}$$

Schoklitsch is reported (Graf, 1971) to have suggested that $m = 2/3$ for $D < 3$ mm. As will be seen in Graf (1971), his suggestion was based on a quite significant number of data. The trend which is similar to that of Shields' curve for $Re_* < 10$, may be explained by viscous effects: At smaller values of D_{50} a larger portion of the sediment mixture is protected by the viscous sublayer than at larger values of D_{50}. Assuming that θ can be described by Eq. 48 with $m = 2/3$, which is the value suggested by Schoklitsch and used for the curve approximating the points in Figure 22, and substituting Eq. 48 into Eq. 45 yields

$$\frac{D}{D_c} = \left(\frac{d}{d_c}\right)^{5/3} \left(\frac{r_c}{r}\right)^{3/2} \tag{49}$$

Substitution of Eq. 49 into Eq. 42 then yields

$$\frac{\overline{V}}{\overline{V}_c} = \left(\frac{d}{d_c}\right)^{7/18} \left(\frac{r_c}{r}\right)^{1/4} \tag{50}$$

In Figures 23, 24, and 25 observed values of (D/D_c) obtained in the Sacramento River bend study are plotted against distance r from the center of curvature, and compared with values computed by Eq. 49 using the measured depth variation. The agreement is reasonable. Figure 26 shows a comparison of observed values of $\overline{V}/\overline{V}_c$ and values computed by Eq. 50, using measured values of d, r, $\overline{V}_c$, and r_c. The values plotted in Figure 26 are from the central portion of the channel sections where bank effects are small. In all cases, the maximum velocity measured in the cross sections were within the central portion of the sections. Although the scatter is large, as is invariably the case with river data, the results plotted in Figure 26 support Eq. 50.

Eqs. 49 and 50 are based on data from bend sections in which the availability of grain sizes were believed to be unlimited. Armor layers had formed in many cases. If the range of grain sizes in the bed sediment is limited, the velocity distribution may be quite different from that of Eq. 50. Eq. 42 shows that if $D = D_c$, the velocity distribution is given by

$$\frac{\overline{V}}{\overline{V}_c} = \left(\frac{d}{d_c}\right)^{2/3} \left(\frac{r_c}{r}\right)^{1/2} \tag{51}$$

If a conservative estimate of the near-bank velocity is needed, this equation should be used rather than Eq. 50.

E. Numerical Example 1

Given a river bend of radius r_c = 2,000 ft. Width b and longitudinal slope S of the river are 500 ft and 0.0003 ft/ft, respectively (based on overall data); and its overall frictional characteristics are given by n = 3 (corresponding to an overall friction factor of f = 0.1). Estimate the maximum depth, d_o, and maximum depth-averaged velocity, $\overline{V}_o$, at a discharge of Q = 40,000 cfs.

Solution:

Cross-sectional average values of depth, d_a, and mean velocity, V_a, are determined by the Darcy-Weisbach relation, Eq. 38, and conservation of volume, $Q = V_a b d_a$:

$$d_a = \left[\frac{Q/b}{n\sqrt{8gS}}\right]^{2/3} = 21.0 \text{ ft}$$

$$V_a = n\sqrt{8gSd} = 3.8 \text{ ft/s}$$

Grain size is the major uncertainty. If all grain sizes are available in the bed sediment, armoring is likely to occur, and D_{50} may be estimated by Eq. 35 with F calculated from Eq. 36:

$$D_{50} = 6.4 \text{ mm}$$

Note that Eq. 35 is based on only the data from the Sacramento River study bend.

The particle Froude number is calculated from the grain-size, D_{50}, using Eq. 20 with $D_{cr} = D_{50}$; $\overline{V} = V_a$; and $(\rho_s - \rho)/\rho = 1.65$:

$$F_D = F_{Dcr} = 3.6$$

and n_f, N_f, and K are calculated from Eqs. 19, 24, and 26/31, respectively, using $\theta = 0.06$; $\alpha = 1.27$; $\kappa = 0.4$; and $p' = 0.4$:

$$n_f = 5.88$$

$$N_f = 0.148$$

$$K = 3.65/3.31$$

Based on the data from the Sacramento River study bend, K must be multiplied by a factor of 2.43/2.7; and the value of K becomes

$$K = 8.9$$

Maximum depth, d_o, and maximum depth-averaged velocities, $\overline{V}_o$, are then estimated by Eqs. 37 and 50, respectively, assuming that $d_c = d_a$, and $\overline{V}_c = V_a$:

$$d_o = 44.4 \text{ ft}$$

$$\overline{V}_o = 4.9 \text{ ft/s}$$

The estimated bed profile is sketched in the figure below. Note that the effective width of the channel is reduced slightly at this discharge. If the reduction in width had been more significant, the calculation procedure should be repeated with the reduced width. In effect, the solution then would be obtained by iteration.

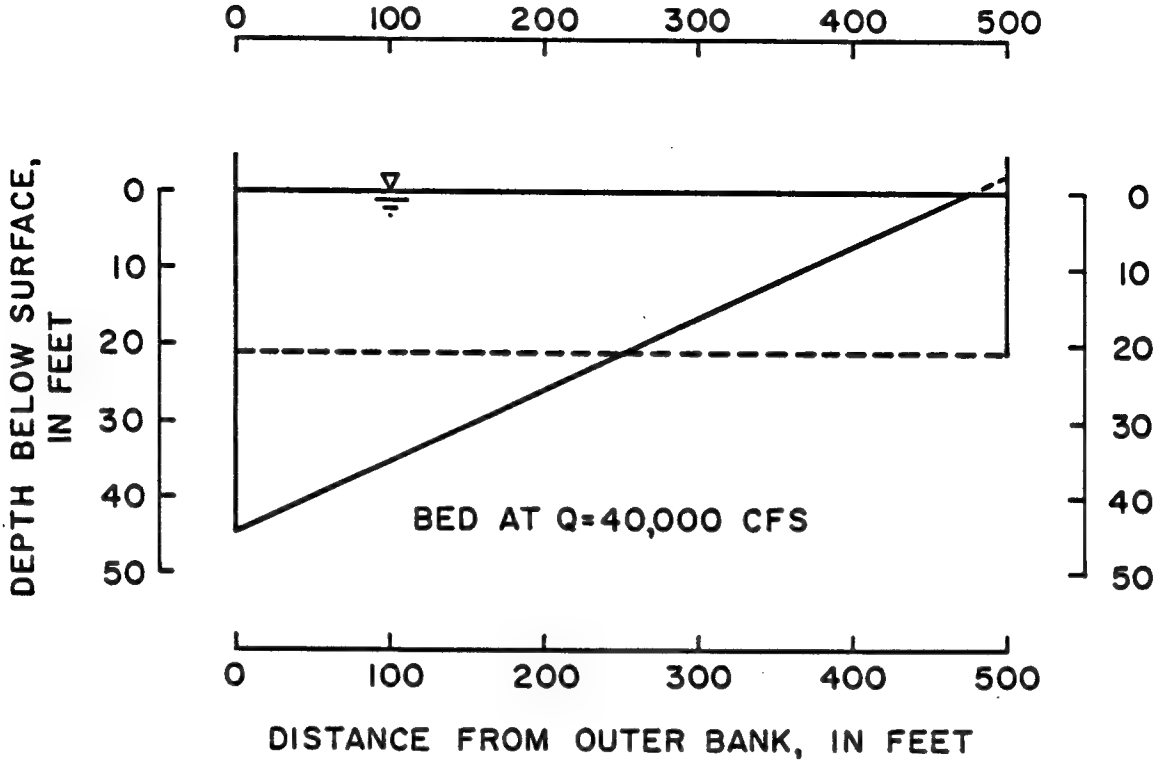

III. NEW METHOD FOR BANK PROTECTION

The recent development in the analytical approaches has prompted the idea that effective bank protection may be obtained by means of deeply submerged vanes placed at strategic points in the bend. From the results of the theories it appears reasonable to expect that the strength of the secondary flow in the bend can be reduced if the vanes are placed at a certain angle of incidence. The vanes will then exert a torque on the flow which will counter the torque produced by the flow (by the interaction of the streamline curvature and horizontal vorticity of the flow), and a reduction of the velocities along the outer bank of the bend is expected.

A. Analysis of Submerged Vanes

The torque produced by the flow through an angular increment $d\phi$ may be estimated using the analysis by Zimmermann and Kennedy (1978). Calculating the torque, dT_{flow}, about the center of the flow yields

$$dT_{flow} = \int_{r_i}^{r_o} \int_{0}^{d_c} \rho \frac{V^2}{r} \left(y - \frac{d_c}{2}\right) r \, d\phi \, dy dr \qquad (52)$$

in which d_c = depth of flow at channel centerline; V = point velocity at distance y from the bed and distance r from the center of curvature; r_o = outermost channel radius; r_i = innermost channel radius; and ρ = fluid density. The velocity V is a yet unknown function of y and r. Zimmermann and Kennedy (1978), however, assumed that the variation of V with r could be neglected in the computation of dT_{flow}. They substituted the power law velocity distribution, Eq. 5, into Eq. 52 and obtained

$$dT_{flow} = \frac{\rho}{2} \frac{n+1}{n(n+2)} (r_o - r_i) \, d_c^2 \, \overline{V}^2 \, d\phi \qquad (53)$$

This equation will be used for the present analysis. With reference to the definition sketch in Fig. 27, Eq. 53 may be re-arranged to read

$$dT_{flow} = \frac{\rho}{2} \frac{n+1}{n(n+2)} \overline{V}^2 \frac{d_c}{r_c} \, d\forall \qquad (54)$$

in which $d\forall = b d_c r_c \, d\phi$, the volume element corresponding to the area, dA, hatched in Fig. 27(a); $r_c = (r_o + r_i)/2$; and $b = r_o - r_i$. The torque produced by the flow over a length $ds = r_c d\phi$ of the bend is

$$dT_{flow} = \frac{\rho}{2} \frac{n+1}{n(n+2)} \bar{V}^2 b \frac{d_c^2}{r_c} ds \qquad (55)$$

The torque produced by a submerged vane may be estimated using the Kutta-Joukowski theorem (see, for example, Daugherty and Franzini 1977). According to this theorem the combination of rotational flow and uniform flow around a vane or foil of length L and width (height in the present application) H gives rise to a lift force, F_ℓ, given by

$$F_\ell = \rho HV\Gamma \qquad (56)$$

in which V = uniform flow velocity and Γ = the circulation around the vane. When the angle of incidence is α , the circulation is given by

$$\Gamma = \pi VL \sin \alpha \qquad (57)$$

Combining Eqs. 56 and 57 yields

$$F_\ell = \frac{1}{2} c_L \rho V^2 HL \qquad (58)$$

in which

$$c_L = 2\pi \sin \alpha \qquad (59)$$

Eq. 59 applies only to thin plates. Theoretically, α may attain any possible value; however, experience has shown that α should be less than about 20° in order that Eq. 59 give reasonable estimates of c_L; otherwise flow separation alters the pressure distribution around the foil. For α less than about 20°, wind-tunnel experiments have yielded values of c_L typically of the order of 90% of the values computed by Eq. 59.

The torque about the center of the flow exerted by a vane, T_{vane}, is

$$T_{vane} = F_\ell \left(\frac{d_c}{2} - \frac{H}{2}\right) \qquad (60)$$

in which H = height of the submerged vane. The height H may realistically be chosen to be of the order of one third the water depth; that is, $H = d_c/3$. Hence,

$$T_{vane} = \frac{\pi}{9} \beta\rho \sin\alpha \, L \, \tilde{V}^2 \, d_c^2 \tag{61}$$

in which β = ratio of actual to theoretical value of c_L; and $\tilde{V}$ = the flow velocity averaged over the height of the vane. Averaging the velocity given by Eq. 5 over the lower one third of the depth yields

$$\tilde{V} = 3\left(\frac{1}{3}\right)^{\frac{n+1}{n}} \bar{V} \tag{62}$$

The torque produced by N_v identical submerged vanes, all placed at the same angle of incidence, is then

$$T_{vanes} = \pi\beta\rho \sin\alpha \, d_c^2 \, L \, \left(\frac{1}{3}\right)^{(2n+2)/n} \bar{V}^2 \, N_v \tag{63}$$

In order for the flow-induced torque to be balanced by the torque produced by these submerged vanes, Eq. 63 must equal Eq. 55; that is

$$\frac{n+1}{n(n+2)} \frac{b}{r_c} ds = 2\pi\beta \sin\alpha \, L \, N_v \left(\frac{1}{3}\right)^{(2n+2)/n} \tag{64}$$

Use of typical data from the Sacramento River bend (b = 400 ft, r_c = 2,000 ft, and n = 8), and β = 0.9, reduces Eq. 64 to

$$0.0225 \, ds = 0.477 \, L \, N_v \sin\alpha \tag{65}$$

Thus, if, for example, α = 20°, L = 50 ft, and N_v = 2,

$$ds = 725 \text{ ft}$$

That is, for every 725 ft along the bend, two 50-foot-long vanes, placed at an angle of incidence of 20° to the local channel axis, should be able to counter-balance the torque produced by the flow. Note that this result is independent of the flow velocity.

B. Physical Model Tests

The foregoing theory has been tested in a curved, recirculating sedimentation flume at IIHR, constructed with support from the U.S. Army Corps

of Engineers, Waterways Experiment Station, MI. The layout and cross-section of the flume are shown in Figures 28 and 29. The flume models, with some idealization, the Sacramento River bend at an undistorted scale of approximately 1:48. The flume is constructed from epoxy-coated plywood. Accurately leveled 2 in. by 4 in. plates on top of the sidewalls of the flume support a 4 ft by 8 ft instrument carriage. The plates serve as vertical reference for all elevation measurements. Water enters the flume through a manifold at the upstream end of the flume and leaves the flume at the downstream end through an adjustable drop gate.

An approximately 9-in. thick layer of quartz sand was placed in the flume. The mean diameter and geometric standard deviation of the sand were 0.30 mm and 1.45, respectively. Water from an underground sump was then propelled through the flume at a given flow rate until the flow condition became steady. Once a steady-state condition was obtained water-surface elevations, and distributions of velocity and depth were measured. Velocities were measured with a miniature propeller-current meter, and depths with a sonic depth sounder. Both current meter and sounder were computer controlled (Figures 30 and 31) and were interfaced directly with the Institute's HP 1000 Data Acquisition and Control System to permit online processing of data.

C. Results of Physical Model Tests

Numerical values presented in the following are prototype values. The model-prototype scale ratios used are (Froude scaling):

Length: 1:48
Velocity: 1:6.9
Time: 1:6.9
Discharge: 1:15,963

Figure 32 shows the steady-state bed topography measured in the model at a discharge (prototype) of 87,000 cfs, before turning vanes were installed. The numbers by the depth contours are depths in feet. The numbers along the inside of the flume are transverse bed slopes and section numbers (model distances, in ft, from the manifold, measured along the right flume wall). Two of the most conspicuous features of the bed topography are the point bar

along the inner bank between Sections 72 and 92; and the relatively deep scour hole along the outer (concave) bank between Sections 72 and 100. The maximum depth measured was 41 ft (at Section 88). The same features were observed in the Sacramento River bend between Sections 6 and 3. As will be seen in Figure 33, which shows the variations along the Sacramento River study bend of water level (WL), cross-sectional average of bed level (BL), and level of deepest points (SL) measured in the 1980 survey, a severe scour hole occurred between Sections 6 and 3 with the maximum depth increasing from 17.4 ft at Section 6 to 40.0 ft at Section 5 and 34.5 ft at Section 4. At Section 3 the maximum depth was 16.5 ft. The maximum transverse bed slope measured in the model is seen in Figure 32 to have been 0.14 (over the point bar at Section 84). The same slope was observed in the Sacramento River bend at Section 5. Downstream from the point bar a very significant decrease of the transverse bed slope occurred. At mid-bend (section 112) the transverse bed slope was reduced to 0.02. This feature agrees with that observed in the Sacramento River bend between Sections 4 and 3. Downstream from Section 136 in the model the transverse bed slope increased again to reach a value of 0.08 at Sections 144 through 152. In the prototype, a similar increase was not observed. This may have been due to the heavy armoring of the prototype river bed between Sections 3 and 1, combined with the increase of radius of curvature. Figure 34 shows Sections 64, 80, 88, 96, 112, and 144 in the model before vanes were installed. The n-values were determined from the slope of the best fitting line through log-log plots of $V/\overline{V}$ versus y/d. The average value of n for the entire model bend was 4.3. Substituting n = 4.3 and $r_c/b = 43/8$ into Eq. 64 yields

$$ds = 7.3\ N_v\ L \sin \alpha \qquad (66)$$

Vanes were then installed in two arays in the outer half of the bend-cross section, as shown in Figure 35. Each vane was 56 ft long and was placed at an angle of incidence of 15°. At discharge 87,000 cfs the top of the vanes was at a depth of 2/3 the water depth, initially. The spacing between the vanes, ds (for $N_v = 2$), was determined, by Eq. 66, to be 212 ft. The total number of vanes used was 52. After a period of 1500 prototype hours with a discharge of 87,000 cfs the cross sections were measured to be as shown in Figure 36.

By comparing the cross sections before (Figure 34) and after the vanes were installed (Figure 36) it is obvious that the vanes had a very significant restoring effect on the bed topography. The point bar disappeared and so did the scour hole. The transverse bed slope was reduced to less than 0.03. At sections 80, 88, and 96, where the scour hole occurred before the vanes were installed, the vanes reduced the near-bank depth and velocity by approximately 25%. The effect of the vanes is even more impressive when it is considered that the ratio of near-bank to centerline velocity undoubtedly was significantly higher in the model than they would have been in the prototype. This is due to the smoothness of the flume wall. Before vanes were installed, a significant percentage of the wetted perimeter was flume wall (as will be seen in Figure 34) with a much lesser friction than that of the sand bed. Had the roughness of the flume wall been comparable to that of the sand bed the initial transverse velocity gradient would have been smaller, and fewer vanes might have accomplished the same bed changes.

Very little scouring occurred around the vanes. Immediately after the installation of the vanes some scouring was observed at the upstream end of each vane. However, as the outer part of the sections filled up, as a result of the vanes, this scouring diminished. After a certain period of time the scouring was negligible.

Tests also were conducted with a smaller number of vanes (ranging from 9 to 52). It appeared that it made little difference with respect to velocity distributions whether the total number of vanes was 36 or 52, or somewhere between, as long as there were two vanes per 212 ft length (approximately) in the beginning of the bend and at least one vane per 212 ft length in the remaining part of the bend. However, the transverse bed slope increased slightly as the number of vanes was reduced toward 36. Figure 37 shows the steady-state cross sections with two rows of vanes in the first part of the bend up to Section 96 (in the configuration shown in Figure 35) and one outer row beyond Section 96, giving a total of 36 vanes. It is seen that the reduction in near-bank velocity is about the same as in the case of 52 anes, whereas the reduction in near-bank depth is slightly less.

The angle of incidence, α , also was varied. For values of α larger than 20°, flow separation occurred around 30%, or more, of the vanes causing a small, permanent, scour hole at these vanes. As the angle was reduced, the

number of "scouring" vanes was reduced. The optimum angle, at which no significant scour occurred, was found to be between 15° and 18°.

The overall effect of the vane system on the river flow was judged to be minor. As will be seen in Figure 38, a minor, although hardly significant, change of the longitudinal slope of the water surface occurred when 52 vanes were installed in the bend. The change was less in the case of 36 vanes. The changes in water depth also were judged to be minor, and possibly insignificant. As will be seen in Table 3 the measurements did not disclose any trends as to overall changes of neither depth nor velocity of bend flow as a result of the vane systems tested.

D. Numerical Example 2

Design a vane system for the bend in Example 1, assuming that the maximum flow is Q = 40,000 cfs during the time from the installation of the vanes to full recovery of the bed topography.

The present study did not include optimization of the vane-system parameters. Therefore, the configuration sketched in Figure 34 with L = 50 ft and N_V = 2 will be adopted. This configuration was found in the model study to be reasonable. The value of n to be used in Eq. 64 should be the value based on local flow characteristics rather than overall characteristics. The analysis of the Sacramento River bend data showed that the local value of n was of the order of 8 (whereas the overall-value was of the order of 3). Substituting the values

$b = 500$ ft
$r_c = 2{,}000$ ft
$\alpha = 15°$
$\beta = 0.9$
$L = 50$ ft
$n = 8$

into Eq. 64 yields

$$ds = 439 \text{ ft}$$

That is, for every 439 ft along the bend, two 50-foot-long vanes, placed at an angle of incidence of 15° to the local channel axis, should be able to restore the bed profile. Installing the outer row of vanes at a distance of 100 ft from the outer bank requires the height H of these vanes (above the mudline) to be

$$H_{outer} \approx \frac{36}{3} = 12 \text{ ft}$$

The maximum depth-averaged velocity at these outer vanes is estimated (by Eq. 50) to be

$$\overline{V} = (3.8)\left(\frac{36}{21}\right)^{7/18}\left(\frac{2,000}{2,150}\right)^{1/4} = 4.6 \text{ fps}$$

The maximum average velocity over the height of the vanes is estimated by Eq. 62:

$$\tilde{V} = (3)\left(\frac{1}{3}\right)^{9/8}(4.6) = 4.0 \text{ fps}$$

The total "lift" force on each vane is then calculated, by Eq. 58, to be

$$F_\ell = \left(\frac{1}{2}\right)(2\pi)(\sin 15^0)(1.94)(4.0)^2(12)(50) = 15,140 \text{ lbf}$$

Installing the inner row of vanes at a distance of 200 ft from the outer bank requires the height of these vanes to be

$$H_{inner} = \frac{26}{3} = 8.7 \text{ ft}$$

Using the same formulas as were used for the outer vanes, the total "lift" force on each of the inner vanes is estimated at

$$F_\ell = 8,900 \text{ lbf}$$

IV. CONCLUSIONS AND RECOMMENDATIONS

The study has: (1) reviewed existing models for the prediction of the steady-state transverse bed profile in channel bends; (2) formulated and validated alternative models; (3) compared the models, analytically and by laboratory and field data; (4) formulated and validated models for the prediction of the steady-state transverse distributions of mean velocity and grain size; and (5) evaluated, theoretically and experimentally, the effectiveness of vertical, submerged vanes as a means of bank protection.

Eq. 50 has been found to give a reasonably accurate relationship between near-bank velocity (depth-averaged), centerline velocity, near-bank depth, centerline depth, and the corresponding radii of curvature. For a conservative estimate of the near-bank velocity, Eq. 51 is recommended. The near-bank depth may be estimated by Eq. 37 with K being determined by Eq. 26 or 31. Based on the data from the Sacramento River study bend, K must be multiplied by a factor of 2.43 if Eq. 26 is used; and by a factor of 2.7 if Eq. 31 is used. The key parameter in all the model is grain size. In the field surveys in the Sacramento River bend the mean-grain size was found to vary significantly throughout the bend. No technique or model is yet available that can simulate or predict these variations in a given bend, given the flow data. The grain-size variation observed in the field surveys conforms approximately to Eq. 35. This equation may apply only to the Sacramento River data. Due to the importance of the grain size for the velocity and depth predictions, it is recommended that future research be focussed on this parameter and, in general, on the bed processes of grain sorting and armoring.

The field data from the Sacramento River study bend clearly show that the near-bank velocity, and therefore also the intensity of the bank attack and erosion, vary widely around the channel. For example, in the 1980 survey the depth-averaged velocity at the outer bank at Section 5 was measured to be more than 100% higher than that at Section 3, 2800 feet downstream from Section 5. Therefore, it is probably not efficient to use the same bank-protection design around a whole curve. Instead, it should be made deeper and heavier at some points (notably opposite the point bar) and tapered down to smaller depth and thickness along other reaches. The analytical models developed in this

study can provide a guide to the depth of bed erosion and depth-averaged velocity near the outer banks, given the discharge, cross-sectional area, surface width, radius of curvature, and grain size. The models cannot predict the formation of point bars.

A physical model study is still the most reliable means of obtaining information about the behavior of flow and sediment transport in a river bend. A physical model has been built which models, with some idealization, the Sacramento River study bend at an undistorted scale of approximately 1:48. The model reproduces the main features (point bar, scour hole, transverse bed slope) very satisfactorily. No mathematical model is available that can reproduce these features to an equally high degree of accuracy. Therefore, it is believed that the best guide for the placement of bank protection is a physical model study of the bend in question.

The effectiveness of vertical, submerged vanes as a means of bank protection has been evaluated theoretically and in the physical model mentioned. The studies showed that submerged vanes, placed at a certain angle of incidence in the outer half of the river-bend cross-section have a very significant, restoring effect on the bed topography with a very significant reduction of the near-bank velocities as a result. The results indicate that such vanes offer an effective (and environmentally preferable) alternative to the present bank protection measures. The vanes do not increase the local channel roughness as do other presently used means for reduction of the near-bank velocity (for example, submerged dikes); the vanes are invisible, and they would be far enough below the surface of the water that snags would be prevented from hanging on to them; and they would appear to be more economical than traditional means of bank protection, especially bank armoring. Navigation would not be affected as the vanes would be placed along the outer bank of the river and the thalweg would move to the central portion of the cross section. If either height or total number (or both) becomes a practical problem, lower and (or) fewer vanes might be combined with minimal slope protection on the banks, such as dressing back the banks, rocking the toe, and planting of vegatation.

It is recommended that the vane alternative be given an early prototype test after further investigation in a model of the specified bend in which the vanes are to be placed. The model tests would be performed to optimize the vane configuration. Important variables to analyze would be the number, spacing, and length of the vanes and their angle of incidence.

REFERENCES

1. Allen, J.R.L., "A Quantitative Model of Grain Size and Sedimentary Structures in Lateral Deposits", Journal of Geology, Vol. 7, 1970, pp. 129-146.

2. Anderson, A.G., Paintal, A.S., and Davenport, J.T., "Tentative Design Procedures for Riprap-Lined Channels", National Cooperative Highway Research Program, Report 108, Highway Research Board, National Research Council, 1970.

3. Bhowmik, N.G., "Hydraulics of Flow in the Kaskaskia River, Illinois", Illinois State Water Survey, Urbana, Report of Investigation 91, 1979.

4. Bluck, B.J., "Sedimentation in the Meandering River Endrick", Scottish Journal of Geology, Vol. 7, Part 2, 1971.

5. Brice, J., "Lateral Migration of the Middle Sacramento River, California", U.S. Geological Survey, Water-Resources Investigations 77-43, United States Department of the Interior, July 1977.

6. Bridge, J.S. and Jarvis, J., "Flow and Sedimentary Processes in the Meandering River South Esk, Glen Cova, Scotland", Earth Surface Processes, Vol. I, 1976, pp. 303-336.

7. Daugherty, R.L., and Franzini, J.B., Fluid Mechanics with Engineering Applications, 7th ed., McGraw-Hill Book Co., 1977.

8. Einstein, H.A., and Barbarossa, N.L., "River Channel Roughness", Transactions, ASCE, Vol. 117, pp. 1121-1132, 1952.

9. El-Khudairy, M., "Stable Bed Profiles in Continuous Bends", Thesis presented to the University of California, at Berkeley, California, in 1970, in partial fulfillment of the requirements for the degree of Doctor of Philosophy.

10. Engelund, F., "Flow and Bed Topography in Channel Bends", Journal of the Hydraulics Division], ASCE, Vol. 100, No. HY11, Proc. Paper 10963, November 1974, pp. 1631-1648.

11. Engelund, F., "Experiments in Curved Alluvial Channel", Progress Report No. 34, Institute of Hydrodynamics and Hydraulic Engineering, The Technical University of Denmark, 1974.

12. Engelund, F., "Experiments in Curved Alluvial Channel (Part 2)", Progress Report No. 38, Institute of Hydraulic Engineering, The Technical University of Denmark, April 1976.

13. Engelund, F., and Fredsøe, J., "A Sediment Transport Model for Straight Alluvial Channels", Nordic Hydrology, Vol. 7, 1976.

14. Falcon, M.A., "Analysis of Flow in Alluvial Channel Bends", Thesis presented to The University of Iowa, Iowa City, Iowa, in 1979, in partial fulfillment of the requirements for the degree of Doctor of Philosophy.

15. Falcon, M.A. and Kennedy, J.F., "Flow in Alluvial-River Curves" to be submitted to Journal of Fluid Mechanics, February 1982.

16. Gottlieb, L., "Three-Dimensional Flow Pattern and Bed Topography in Meandering Channels", Series Paper 11, Institute of Hydrodynamics and Hydraulic Engineering, Technical University of Denmark, February 1976.

17. Graf, W.H., Hydraulics of Sediment Transport, McGraw-Hill Book Co., New York, 1971.

18. Henderson, F.M., Open Channel Flow, MacMillan Publishing Co., Inc., New York, 1966.

19. Ideda, S., "On Secondary Flow and Dynamic Equilibrium of Transverse Bed Profile in Alluvial Curved Open Channel", Proceedings of the Japanese Society of Civil Engineers, No. 229, 1974, pp. 55-65.

20. Karim, M.F., "Computer Based Sediment Discharge and Friction Factor Relationships for Alluvial Streams", Thesis presented to The University of Iowa in 1981, in partial fulfillment of the requirements for the degree of Doctor of Philosophy.

21. Kikkawa, H., Ikeda, S., and Kitagawa, A., "Flow and Bed Topography in Curved Open Channels", Journal of the Hydraulics Division, ASCE, Vol. 102, No. HY9, proc. Paper 12416, September 1976, pp. 1327-1342.

22. Luque, R.F., "Erosion and Transport of Bed-Load Sediment", Ph.D. Thesis, Krips Repro B.V.-Meppel, The Netherlands, 1974.

23. NEDECO "River Studies and Recommendations on Improvement of Niger and Benue", Netherlands Engineering Consultants, Amsterdam, 1959.

24. Odgaard, A.J., "Transverse Bed Slope in Alluvial Channel Bends", Journal of the Hydraulics Division, Proceedings ASCE, Vol. 107, No. HY12, December 1981.

25. Rakoczi, L., "Influence of Grain-Size Composition on the Incipient Motion and Self-Pavement of Bed Materials", Proceedings of the 16th Congress of the International Association for Hydraulic Research, Sao Paulo, Brazil, Vol. 2, July 1975, pp. 150-157.

26. Rouse, H., "An Analysis of Sediment Transportation in the Light of Fluid Turbulence", Soil Conservation Service Report No. SCS-TP-25, United States Department of Agriculture, Washington, D.C. 1939.

27. Rozovskii, L.L., "Flow of Water in Bends of Open Channels", Israel Program for Scientific Translations, Jerusalem, Israel, 1961 (available from Office of Technical Services, U.S. Department of Commerce, Washington, D.C., PST Catalog No. 363; OTS 60-51133).

28. Shields, A., "Anvendung der Aenlichkeitsmechanik und der Turbulenzforschung auf die Geshiebebewegung", M,itteilungen der Preussischen Versuchsanstalt fur Wasserbau und Schiffbau, Berlin, Germany, Translated to English by W.P. Ott and J.C. van Uchelen, California Institute of Technology, Pasadena, California, 1936.

29. Simons, D.B., and Senturk, F., "Sediment Transport Technology", Water Resources Publications, Fort Collins, Colorado, USA, 1977.

30. Sundborg, A., "The River Klaraluen, A Study of Fluvial Processes", Bulletin No. 52, Inst. of Hydraulics, Roy. Inst. nof Tech., Stockholm, Sweden, 1956.

31. van Bendegom, L., "Eenige Beschouwingen over Riviermorphologie en rivierverbetering", De Ingenieur, Vol. 59, No. 4, 1947, pp. 1-11.

32. Vanoni, V.A., ed., Sedimentation Engineering, Manual and Report on Engineering Practice No. 54, ASCE, 1976.

33. White, C.M., "The Equilibrium of Grains on the Bed of a Stream", Proceedings Royal Society of London, Series A, No. 958, Vol. 1974, Feb., 1940, pp. 322-338.

34. Yen, C.L., "Bed Configurations and Characteristics of Subcritical Flow in a Meandering Channel", thesis presented to The University of Iowa, Iowa City, Iowa, in 1967, in partial fulfillment of the requirements for the degree of Doctor of Philosophy.

35. Zimmermann, C., and Kennedy, J.F., "Transverse Bed Slopes in Curved Alluvial Streams", Journal of the Hydraulics Division, ASCE, Vol. 104, No. HY1, January, 1978, pp. 33-48.

TABLE 1

Summary of Key Relations in Bed-Topography Models Reviewed

Author or Authors (1)	Bed-Friction Parameter (2)	Ratio of Local Bed Slope to Depth/Radius Ratio, K (3)
van Bendegom (1947)	$C = 50m^{1/2}/s$	$0.0585\ F_D^2$
Engelund (1974)	$\mu = \tan \Phi$	7μ
Kikkawa, Ikeda, Kitagawa (1976)	$M = \lambda(2.75\text{-}4.35\ V_*/\overline{V})f_v^2$	MF_D
Zimmermann, Kennedy (1978)	$N = (n+1)/[n(n+2)]$	$(\alpha/2)\ NF_D^2$
Falcon (1979)	$N = (n+1)/[n(n+2)]$	$(3\alpha/2)\ NF_D^2$

C = Chezy's coefficient
Φ = dynamic friction angle
f_V = forced vortex distribution
λ = sheltering factor (= 0.592)
$V*$ = $\sqrt{\tau_0/\rho}$
α = ratio of projected surface area to volume for a sediment particle divided by that for a sphere ($\simeq$ 1.27)

Table 2 - Sacramento River Bend Flow Data

Section No.	Flow rate, in cubic feet per second	Cross-sectional area, in square feet	Cross-sectional average velocity, V_a, in feet per second
(1)	(2)	(3)	(4)
1-L	7,800	1,900	4.11
2-L	8,300	3,190	2.60
2-H	24,900	6,510	3.82
3-L	9,900	4,340	2.28
3-H	28,400	7,580	3.75
4-L	9,100	4,290	2.12
4-H	24,900	6,370	3.91
5-L	9,100	4,000	2.28
5-H	24,000	7,600	3.15
6-H	26,800	6,700	4.00

Table 2 (Cont.) - Sacramento River Bend Flow Data

Section No.	Cross-sectional average depth, d_a, in feet	Mean particle diameter, D_{50}, in millimeters	Particle Froude number, F_D, based on D_{50}
(1)	(5)	(6)	(7)
1-L	4.4	21.5	2.12
2-L	5.6	4.9	2.81
2-H	11.1	10.8	2.78
3-L	8.1	6.3	2.17
3-H	12.5	-	-
4-L	12.2	1.6	4.00
4-H	23.1	6.1	3.78
5-L	15.2	0.7	6.51
5-H	19.7	-	-
6-H	8.6	6.1	3.87

Table 2 (Cont.) - Sacramento River Bend Flow Data

Section No.	Radius of curvature, r_c, in feet	Transverse bed slope, S_T	Cross-sectional average velocity profile exponents $n_{*)}$	n_{**}
(1)	(8)	(9)	(10)	(11)
1-L	∞	0.000	7.0	5.8
2-L	3,920	0.010	4.0	6.3
2-H	3,920	0.018	4.1	6.2
3-L	2,640	0.020	2.9	6.4
3-H	2,640	0.018	3.8	5.8
4-L	1,800	0.073	2.2	9.6
4-H	1,800	0.135	2.9	9.4
5-L	1,800	0.150	2.3	10.5
5-H	1,800	0.145	2.6	12.5
6-H	2,000	0.041	4.9	8.9

*) calculated from the longitudinal slope of the water surface

**) cross-sectional average of values calculated from individual velocity profiles

Table 3. Cross-Sectional Average Values of Depth and Velocity in the Cases of 0, 36, and 52 Vanes.

Section No.	Total Number of Vanes	Cross-Sectional Average Value of Depth (ft)	Velocity (fps)*
64	0	23.2	9.8
	36	24.1	9.4
	52	23.6	9.6
80	0	21.3	10.6
	36	21.8	10.4
	52	23.9	9.5
88	0	22.9	9.9
	36	24.2	9.4
	52	21.4	10.6
96	0	25.1	9.0
	36	22.1	10.3
	52	22.3	10.2
112	0	22.4	10.1
	36	21.9	10.3
	52	23.6	9.6
144	0	21.3	10.6
	36	22.5	10.1
	52	23.4	9.7

*Determined as the discharge per unit width divided by the cross-sectional average value of depth.

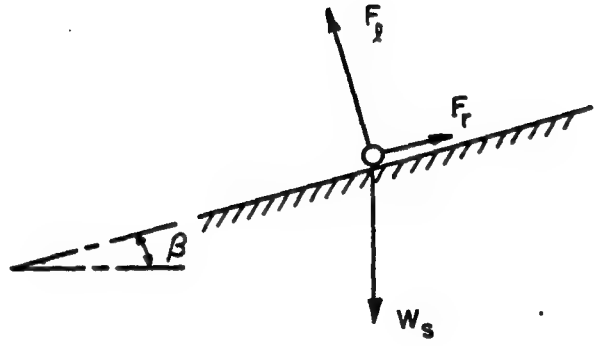

Fig. 1 - Radial-Plane Components of Forces on a Sediment Particle

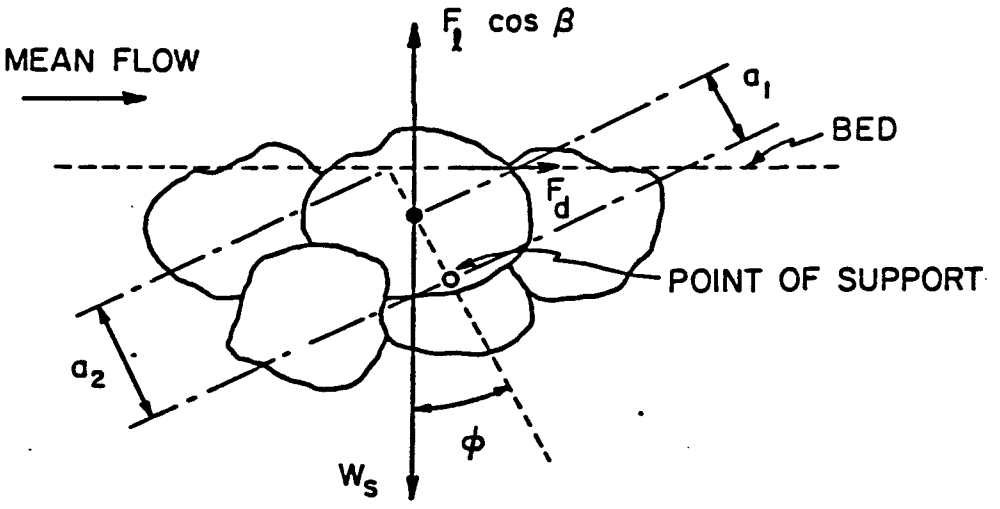

Figure 2 - Vertical Longitudinal-Plane Components of Forces on a Sediment Particle.

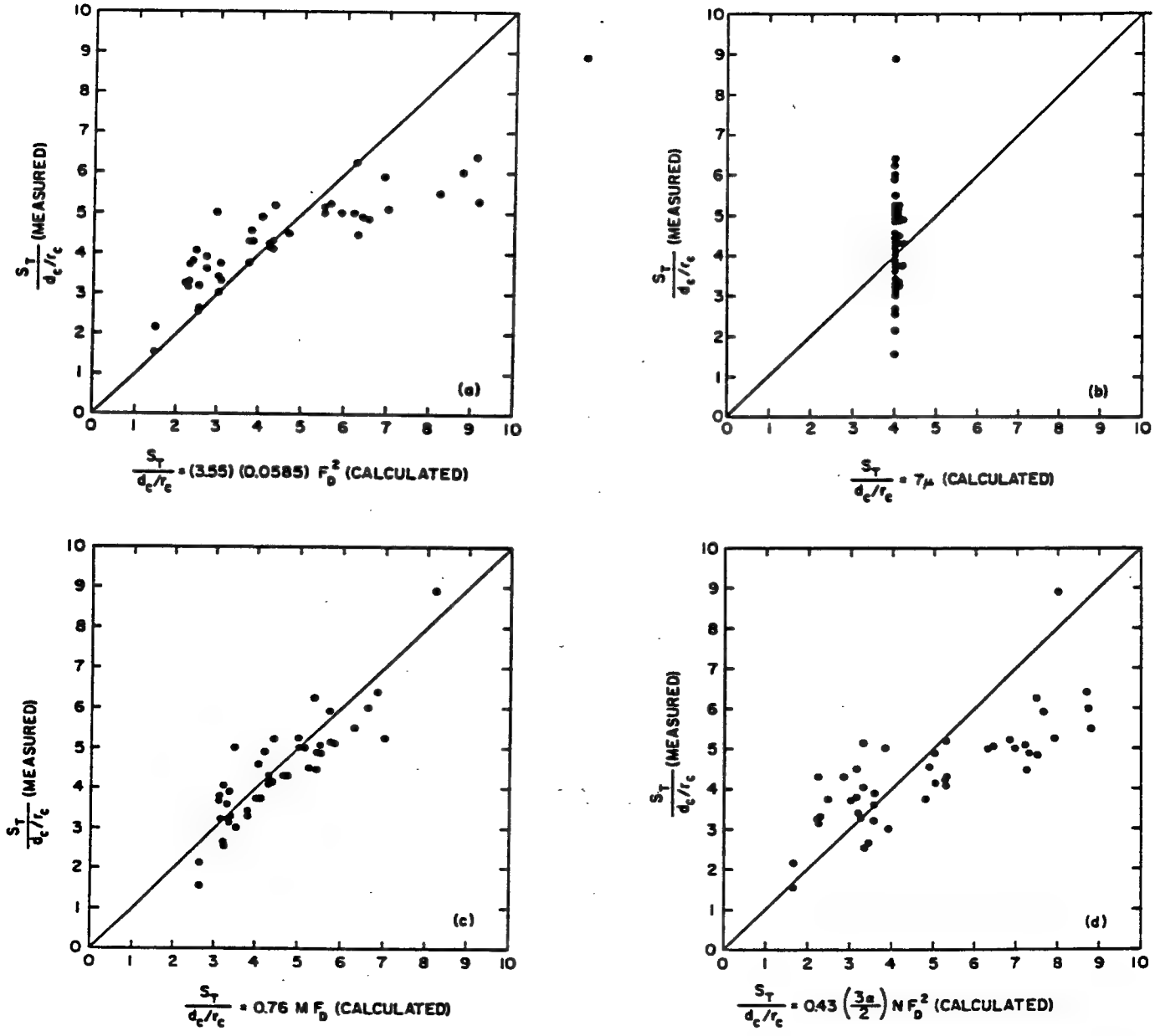

Figure 3 - Comparison of Transverse Bed Slopes Measured by Zimmermann and Kennedy (1978) with Slopes Computed by the Models of (a) van Bendegom (1947); (b) Engelund (1974); (c) Kikkawa, Ikeda, and Kitagawa (1976); (d) Zimmermann and Kennedy (1978) or Falcon (1979); and (e) Odgaard (1981)

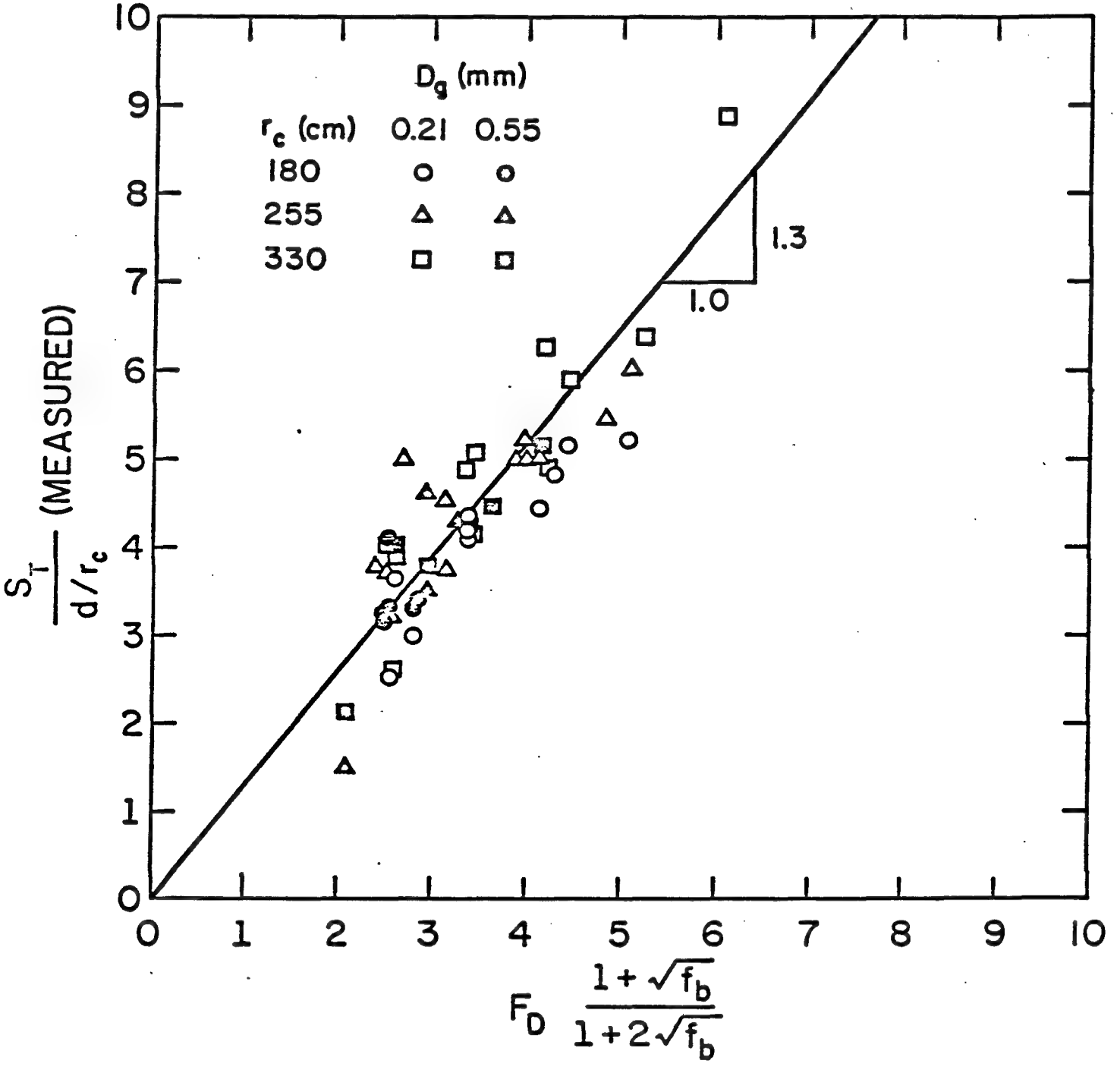

Figure 3(f) - Comparison of Transverse Bed Slopes Measured by Zimmermann and Kennedy (1978) with Slopes Computed by Falcon and Kennedy's (1982) Model

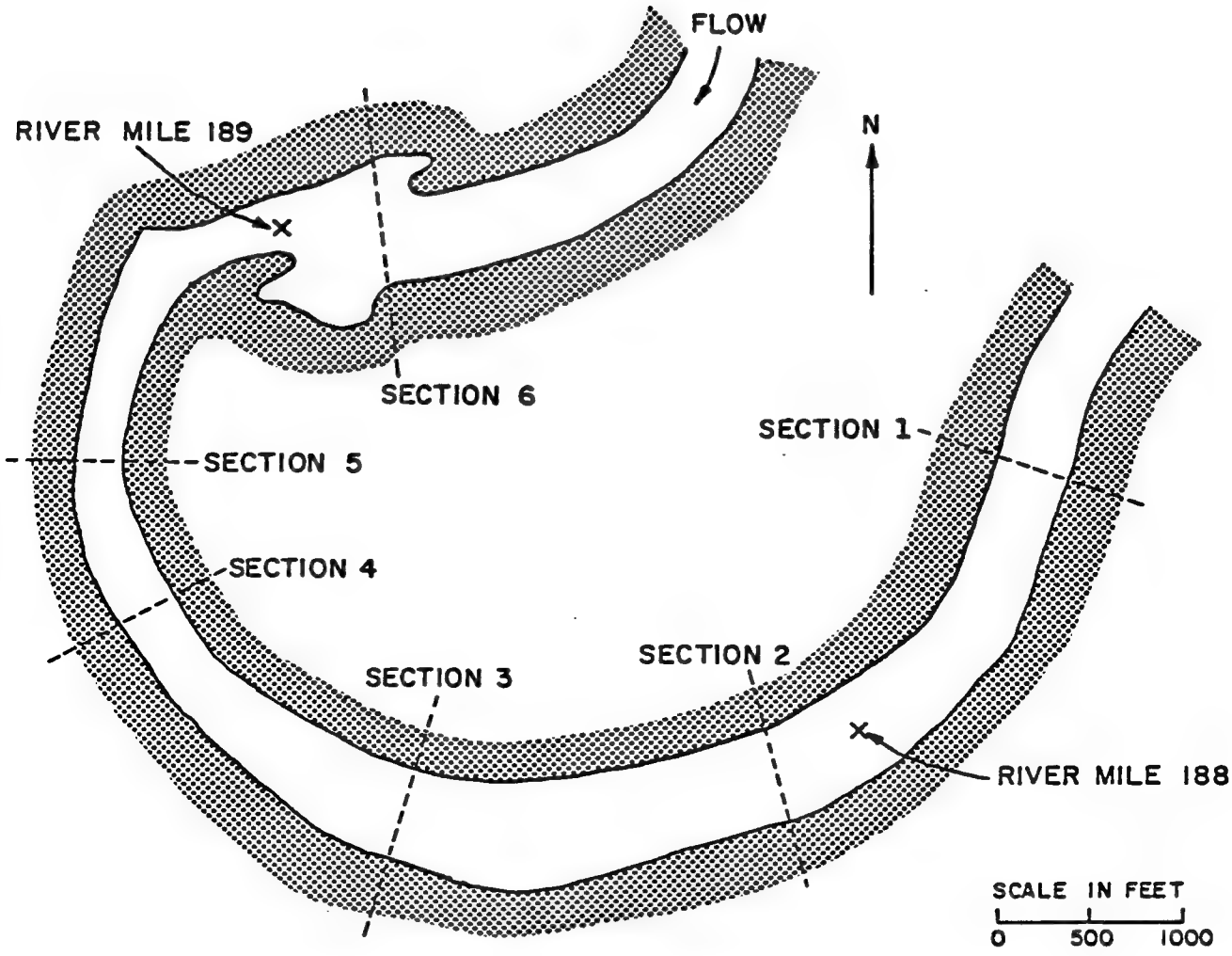

Figure 4 - Schematic Plan View of Sacramento River Study Bend

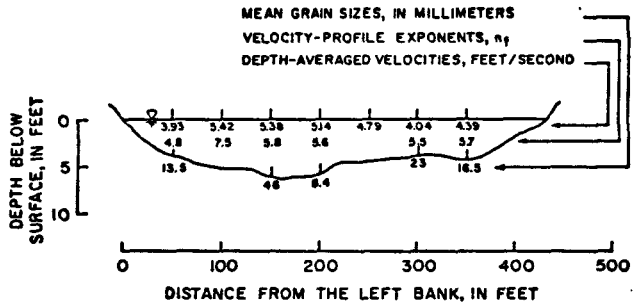

Figure 5 - Cross Section No. 1 at Low Flow, 7,800 Cubic Feet Per Second

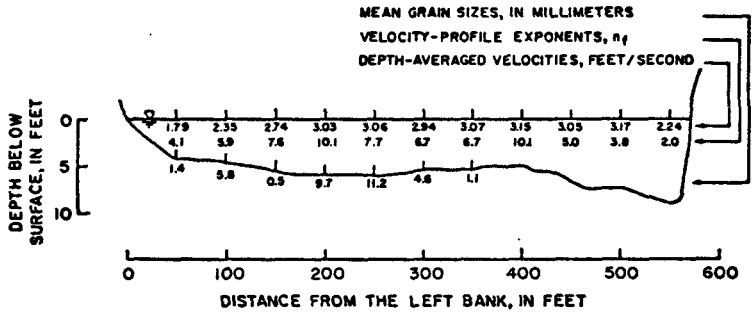

Figure 6 - Cross Section No. 2 at Low Flow, 8,300 Cubic Feet Per Second

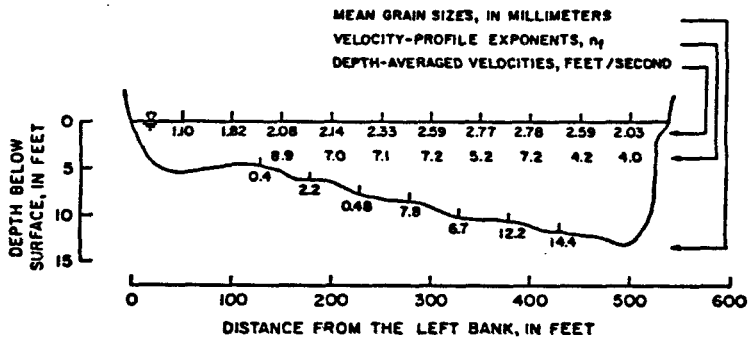

Figure 7 - Cross Section No. 3 at Low Flow, 9,900 Cubic Feet Per Second

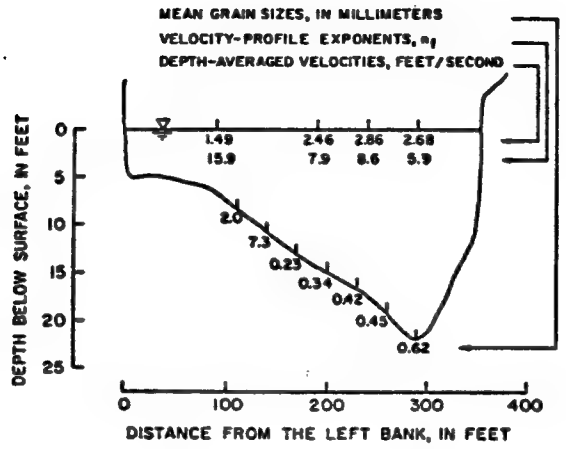

Figure 8 - Cross Section No. 4 at Low Flow, 9,100 Cubic Feet Per Second

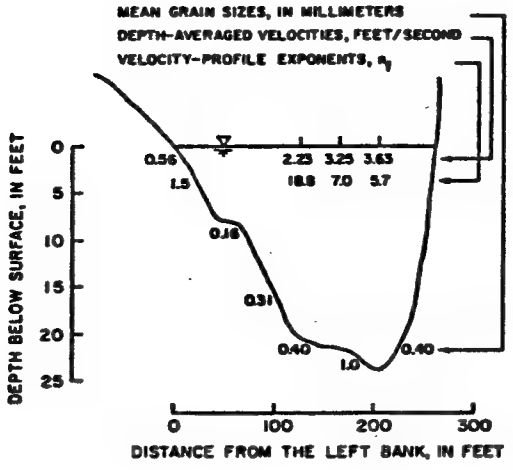

Figure 9 - Cross Section No. 5 at Low Flow, 9,100 Cubic Feet Per Second

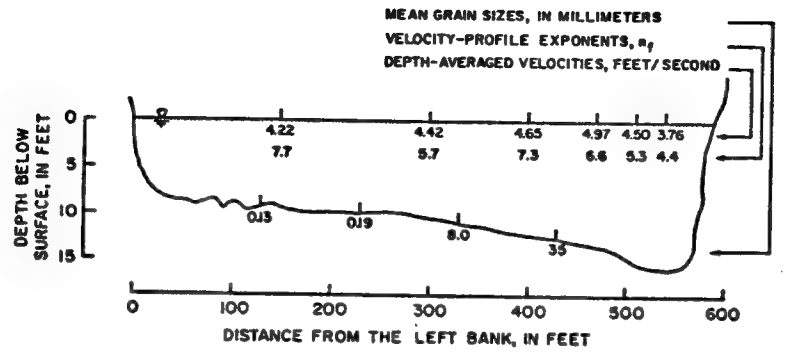

Figure 10 - Cross Section No. 2 at High Flow, 24,900 Cubic Feet Per Second

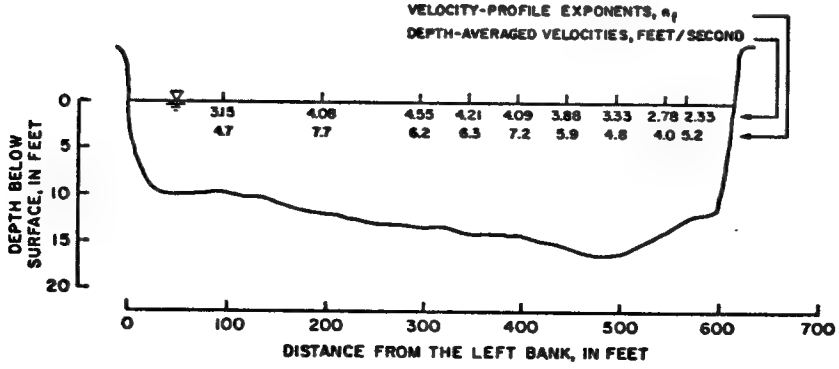

Figure 11 - Cross Section No. 3 at High Flow, 28,400 Cubic Feet Per Second

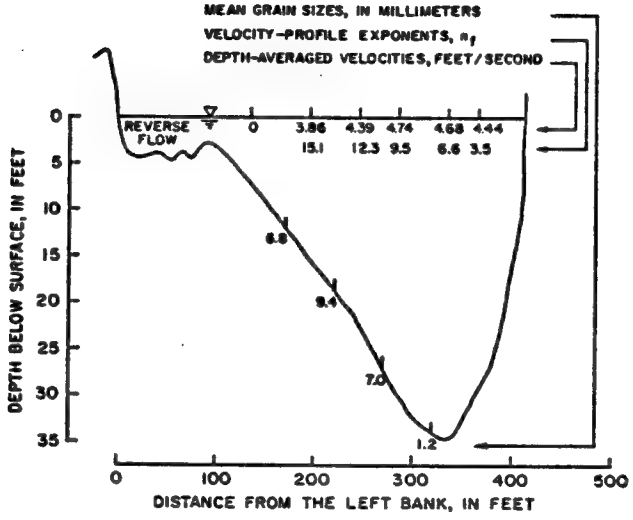

Figure 12 - Cross Section No. 4 at High Flow, 24,900 Cubic Feet Per Second

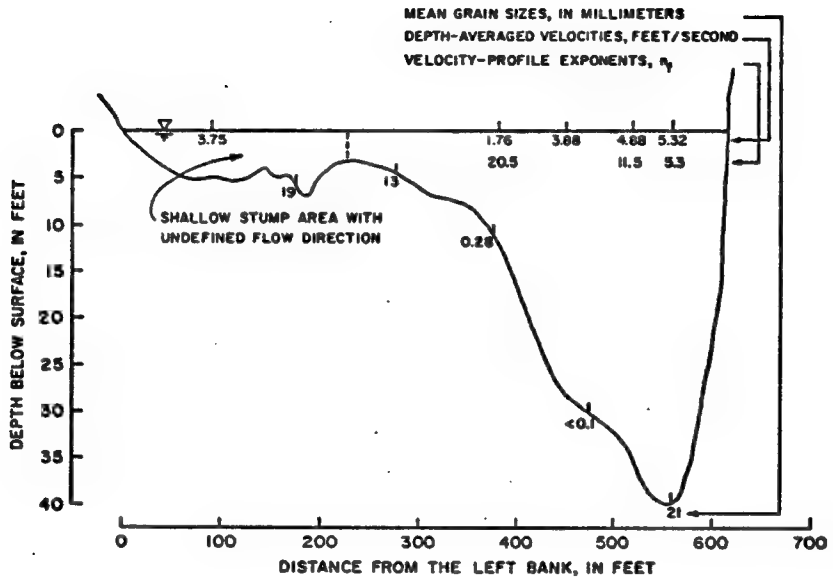

Figure 13 - Cross Section No. 5 at High Flow, 24,000 Cubic Feet Per Second

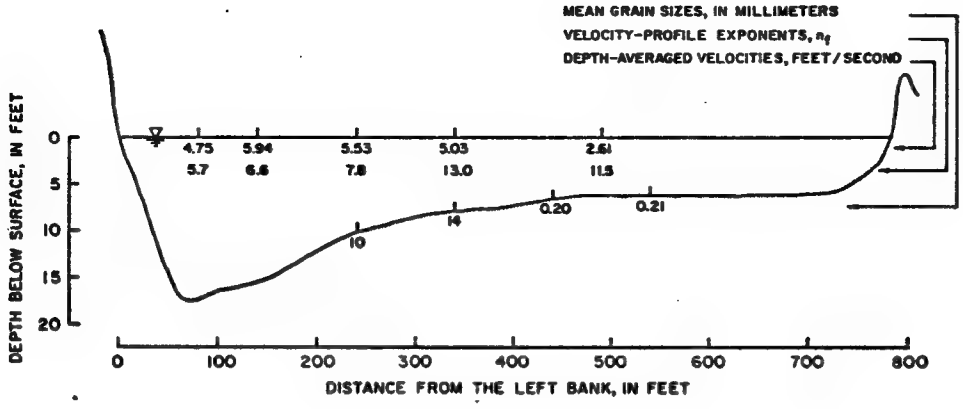

Figure 14 - Cross Section No. 6 at High Flow, 26,800 Cubic Feet Per Second

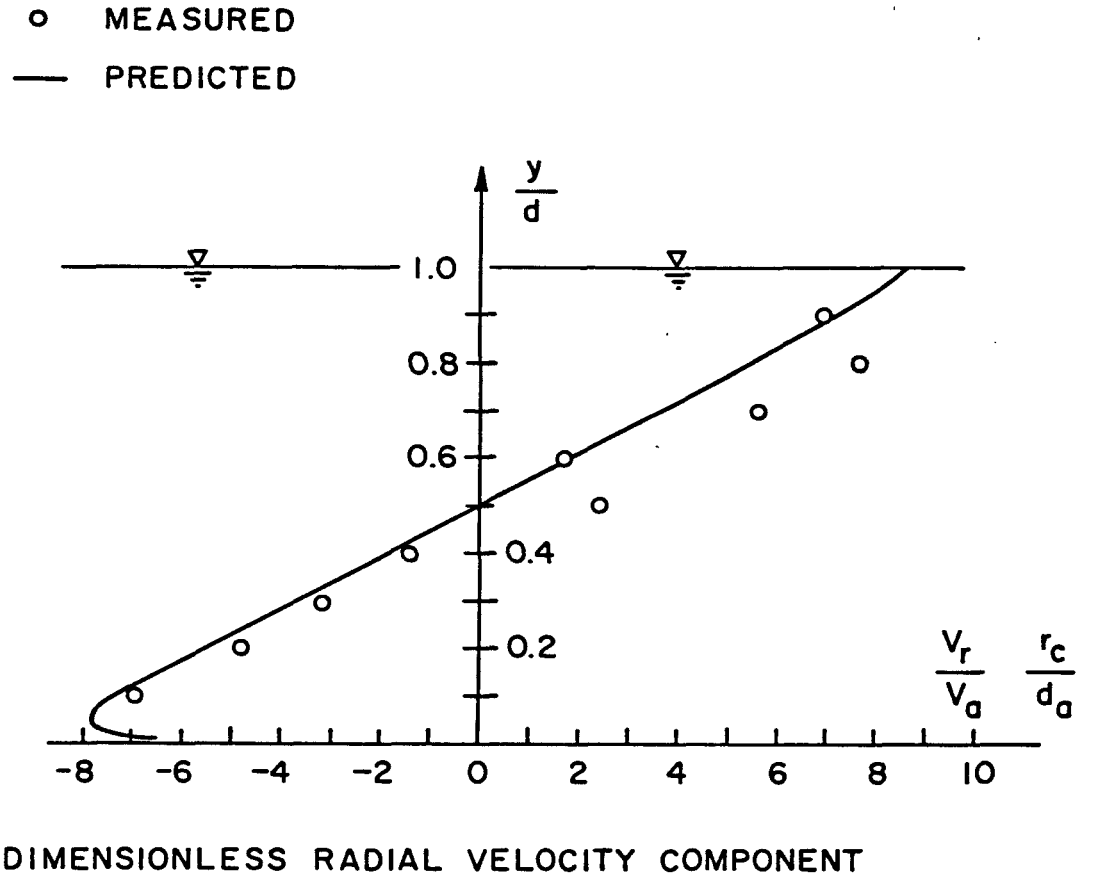

Figure 15 - Measured and Computed Radial Velocity Distribution

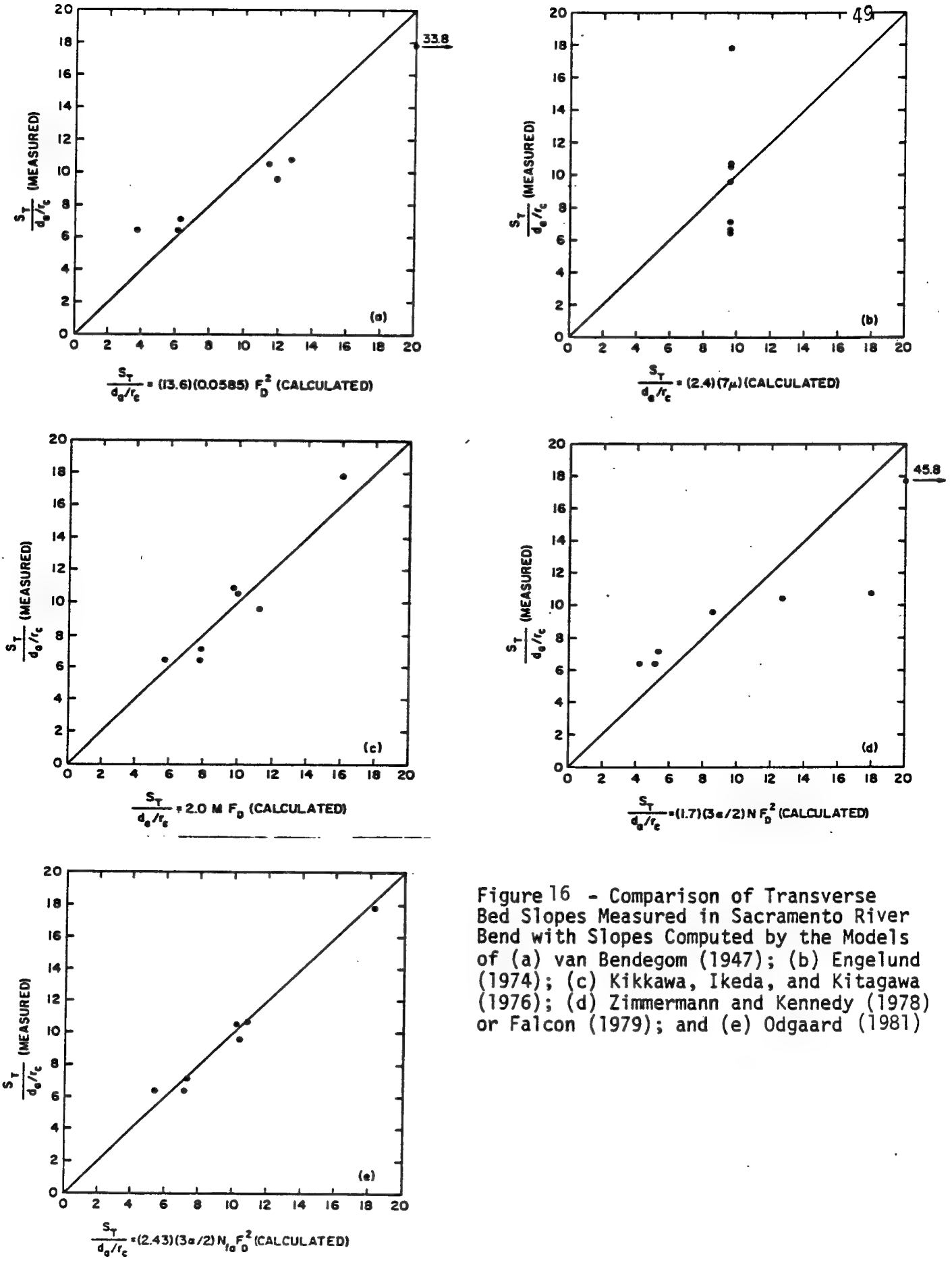

Figure 16 - Comparison of Transverse Bed Slopes Measured in Sacramento River Bend with Slopes Computed by the Models of (a) van Bendegom (1947); (b) Engelund (1974); (c) Kikkawa, Ikeda, and Kitagawa (1976); (d) Zimmermann and Kennedy (1978) or Falcon (1979); and (e) Odgaard (1981)

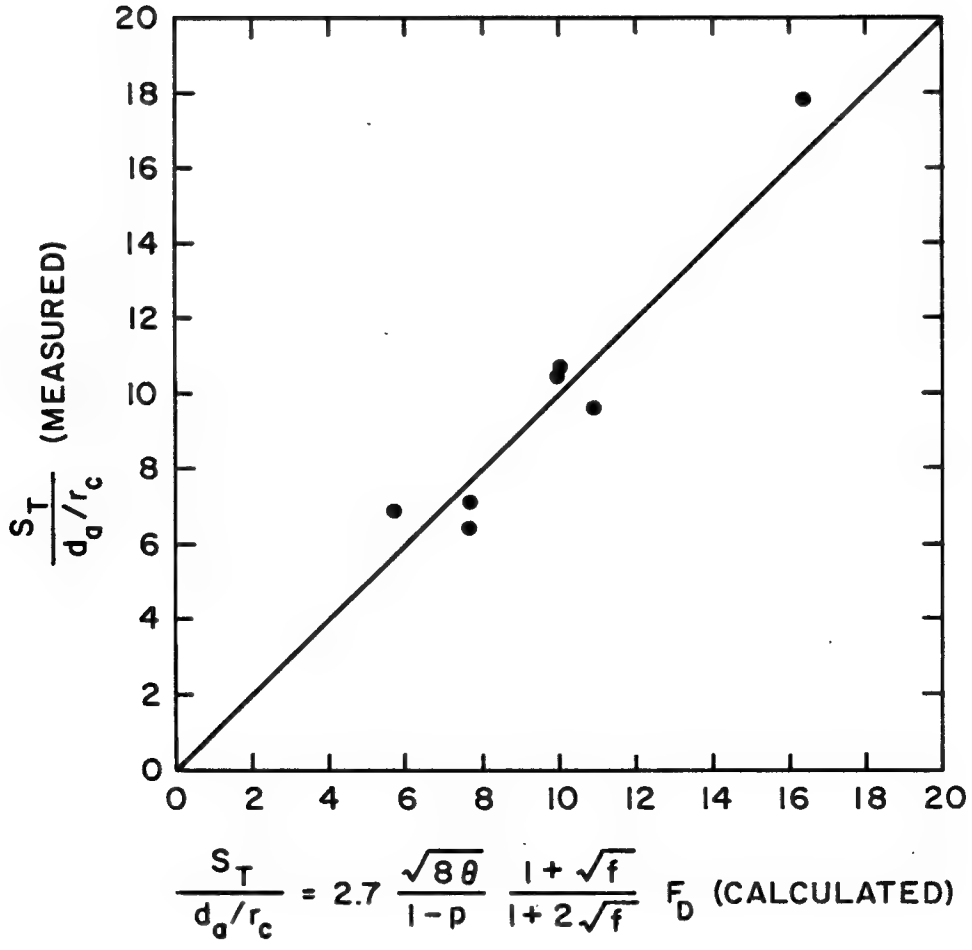

Figure 16(f) - Comparison of Transverse Bed Slopes Measured in the Sacramento River Study Bend with Slopes Computed by Falcon and Kennedy's (1982) Model

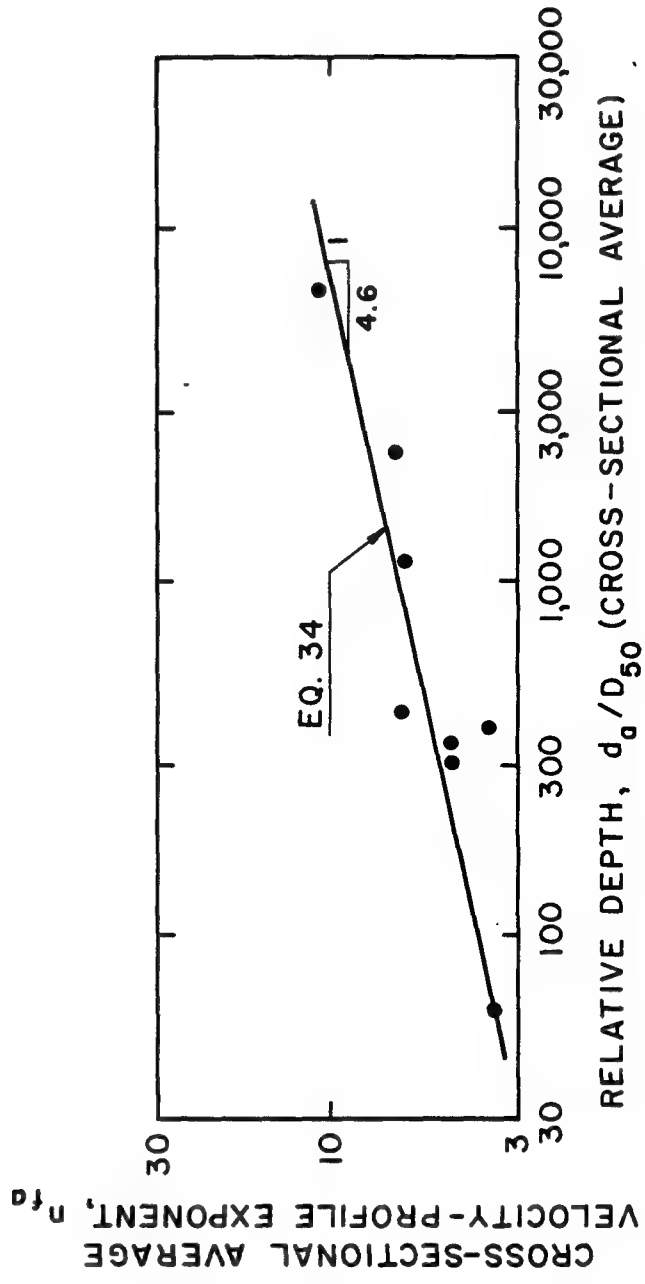

Figure 17 - Velocity-Profile Exponent n_{fa} as a Function of Relative Depth

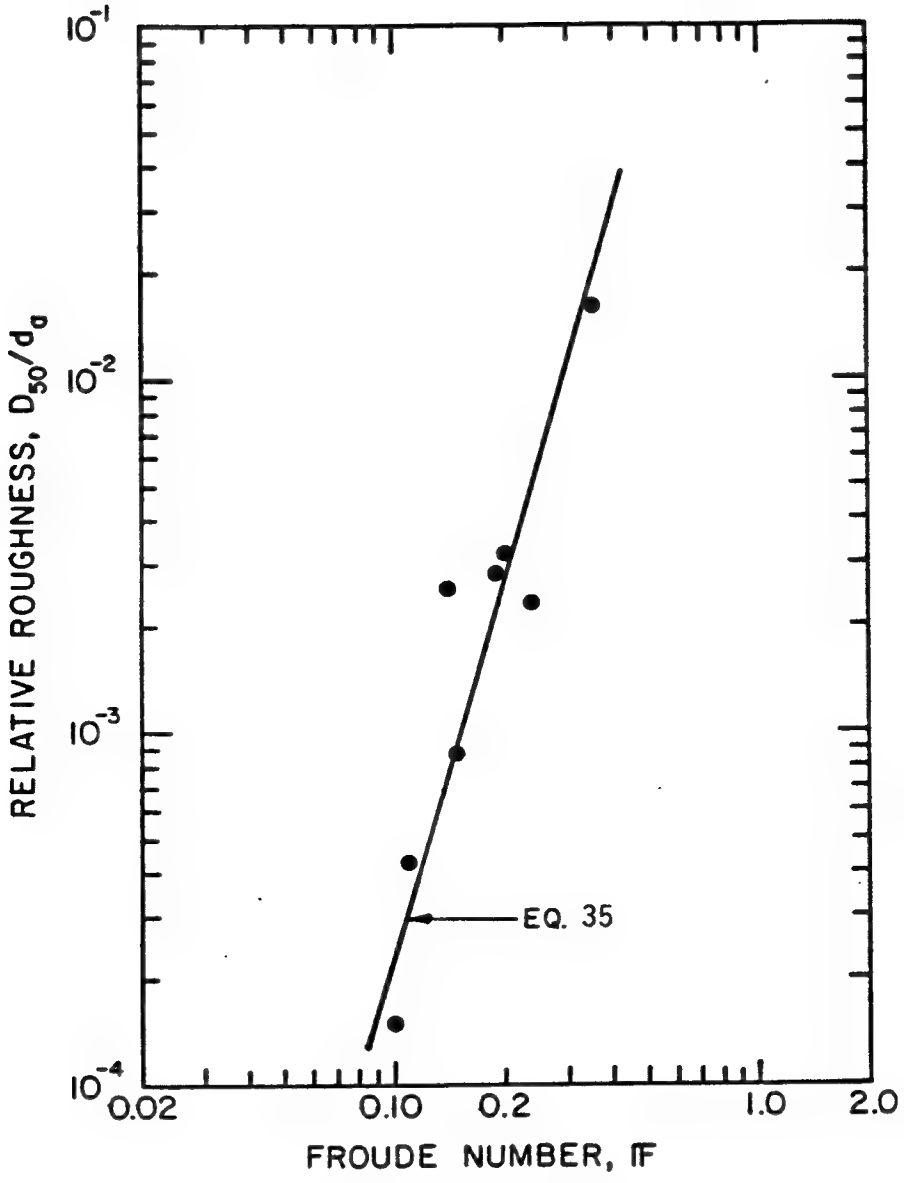

Figure 18 - Relative Roughness as a Function of Froude Number

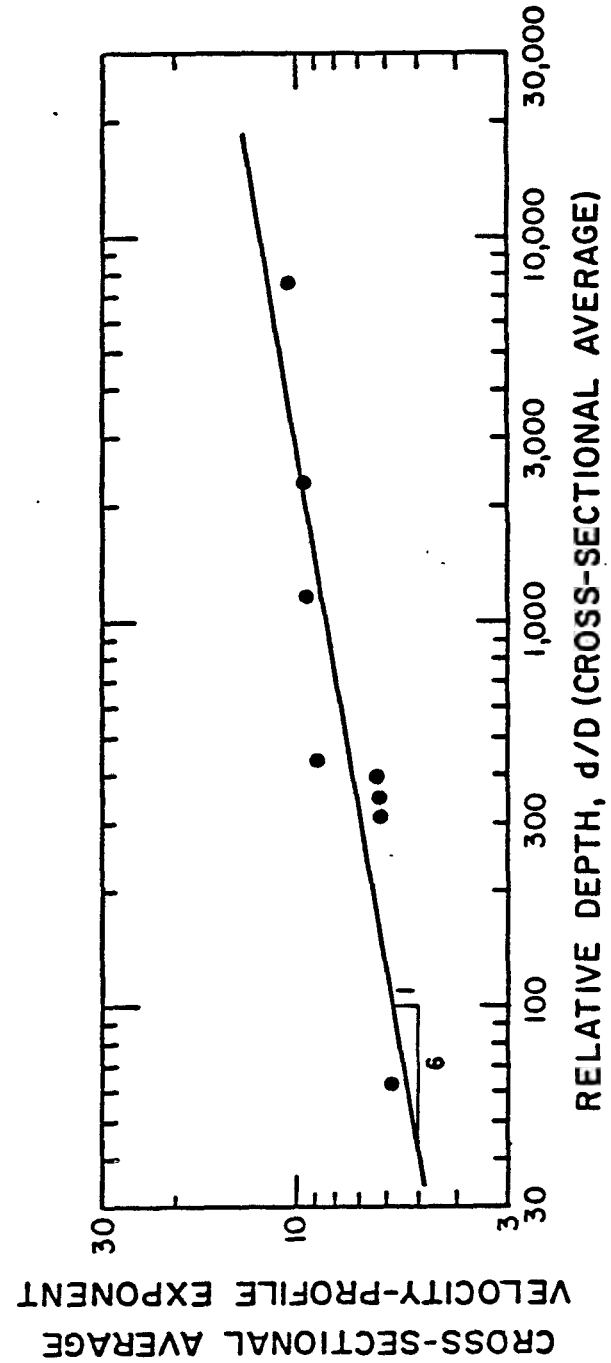

Figure 19 - Velocity Profile Exponent n as Function of Relative Depth, Sacramento River

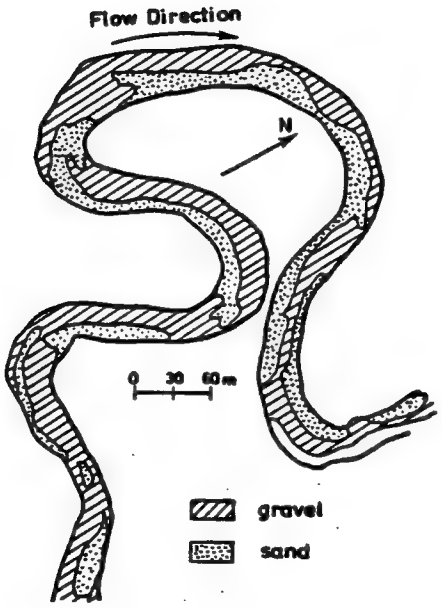

Figure 20 -Distribution of Sand and Gravel on the Bed of River Endrick, Scotland (Bluck 1971).

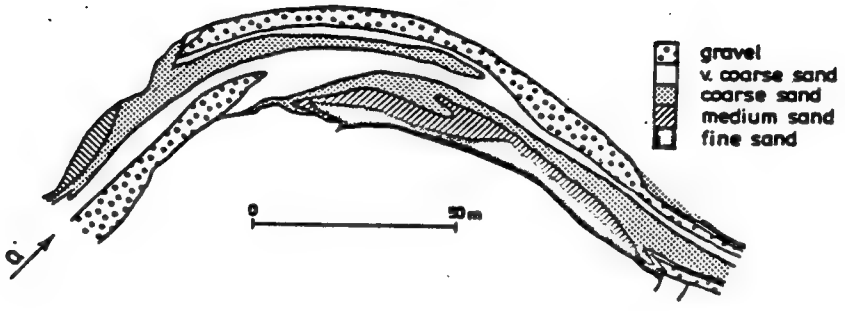

Figure 21 - Distribution of Sand and Gravel on the Bed of River Esk, Scotland (Bridge and Jarvis 1976).

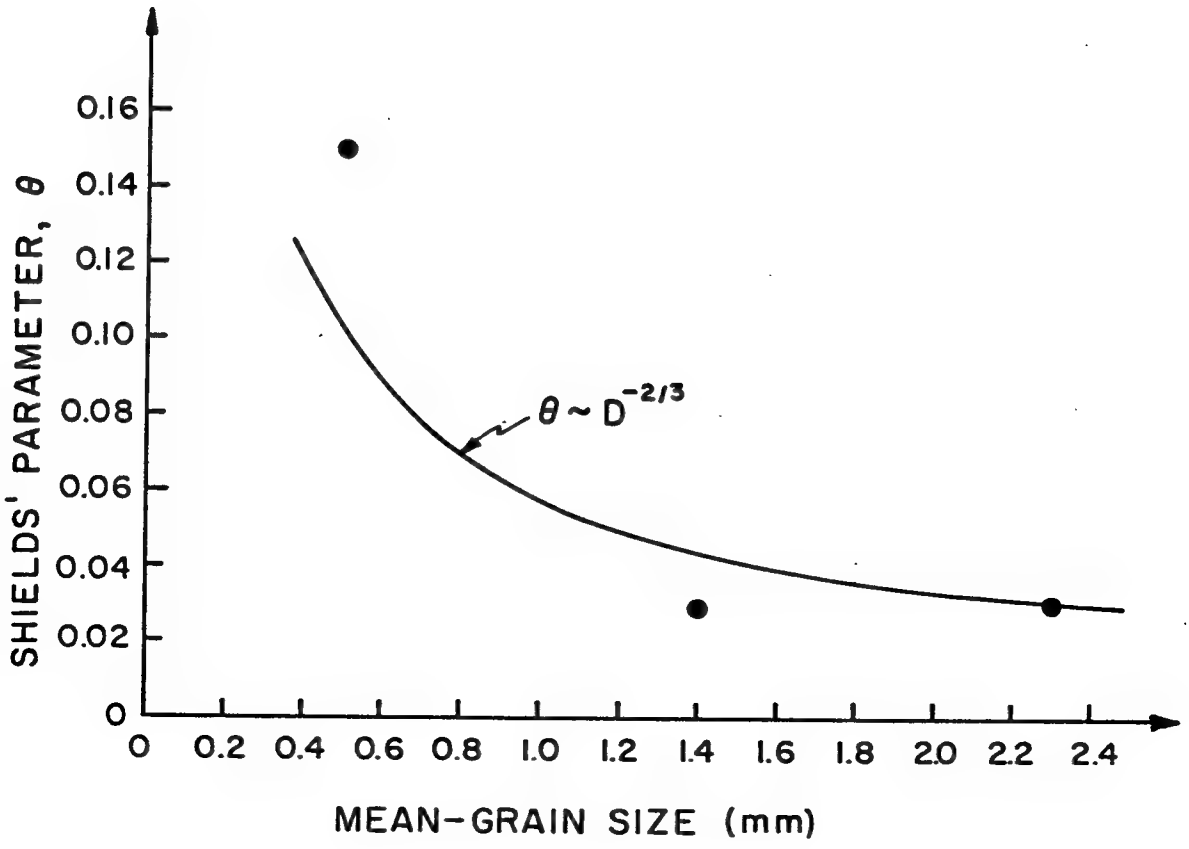

Fig. 22 - Shields' Parameter as a Function of Mean-Grain Size, Based on Rakoczi's (1975) Measurements.

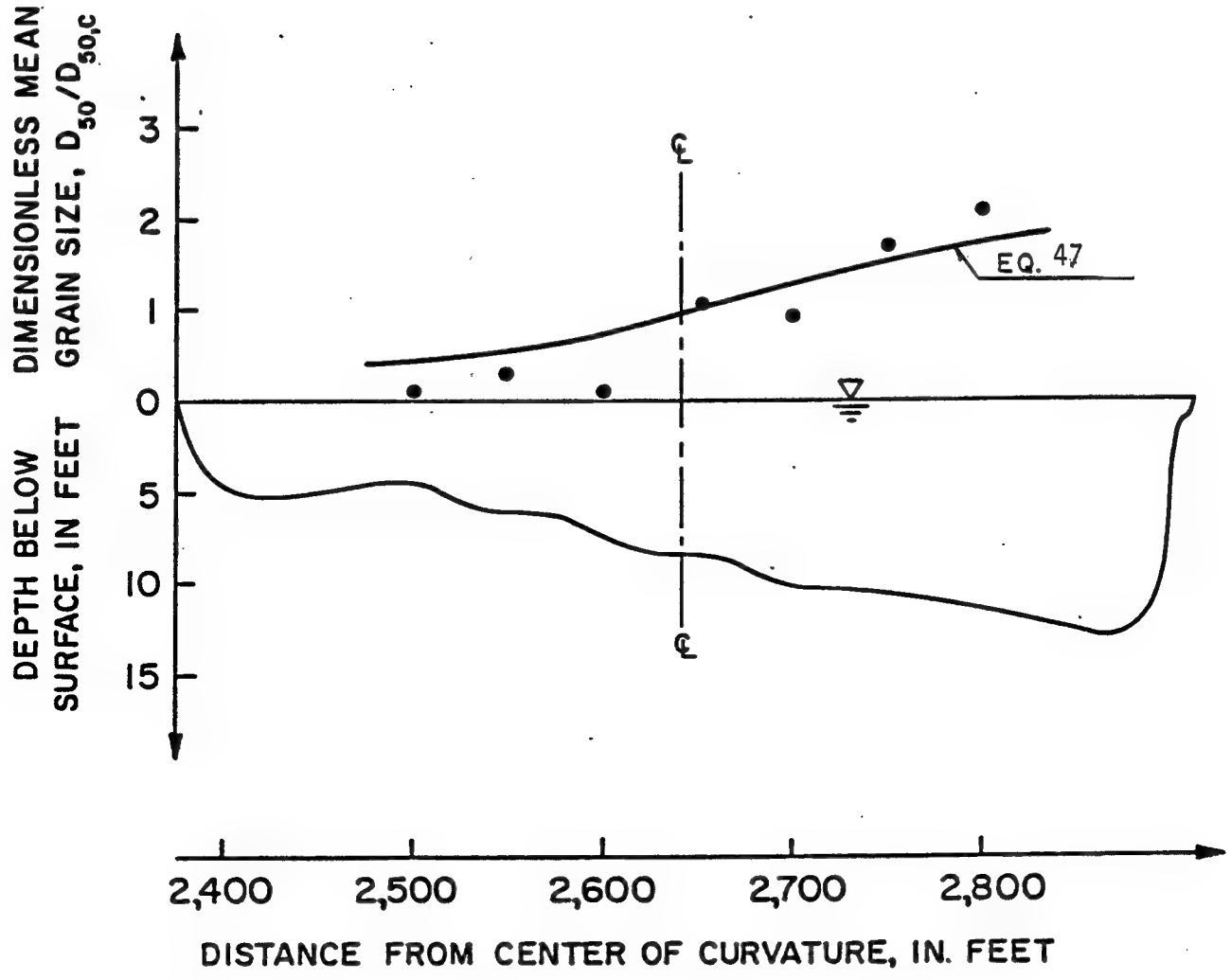

Figure 23 - Observed and Predicted Transverse Variation of Grain Size at Section 3 of the Sacramento River Study Bend.

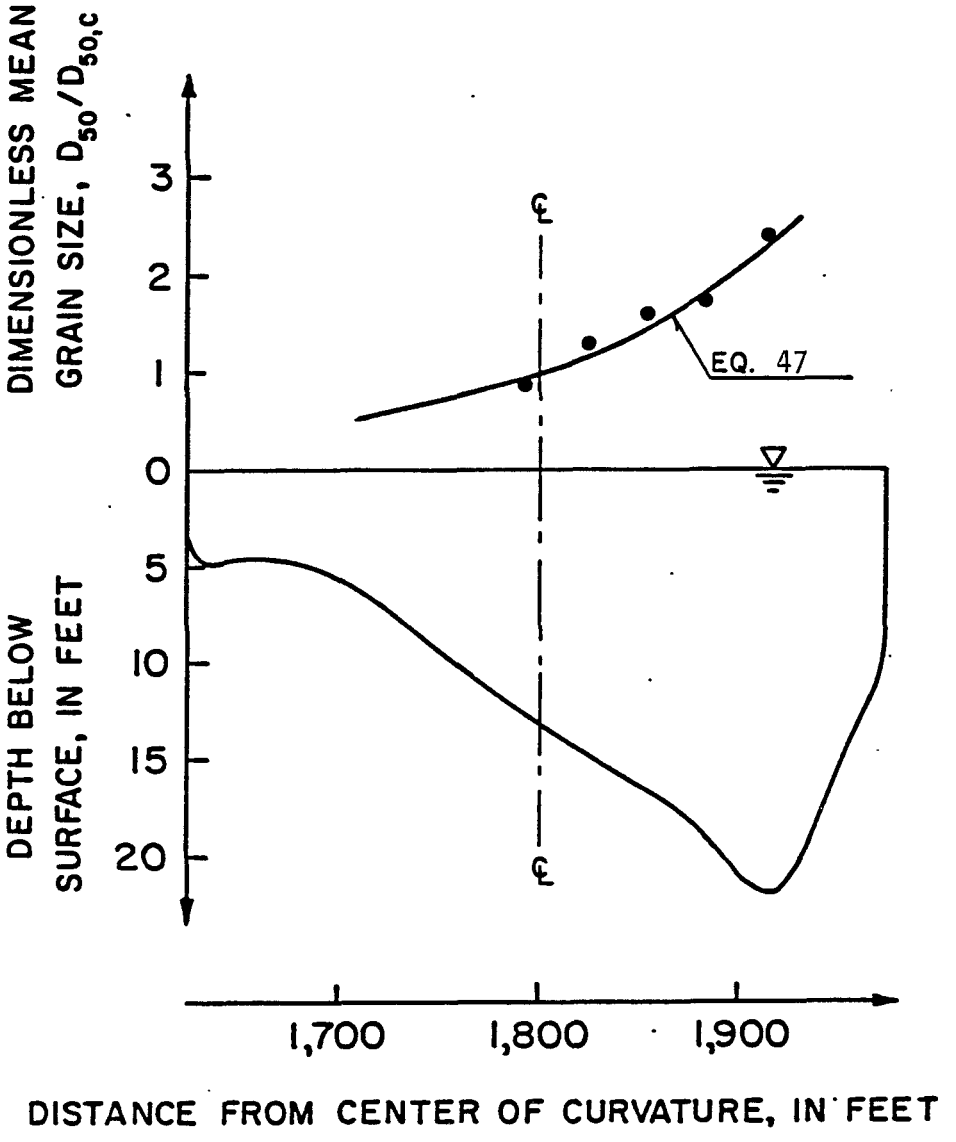

Figure 24 - Observed and Predicted Transverse Variation of Grain Size at Section 4 of the Sacramento River Study Bend (1 ft = 0.305 m).

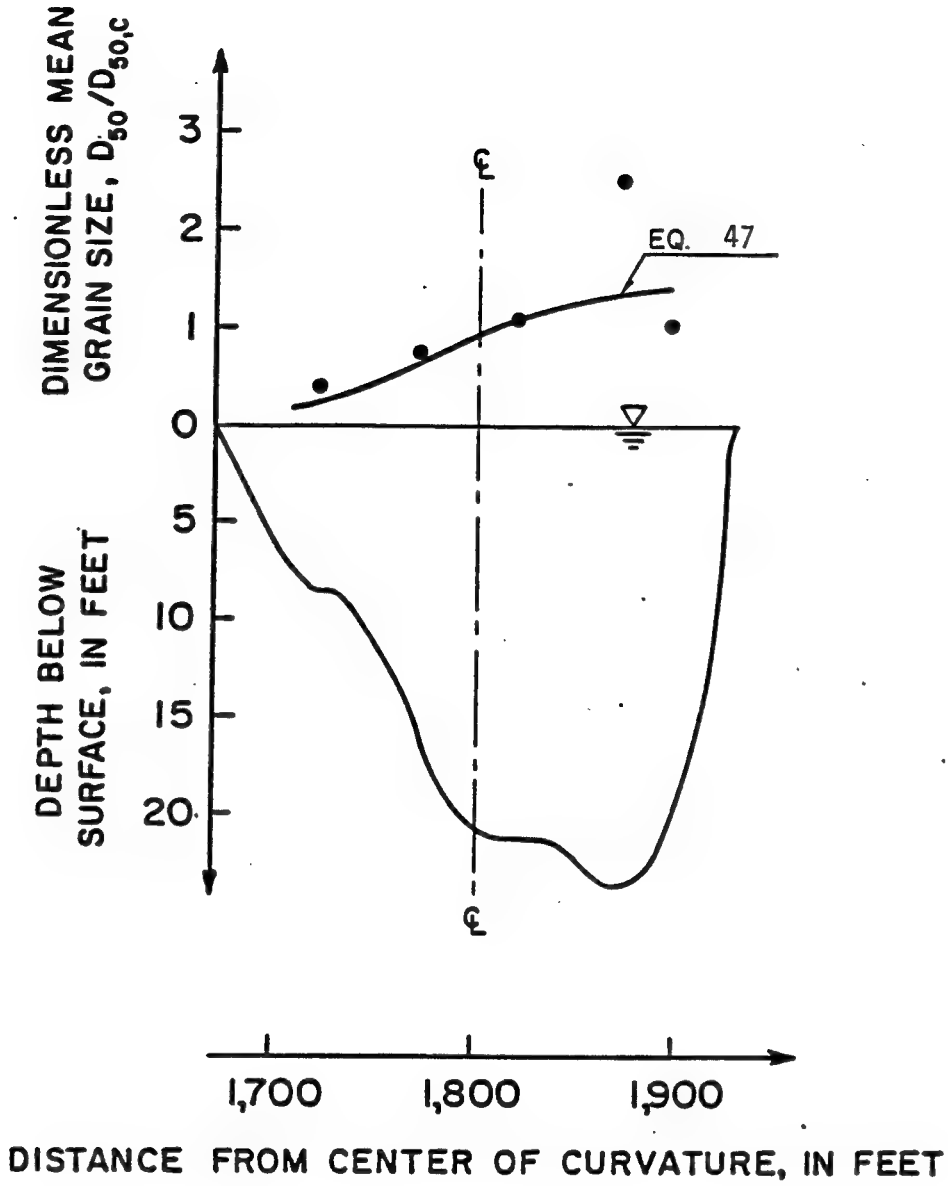

Figure 25 - Observed and Predicted Transverse Variation of Grain Size at Section 5 of the Sacramento River Study Bend (1 ft = 0.305 m).

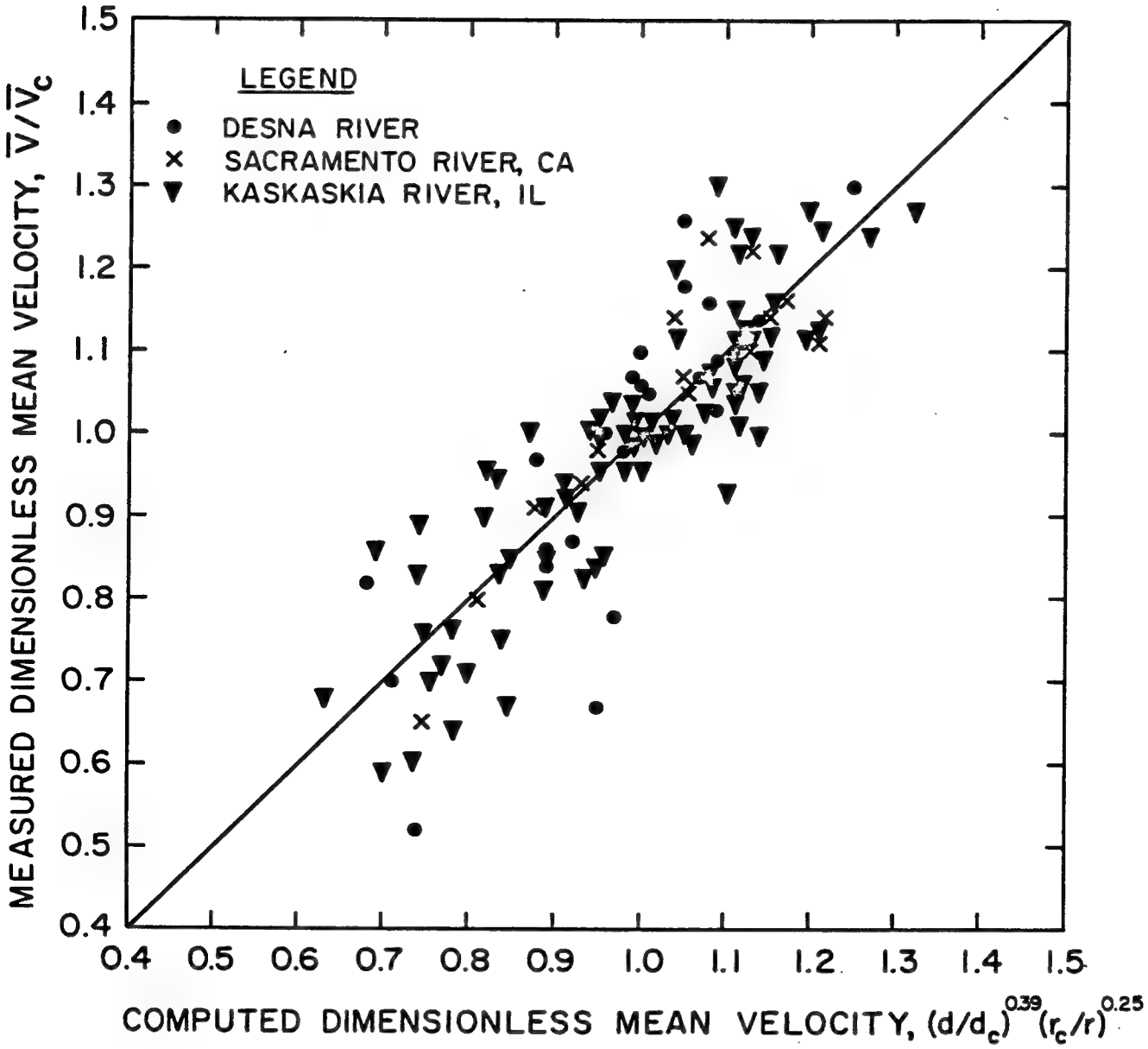

Figure 26 - Comparison of Measured and Computed Transverse Variation of Mean Velocity across Bends of Desna River (Rozovskii (1961)), Kaskaskia River, Illinois (Bhowmik (1979)), and Sacramento River, California.

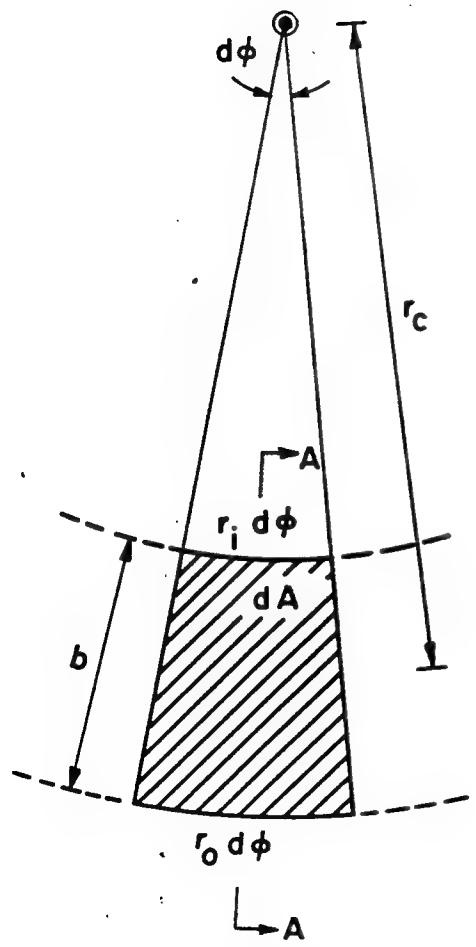

TOP VIEW

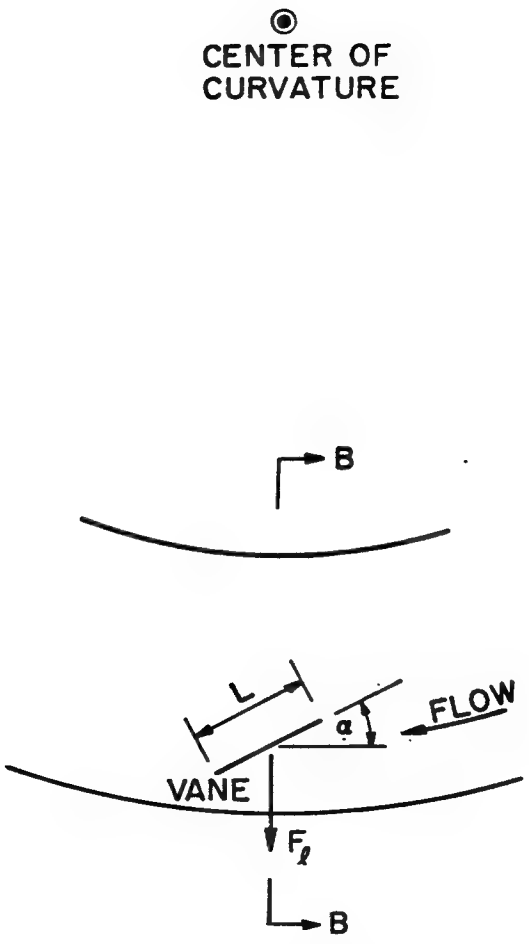

TOP VIEW

FORCE PROFILE

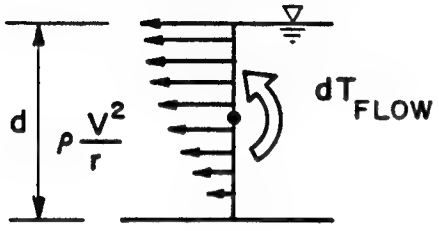

SIDE VIEW
SECTION A-A

(a)

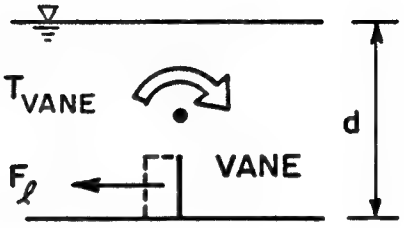

SIDE VIEW
SECTION B-B

(b)

Figure 27 - Definition Sketch for the Calculation of the Torque Produced by (a) the Flow and (b) a Submerged Vane

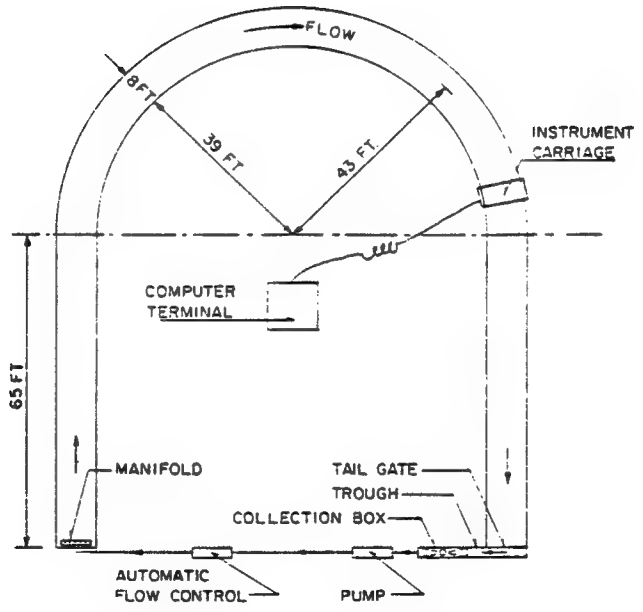

Figure 28 - Layout of the Curved, Recirculating Sedimentation Flume

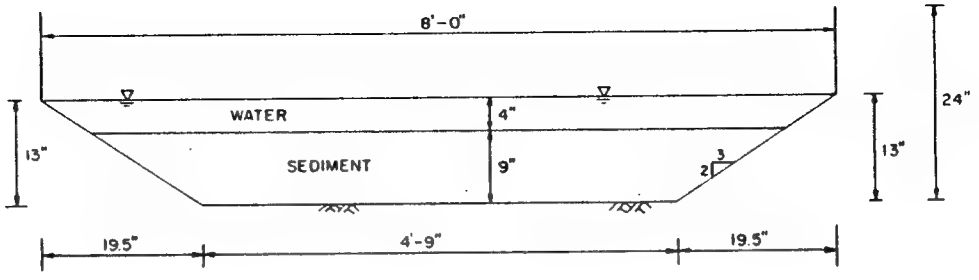

Figure 29 - Cross Section of the Curved, Recirculating Sedimentation Flume

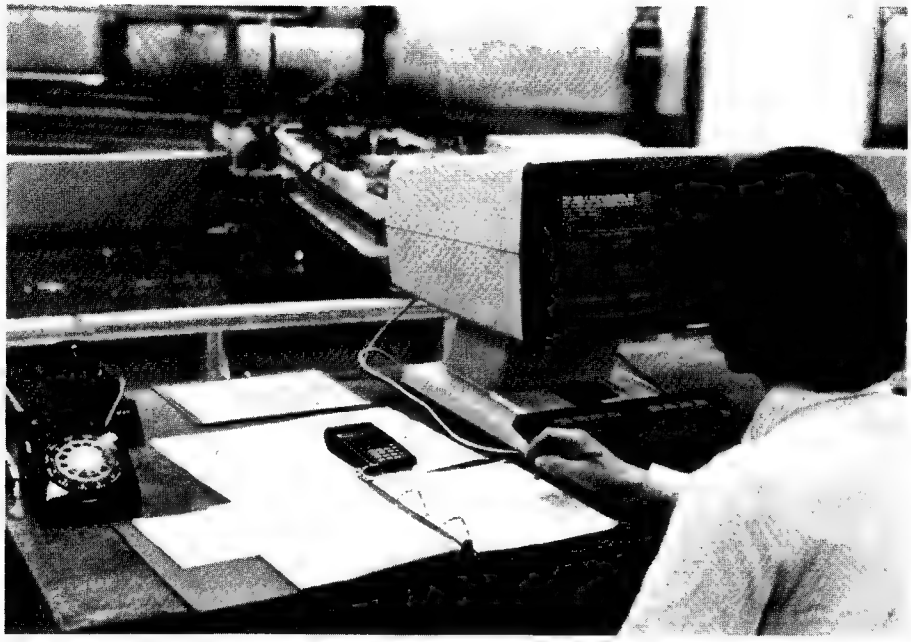

Figure 30 - Computer Operated Depth and Velocity Measurements in the Curved Sedimentation Flume

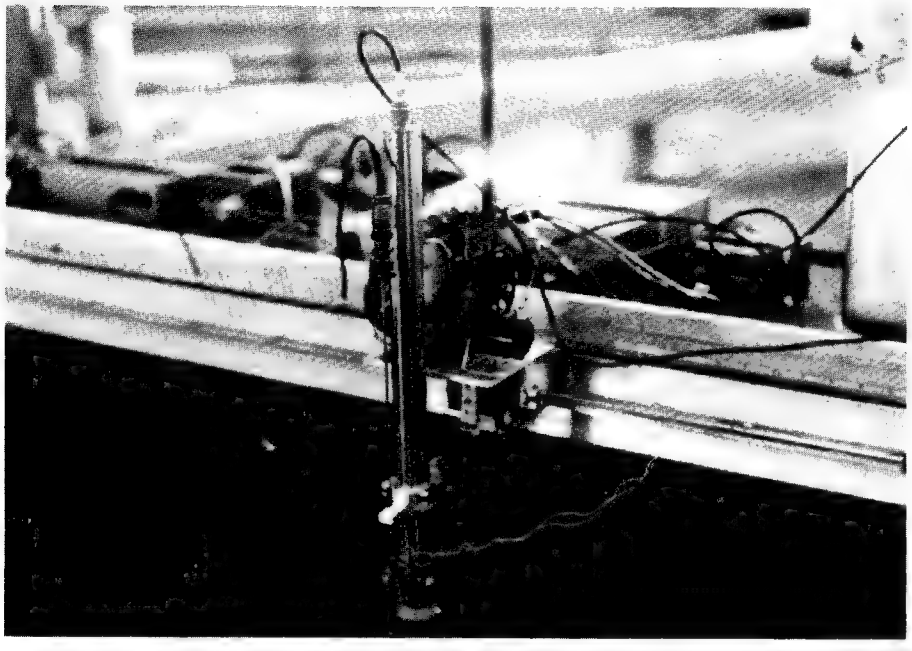

Figure 31 - Close-up of Current Meter and Sonic Depth Sounder

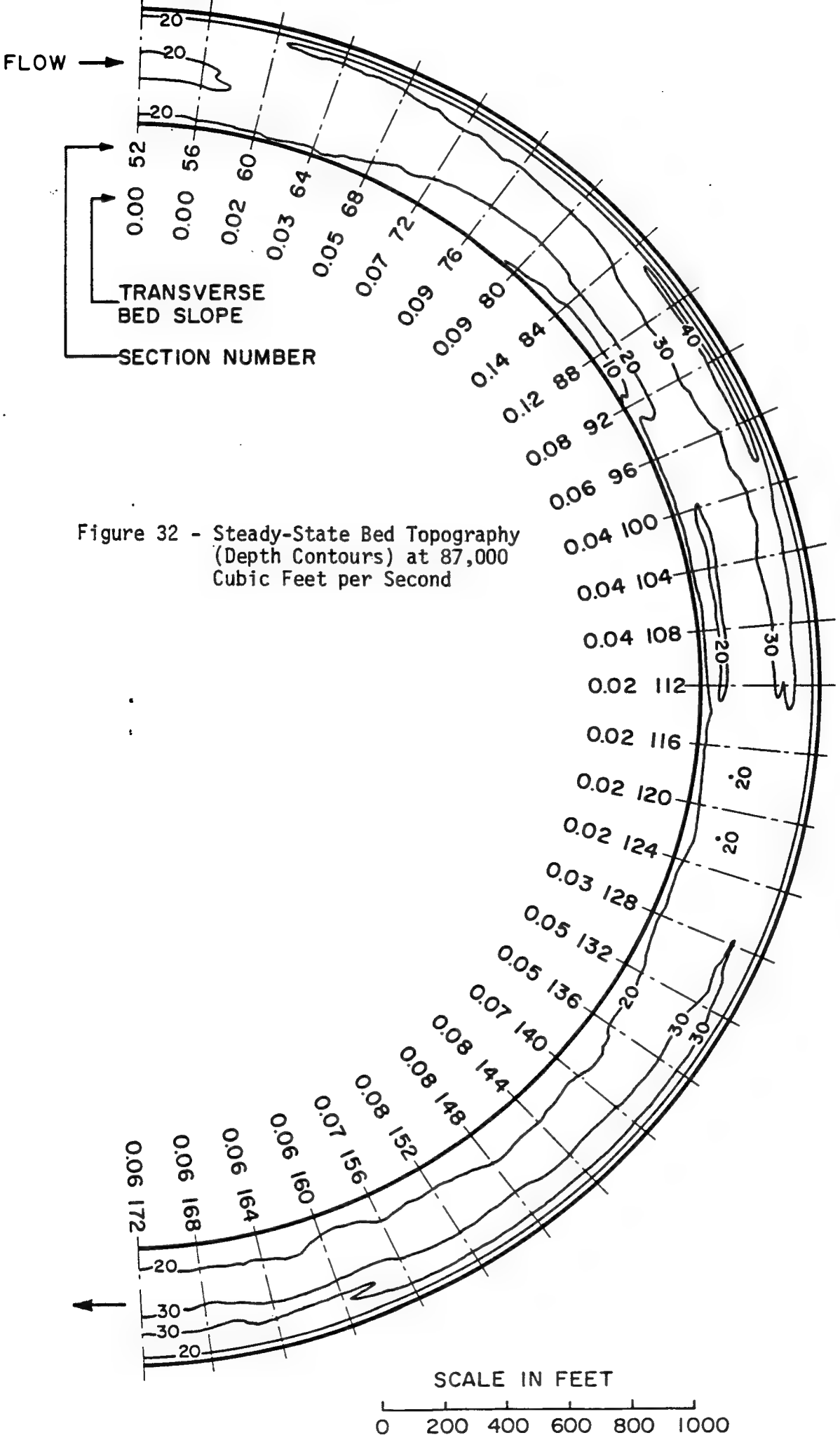

Figure 32 - Steady-State Bed Topography (Depth Contours) at 87,000 Cubic Feet per Second

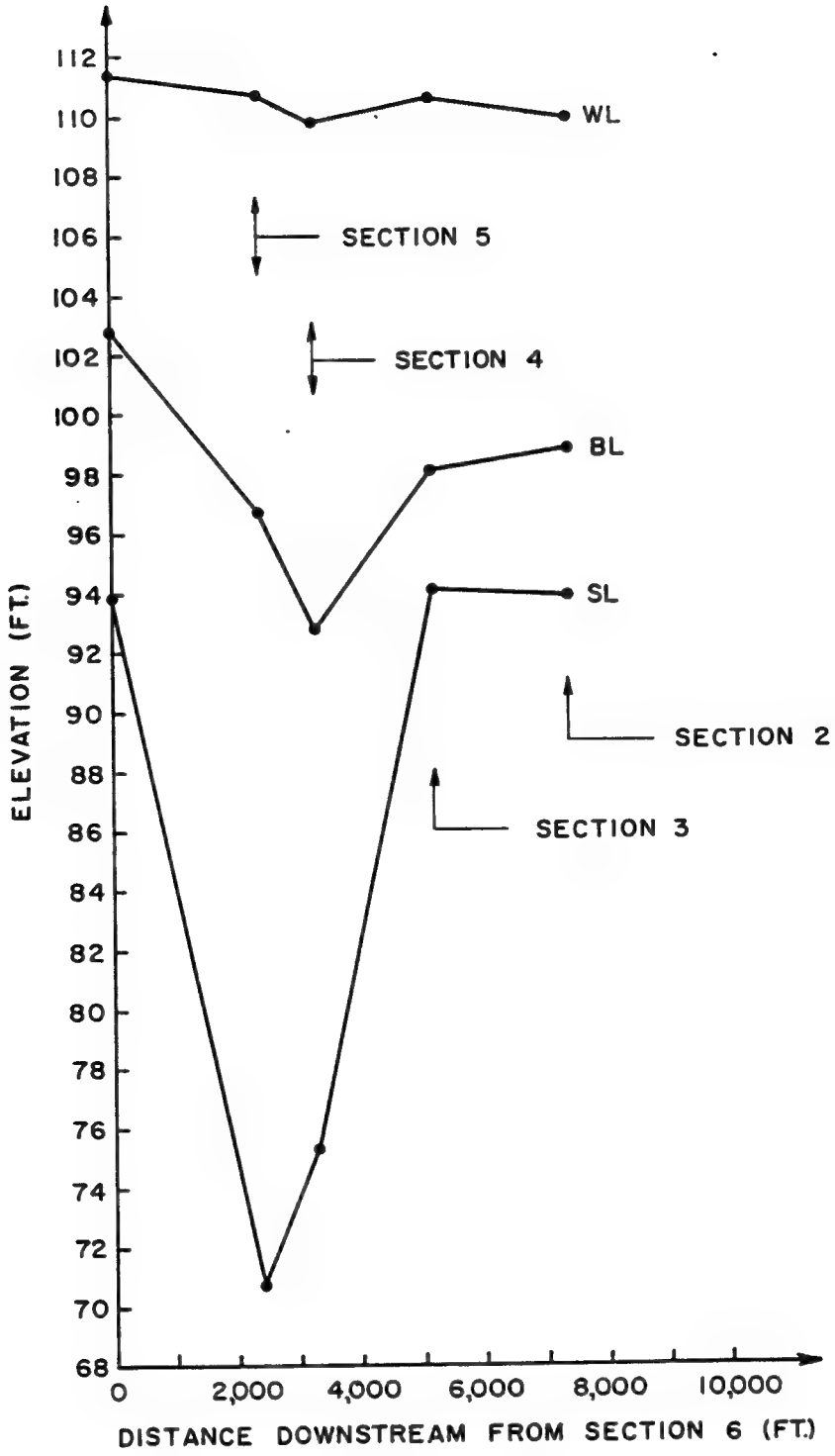

Figure 33 - Variations along the Sacramento River Bend of Water Level (WL), Cross-Sectional Average of Bed Level (BL), and Level of Deepest Point (SL), Measured in the 1980 Survey

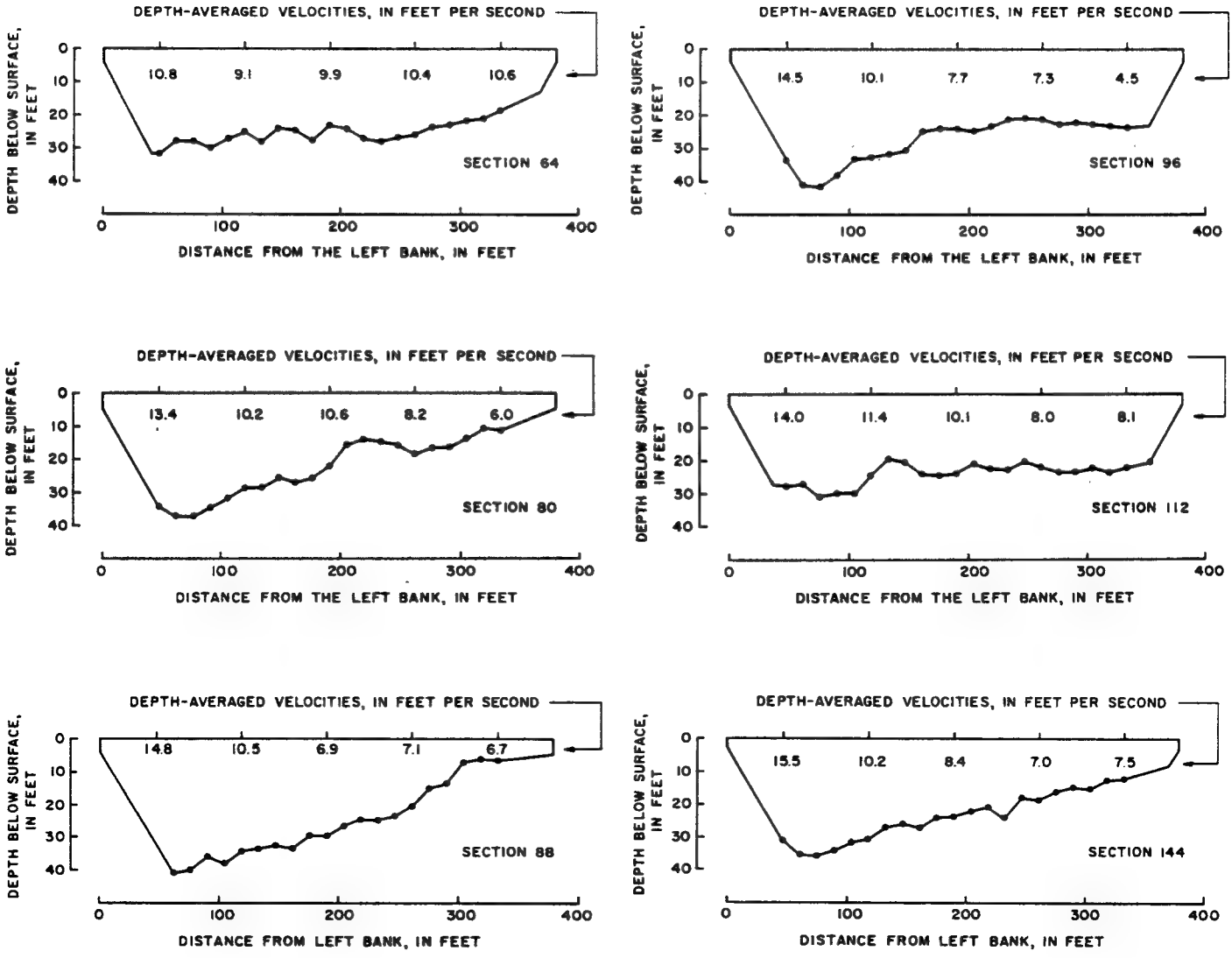

Figure 34 - Steady-State Cross Sections before Installation of Vanes; Discharge = 87,000 cfs

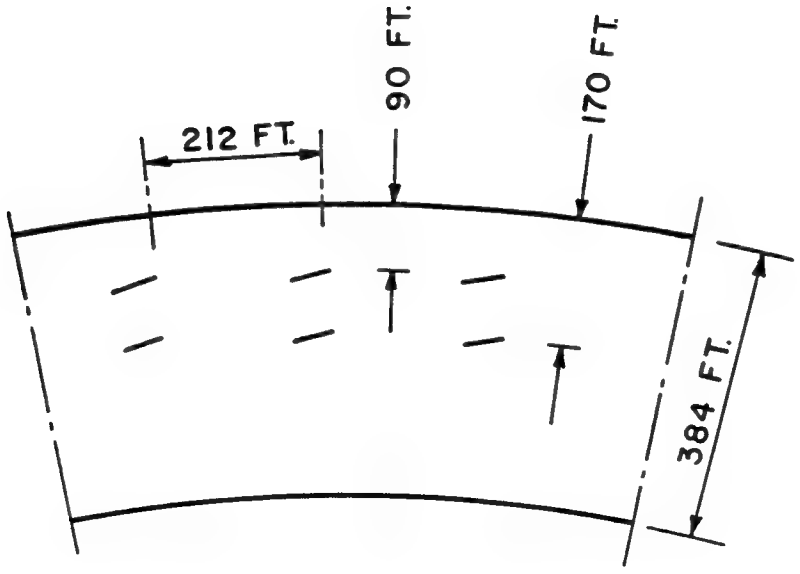

Figure 35 - Vane Configuration Tested

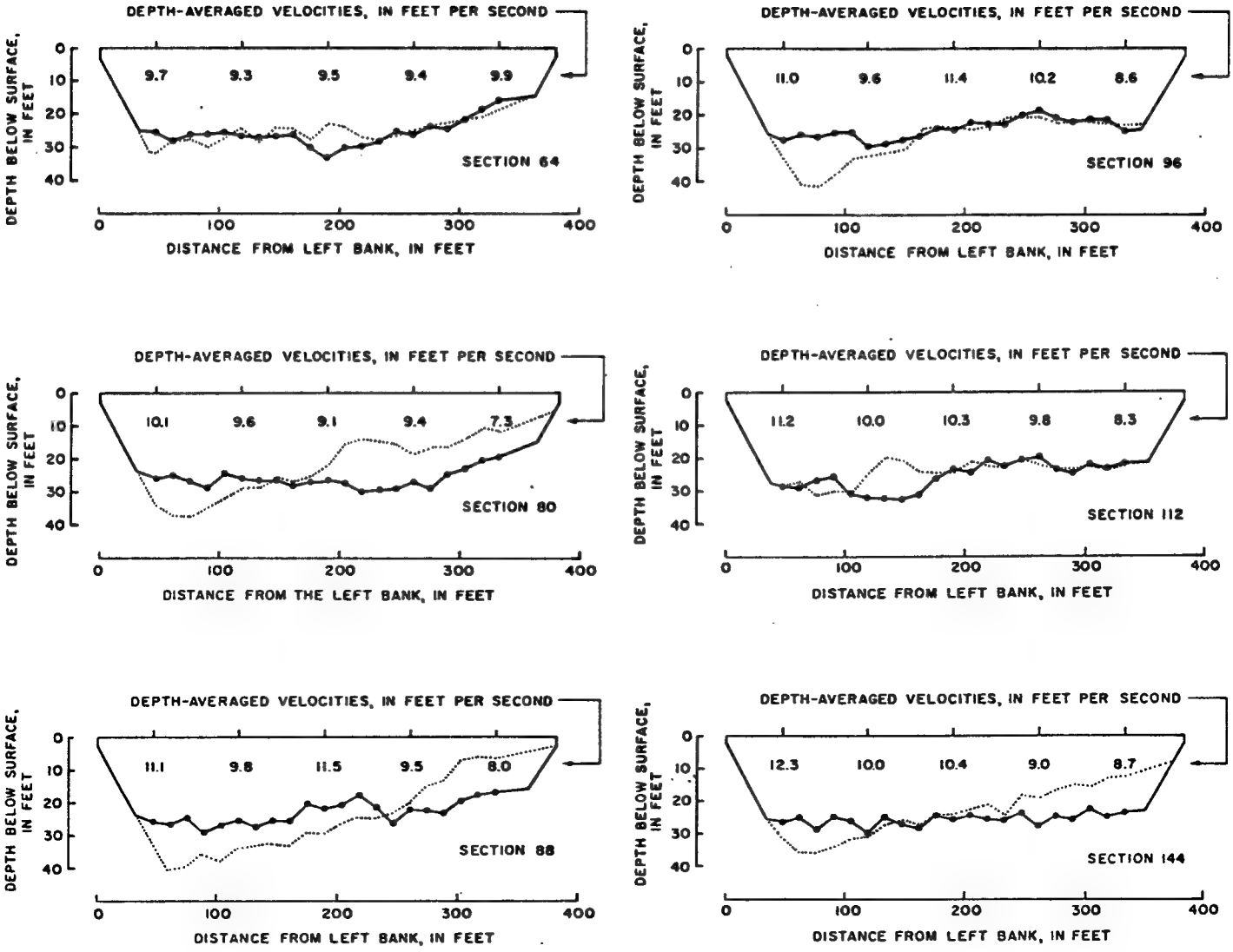

Figure 36 - Steady-State Cross Sections with 52 Vanes Installed; Discharge = 87,000 cfs

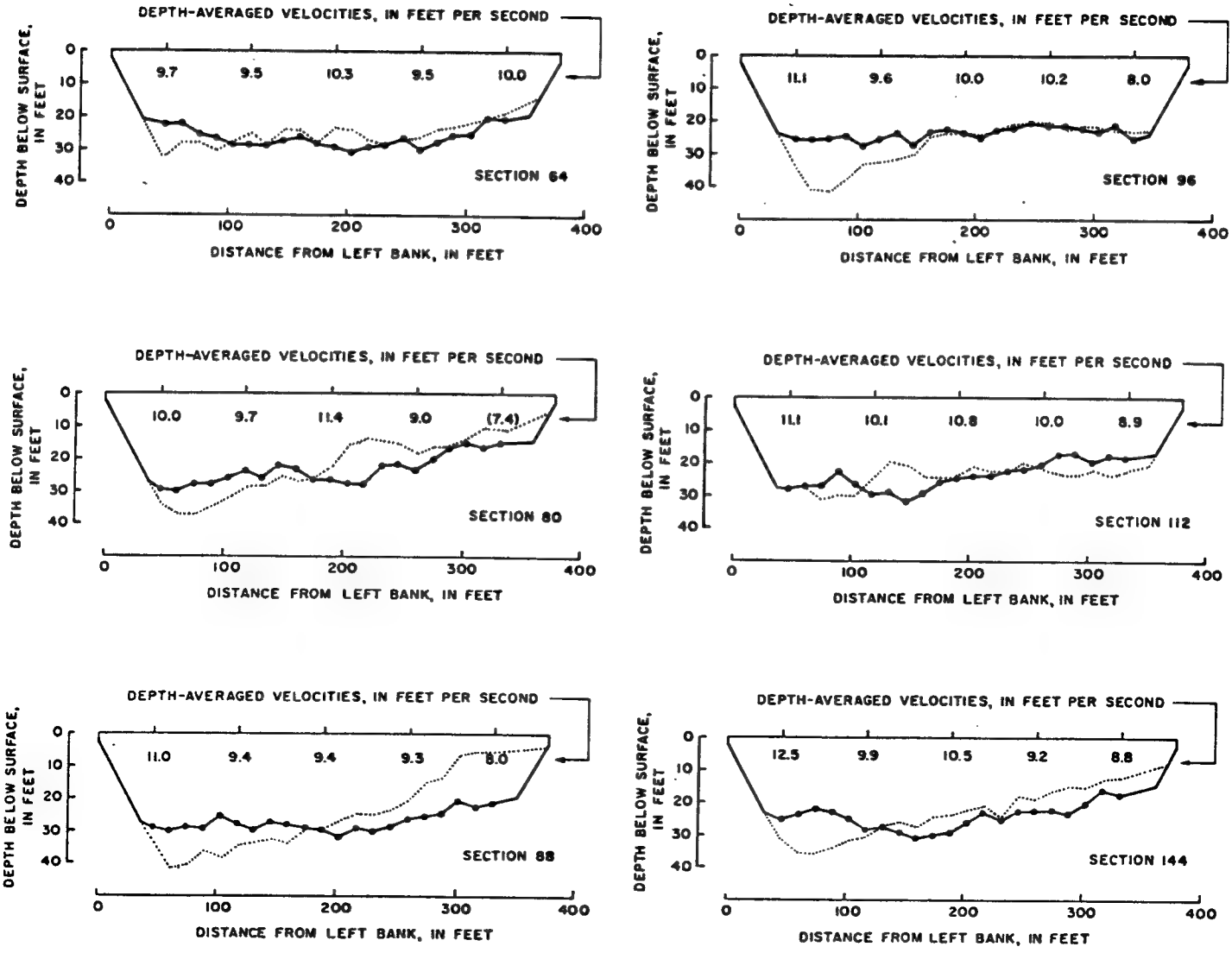

Figure 37 - Steady-State Cross Sections with 36 Vanes Installed; Discharge = 87,000 cfs

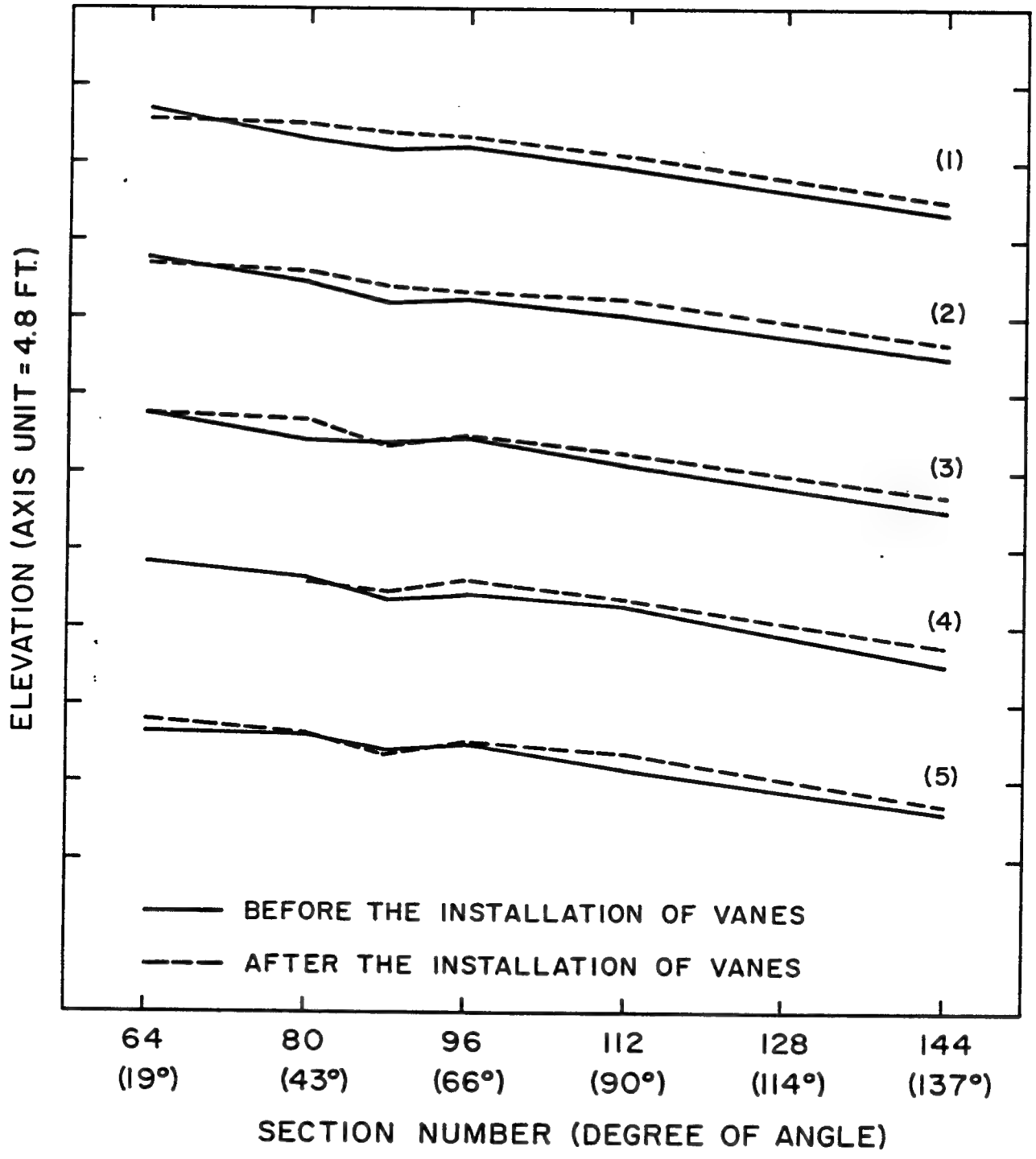

Figure 38 - Longitudinal Water-Surface Profiles Before and After the Installation of Vanes; (1) 48 ft from Inner Bank; (2) 120 ft from Inner Bank; (3) 192 ft from Inner Bank (Centerline); (4) 120 ft from Outer Bank; and (5) 48 ft from Outer Bank

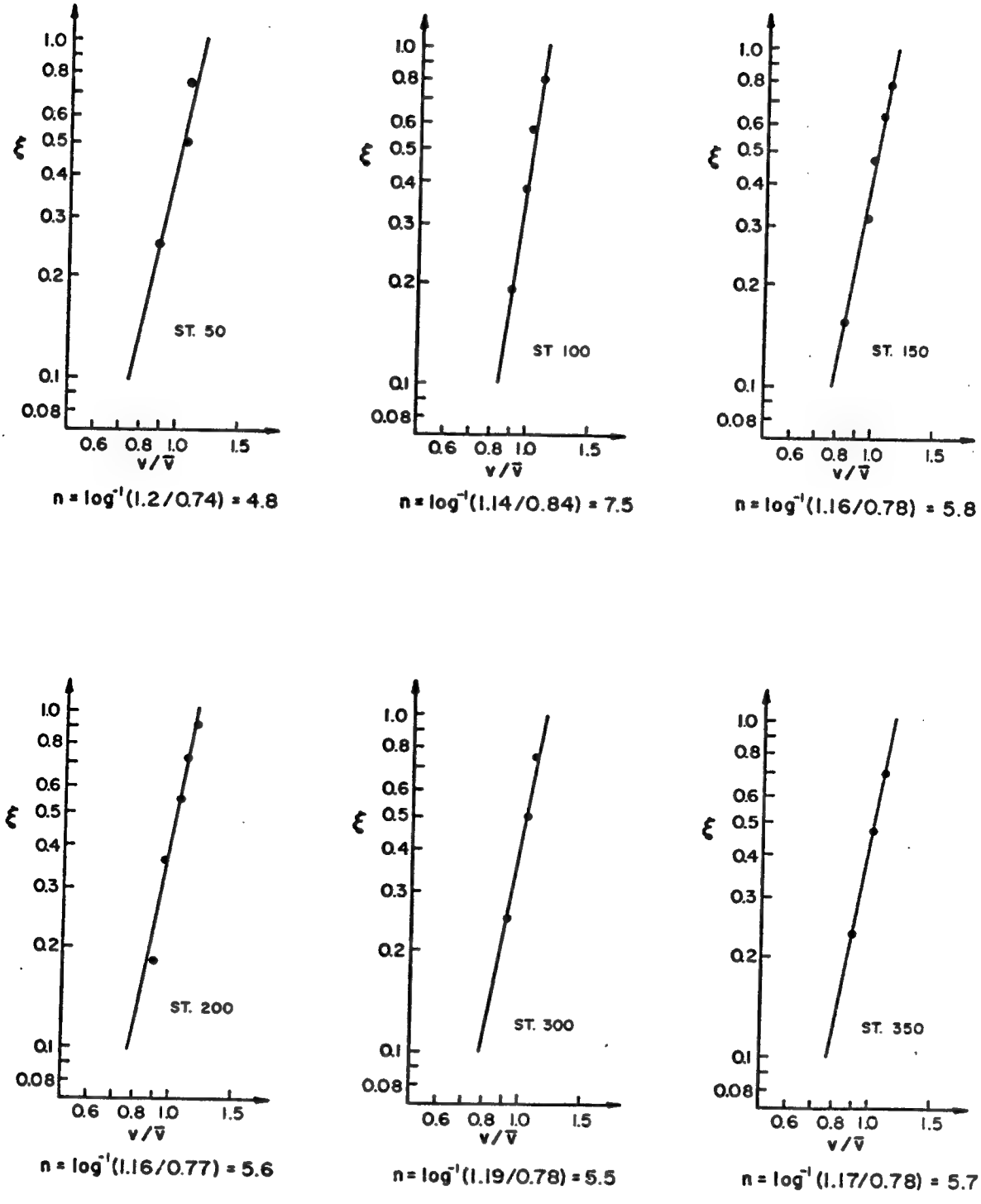

Figure A-1 - Velocity Distributions in Cross Section No. 1 at Low Flow, 7,800 Cubic Feet Per Second

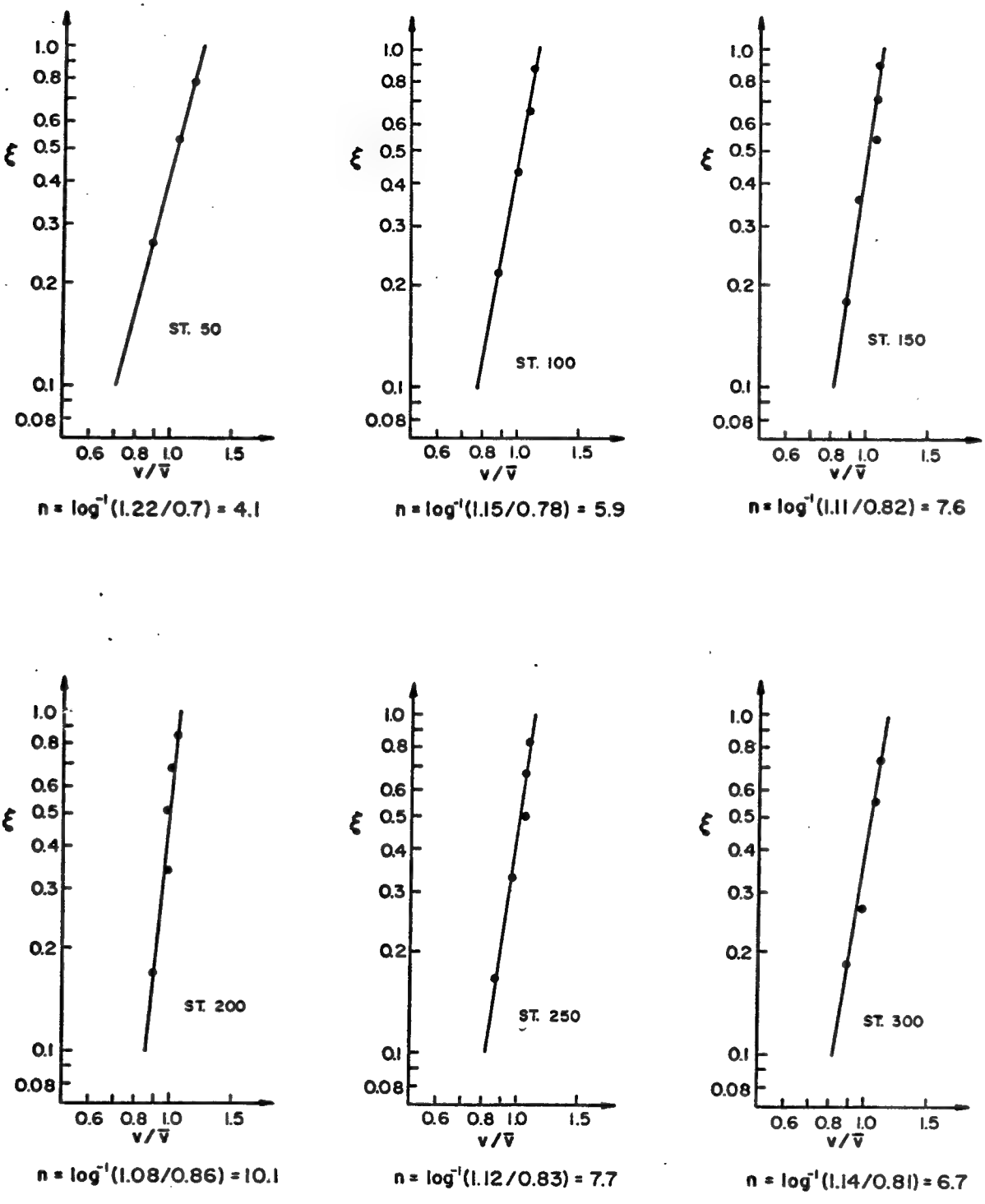

Figure A-2 - Velocity Distributions in Cross Section No. 2 at Low Flow, 8,300 Cubic Feet Per Second

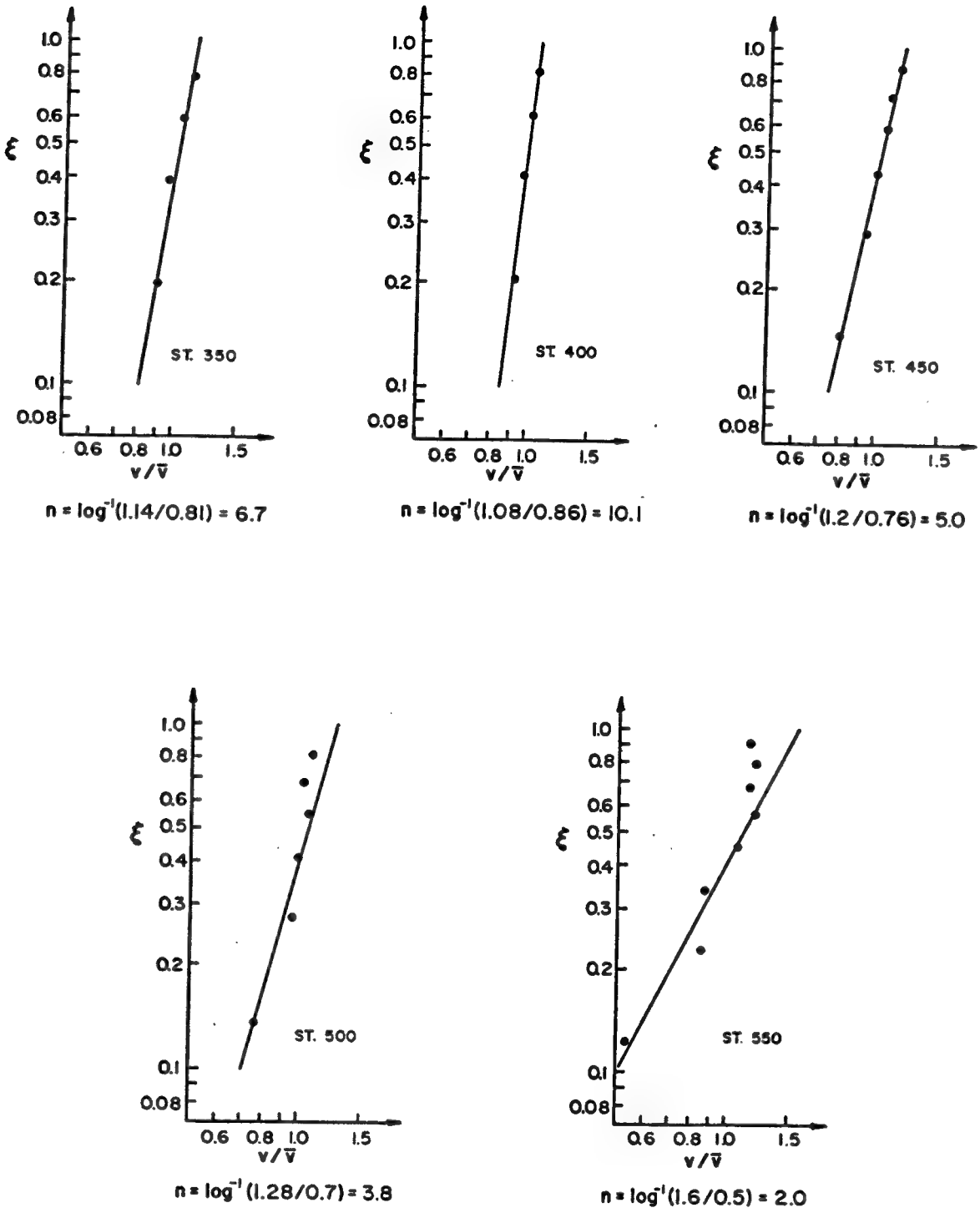

Figure A-2 (Cont) - Velocity Distributions in Cross Section No. 2 at Low Flow, 8,300 Cubic Feet Per Second

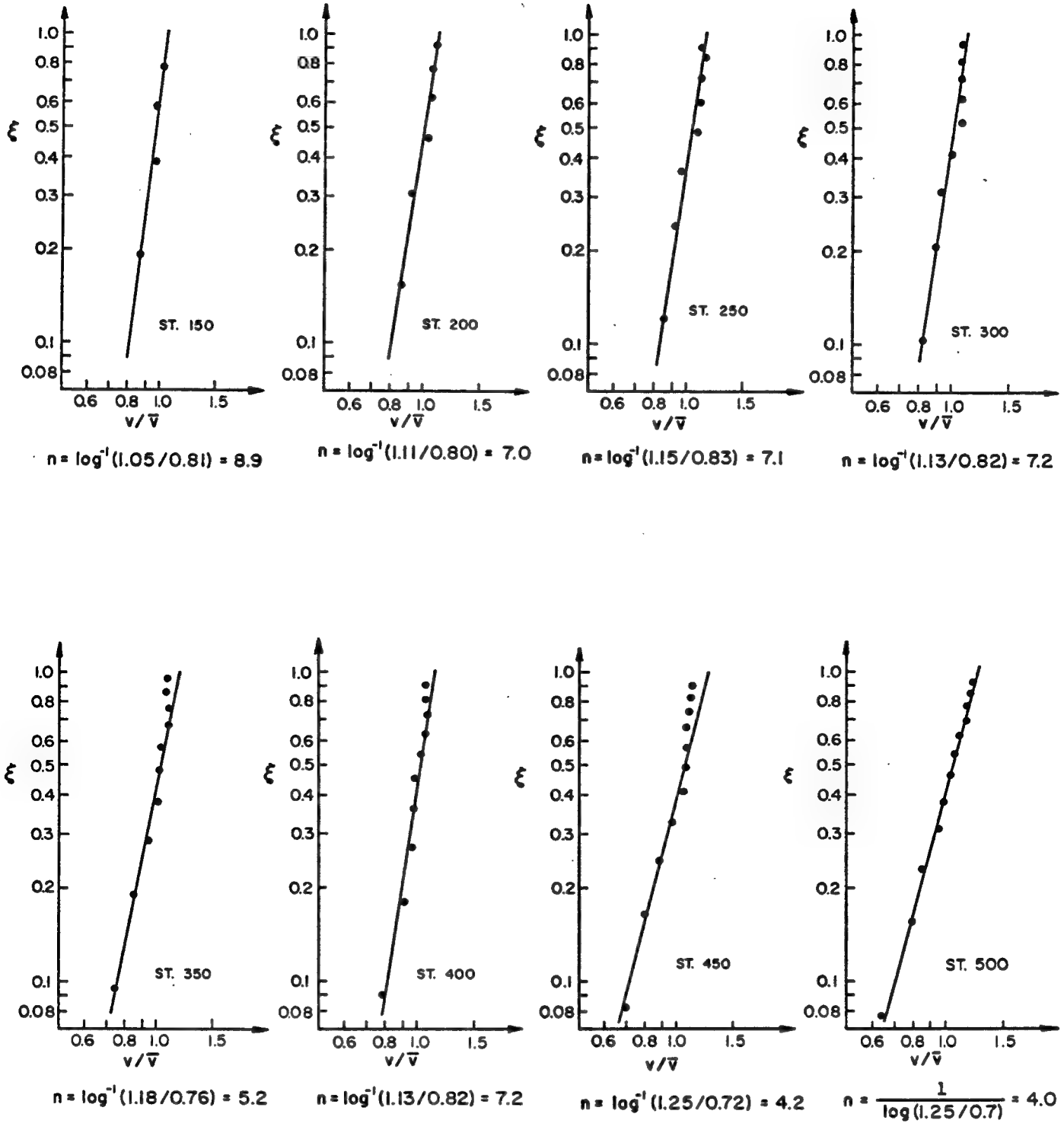

Figure A-3 - Velocity Distributions in Cross Section No. 3
at Low Flow, 9,900 Cubic Feet Per Second

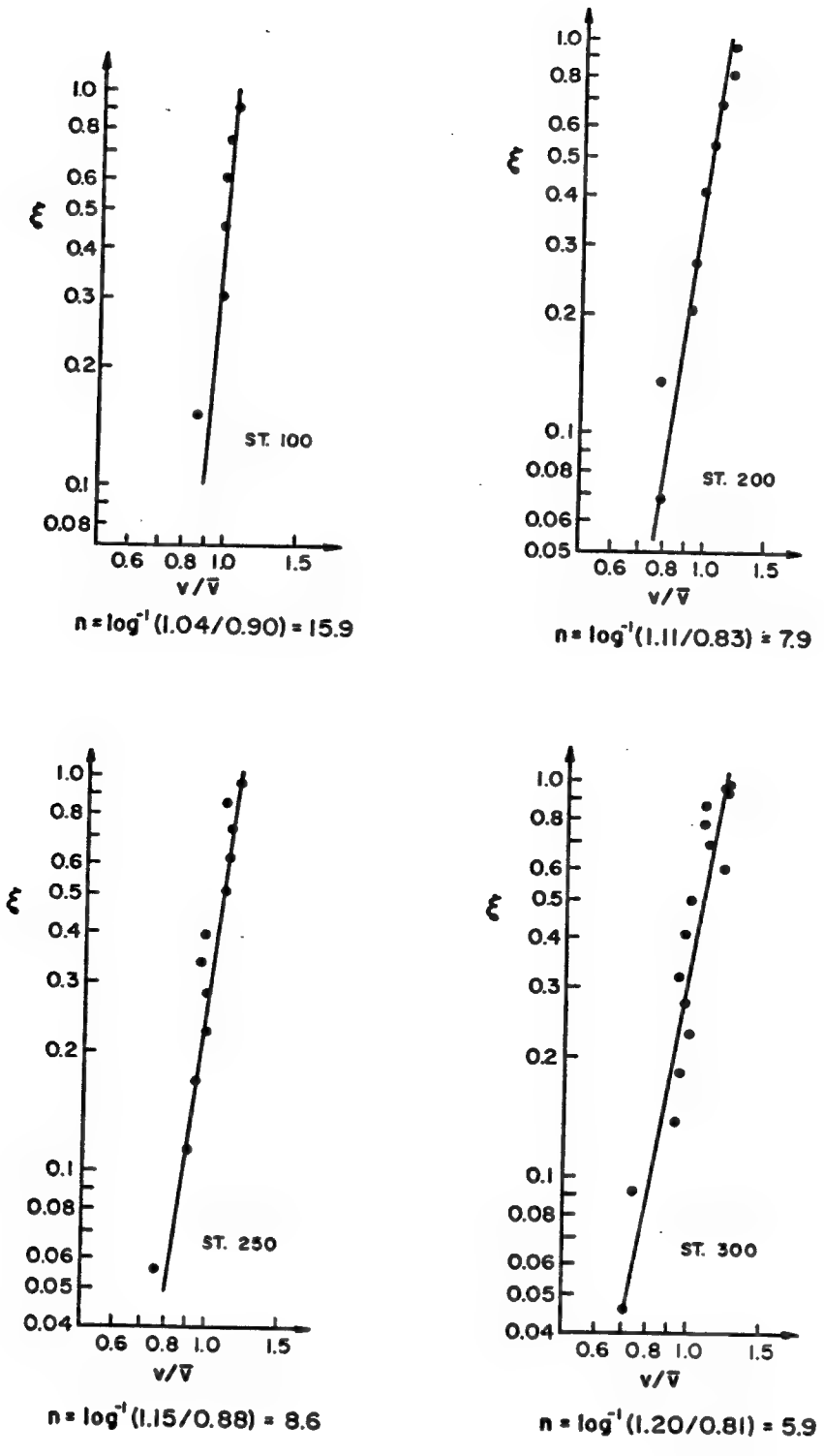

Figure A-4 - Velocity Distributions in Cross Section No. 4 at Low Flow, 9,100 Cubic Feet Per Second

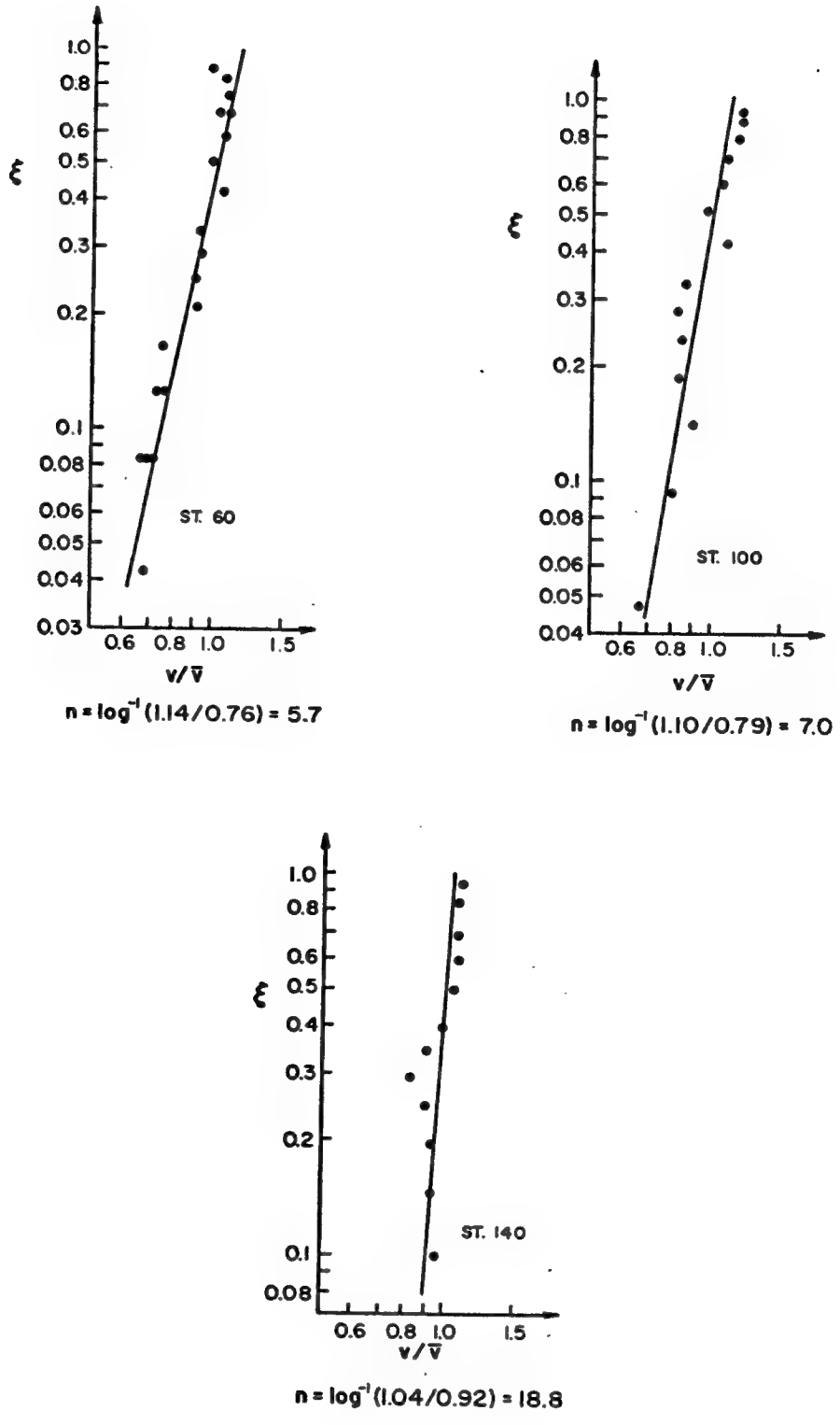

Figure A-5 - Velocity Distributions in Cross Section No. 5 at Low Flow, 9,100 Cubic Feet Per Second

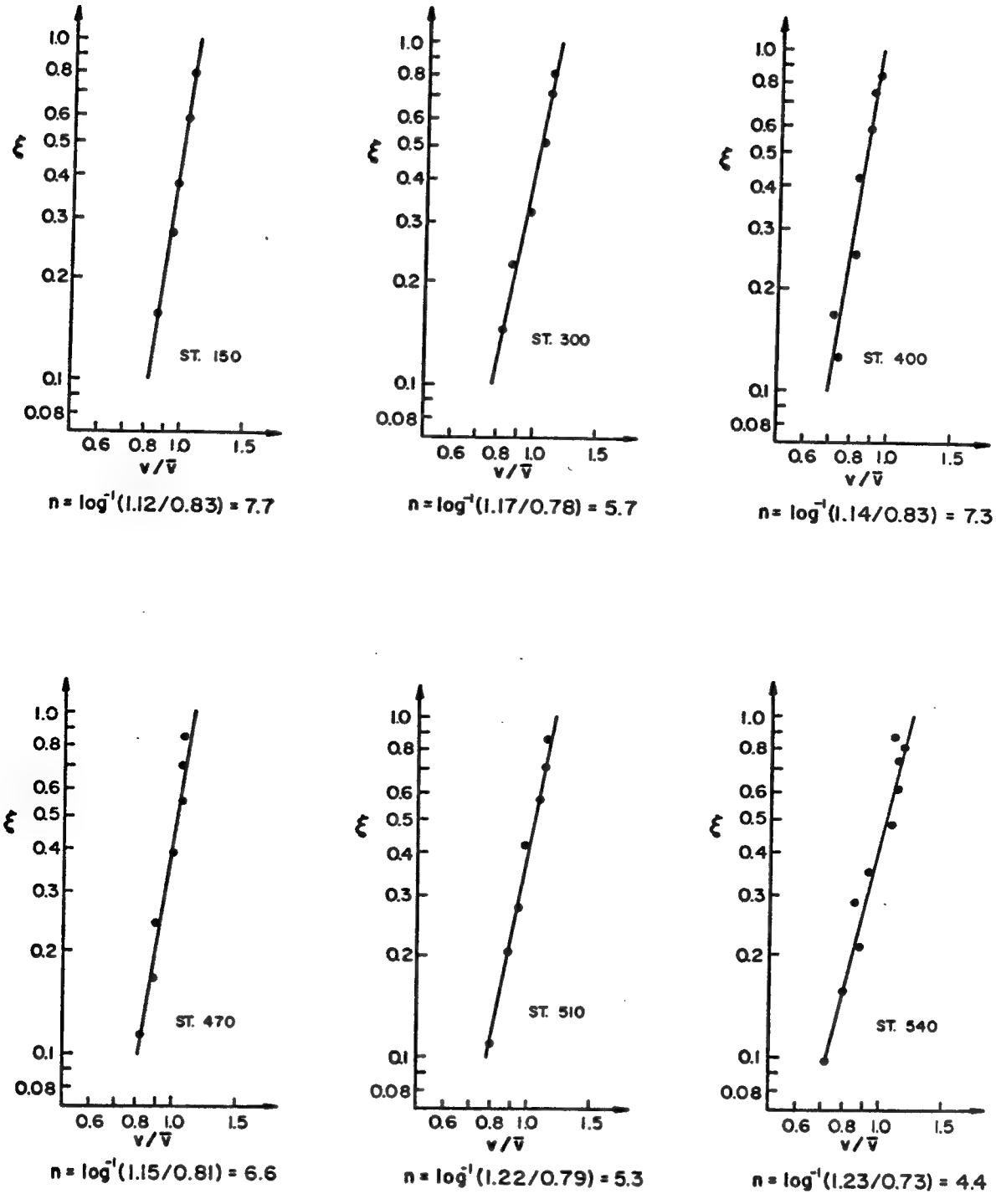

Figure A-6 - Velocity Distributions in Cross Section No. 2 at High Flow, 24,900 Cubic Feet Per Second

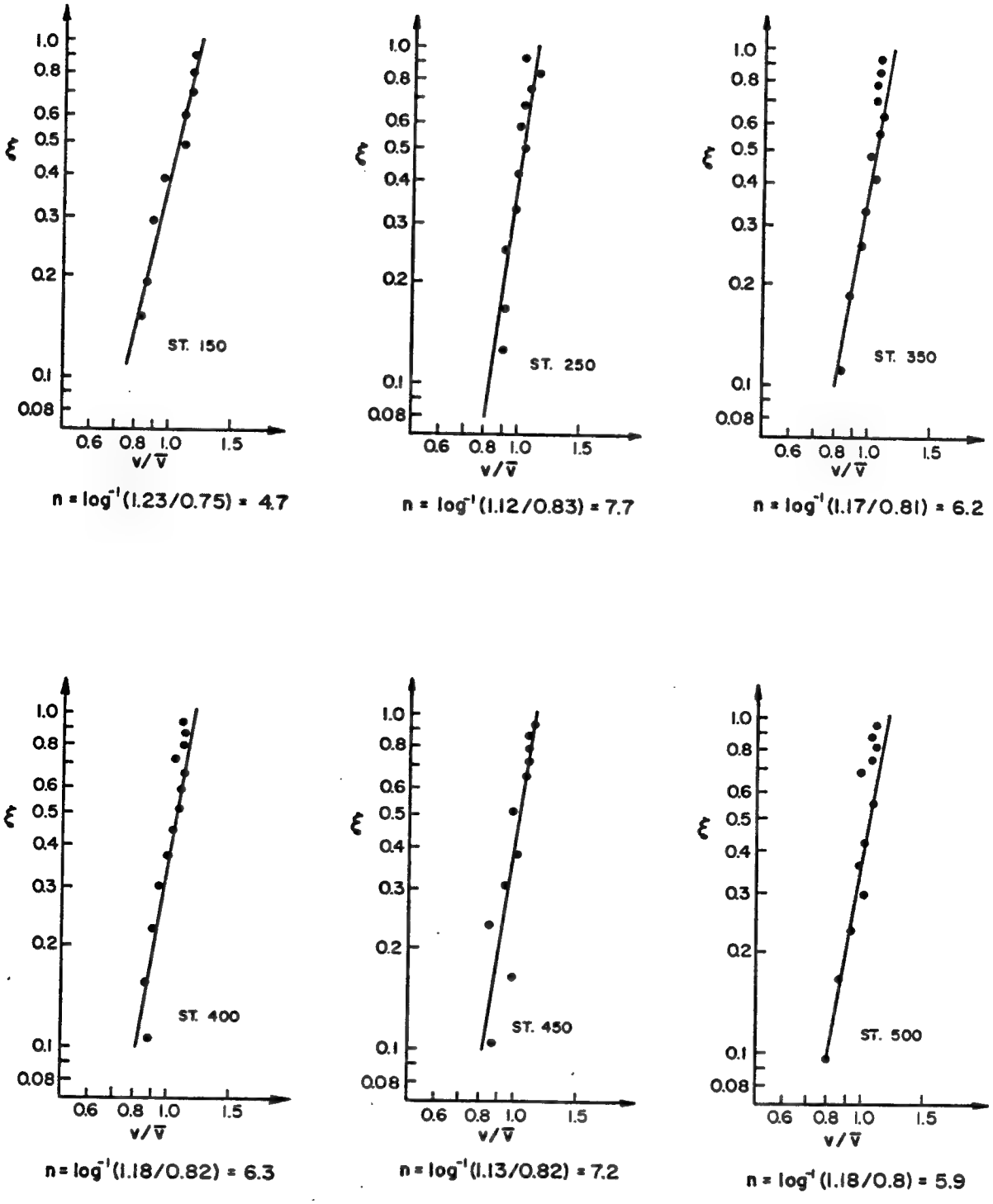

Figure A-7 - Velocity Distributions in Cross Section No. 3 at High Flow, 28,400 Cubic Feet Per Second

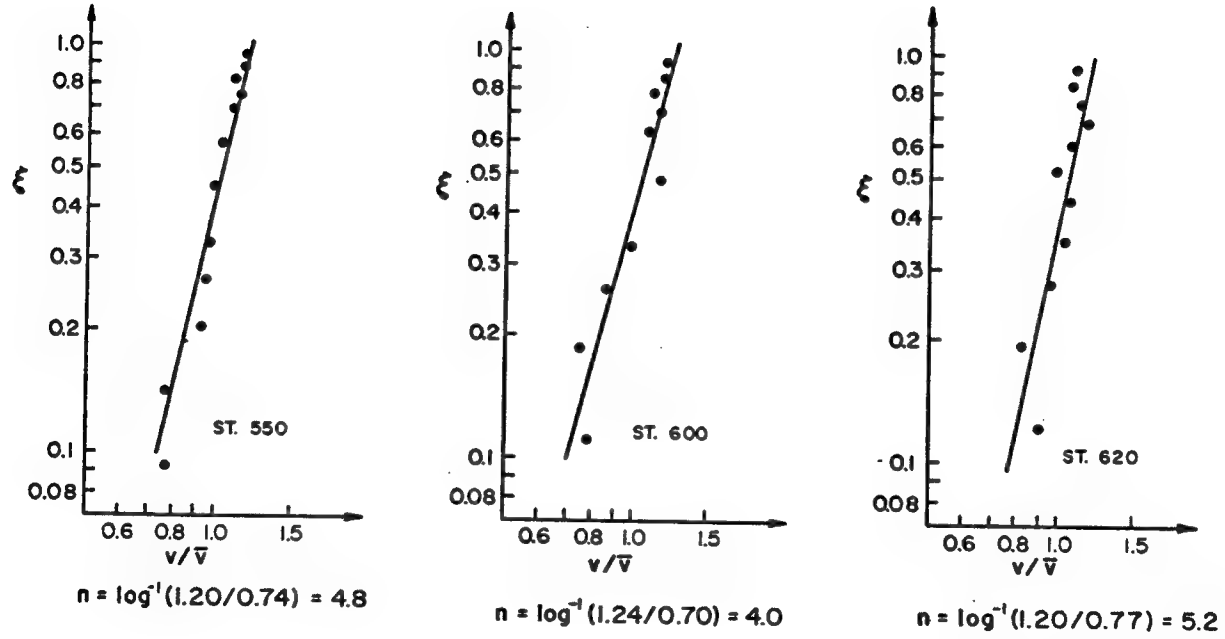

Figure A-7 (Cont) - Velocity Distributions in Cross Section No. 3 at High Flow, 28,400 Cubic Feet Per Second

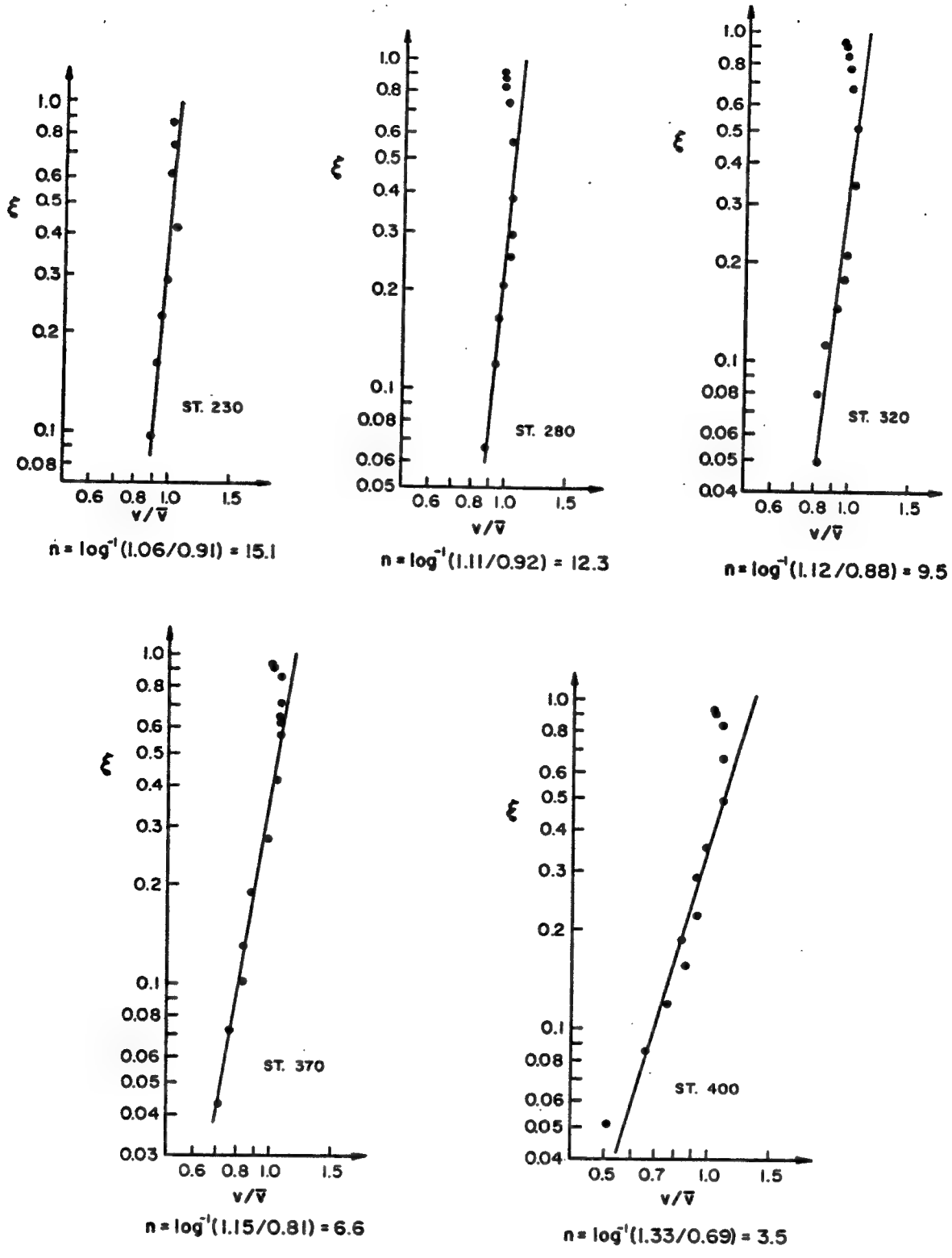

Figure A-8 - Vertical Velocity Distributions in Cross Section No. 4 at High Flow, 24,900 Cubic Feet Per Second

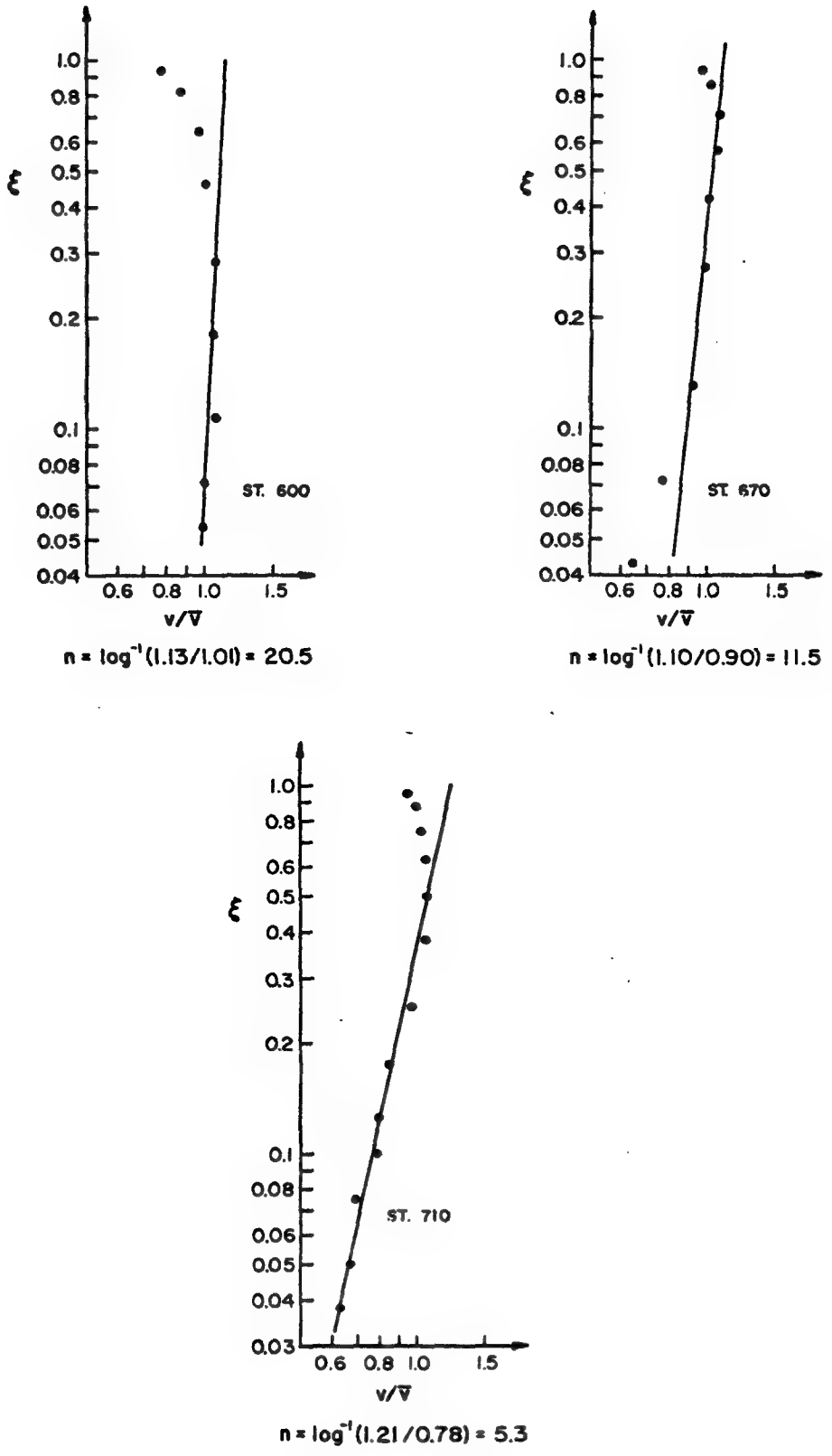

Figure A-9 - Vertical Velocity Distributions in Cross Section No. 5 at High Flow, 24,000 Cubic Feet Per Second

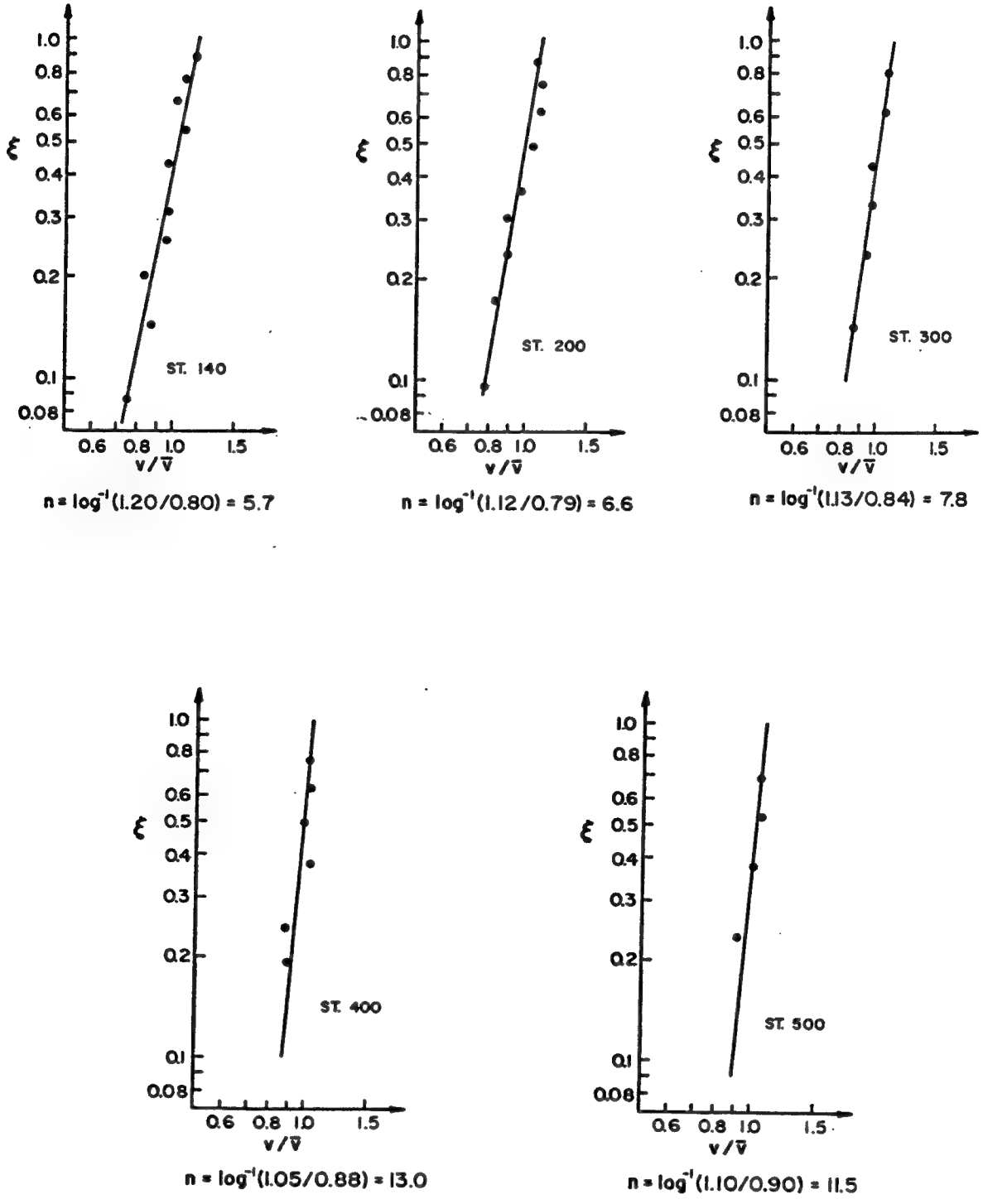

Figure A-10 - Vertical Velocity Distributions in Cross Section No. 6 at High Flow, 26,800 Cubic Feet Per Second

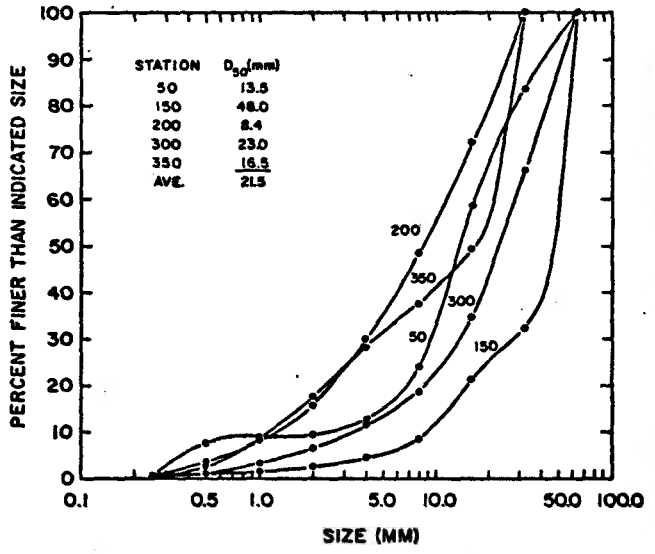

Figure A-11 - Grain-Size Distributions in Cross Section No. 1 at Low Flow, 7,800 Cubic Feet Per Second

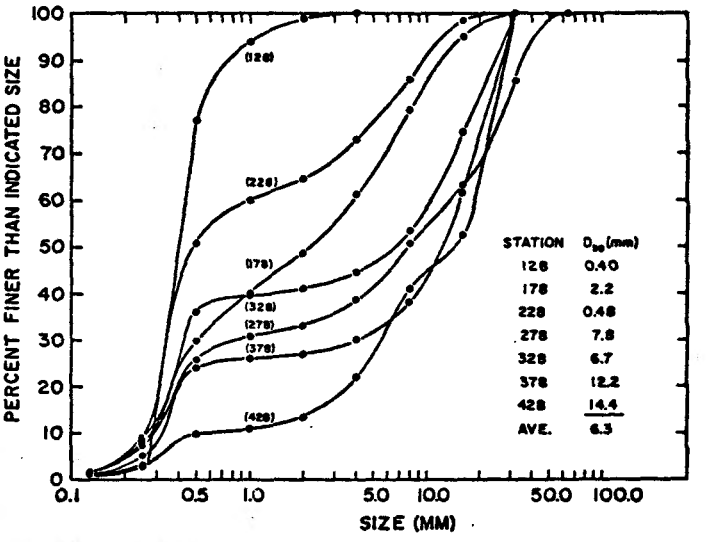

Figure A-12 - Grain-Size Distributions in Cross Section No. 3 at Low Flow, 9,900 Cubic Feet Per Second

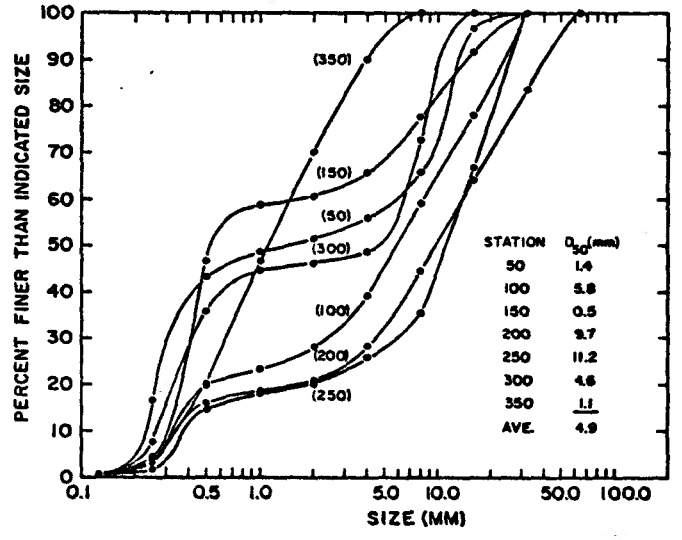

Figure A-13 - Grain-Size Distributions in Cross Section No. 2 at Low Flow, 8,300 Cubic Feet Per Second

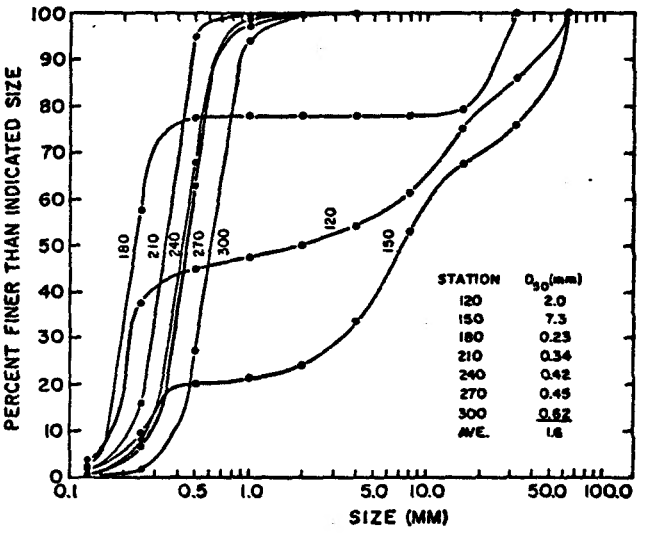

Figure A-14 - Grain-Size Distributions in Cross Section No. 4 at Low Flow, 9,100 Cubic Feet Per Second

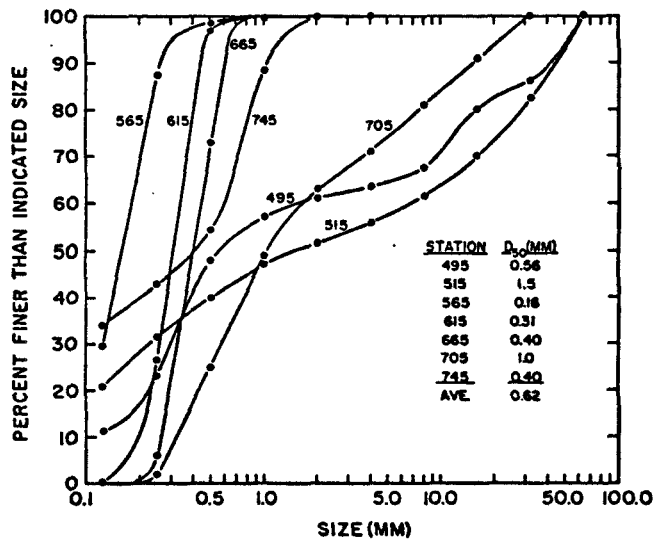

Figure A-15 - Grain-Size Distributions in Cross Section No. 5 at Low Flow, 9,100 Cubic Feet Per Second

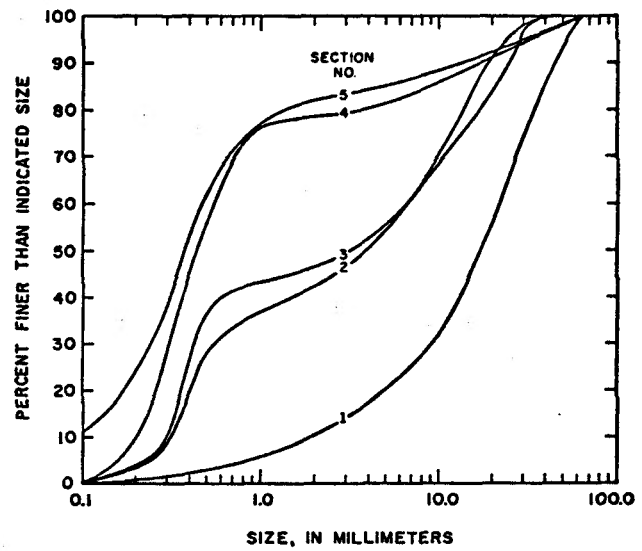

Figure A-16 - Composite Grain-Size Distributions at Low Flow

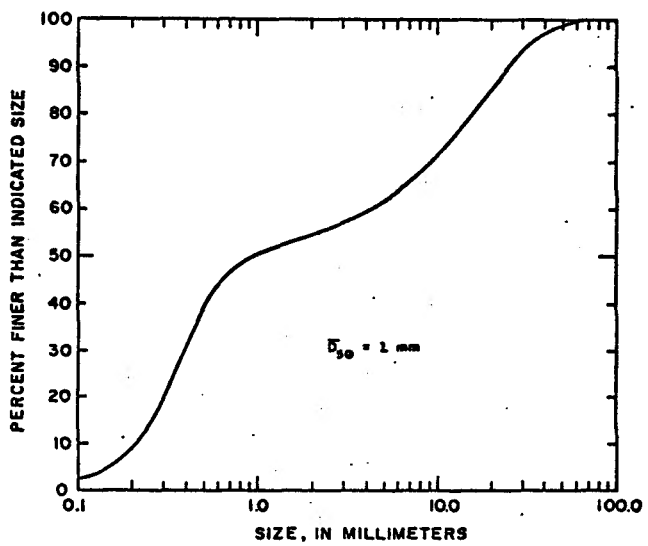

Figure A-17 - Composite Grain-Size Distribution for all Sections at Low Flow

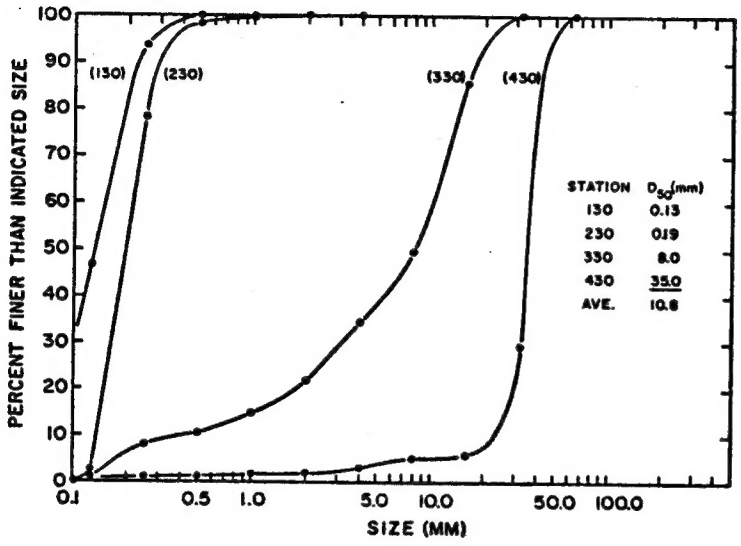

Figure A-18 - Grain-Size Distributions in Cross Section No. 2 at High Flow, 24,900 Cubic Feet Per Second

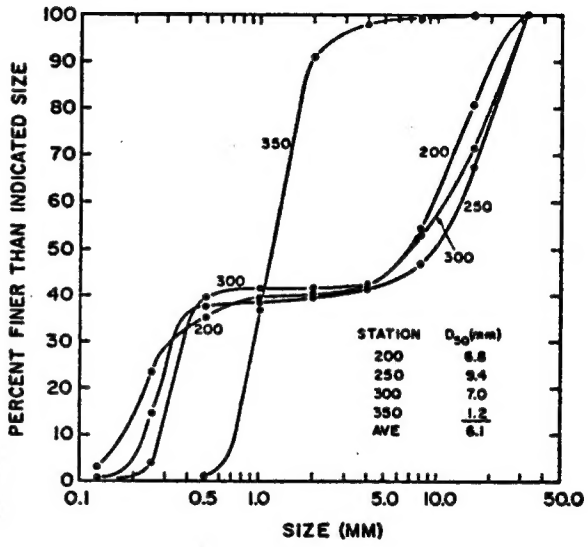

Figure A-19 - Grain-Size Distributions in Cross-Section No. 4 at High Flow, 24,900 Cubic Feet Per Second

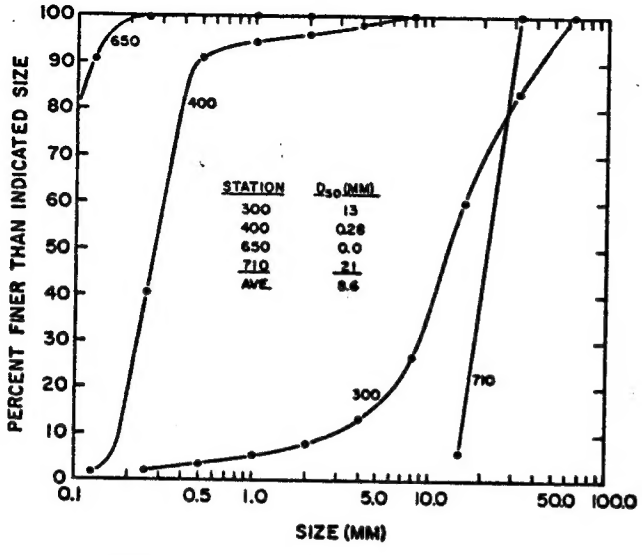

Figure A-20 - Grain-Size Distributions in Cross Section No. 5 at High Flow, 24,000 Cubic Feet Per Second

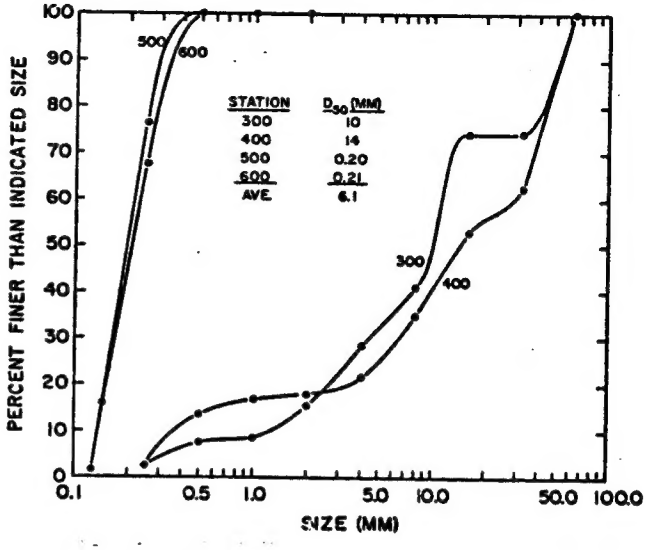

Figure A-21 - Grain-Size Distributions in Cross-Section No. 6 at High Flow, 26,000 Cubic Feet Per Second

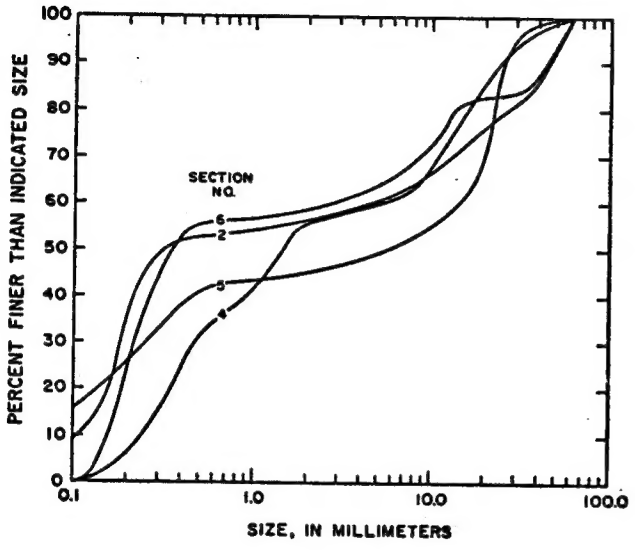

Figure A-22 - Composite Grain-Size Distributions at High Flow

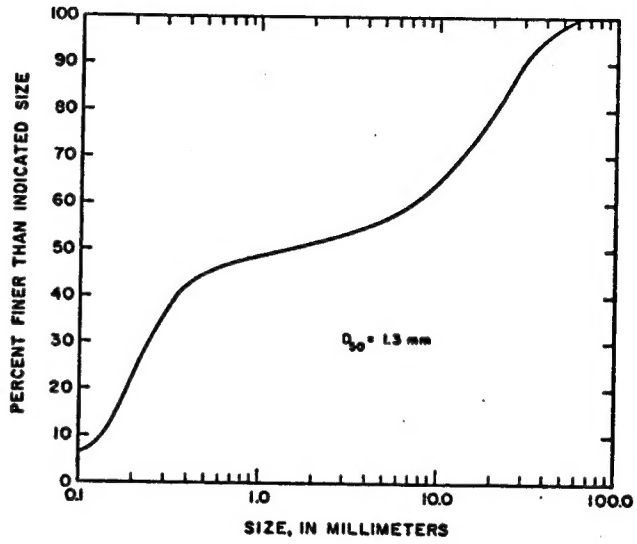

Figure A-23 - Composite Grain-Size Distributions for all Sections at High Flow

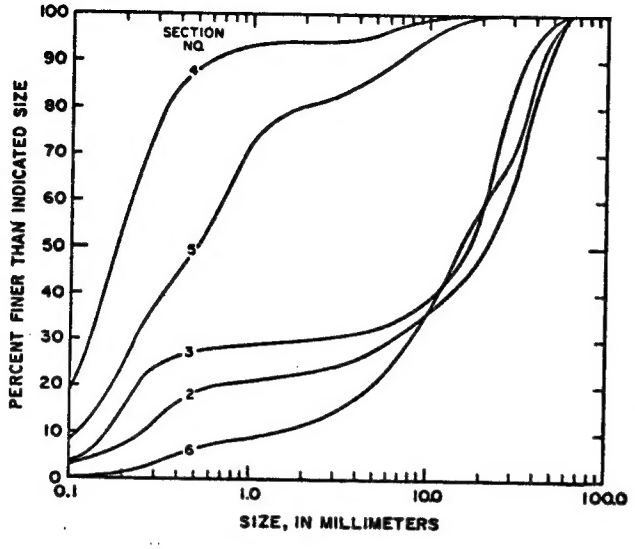

Figure A-24 - Composite Grain-Size Distributions, from Survey in July, 1980

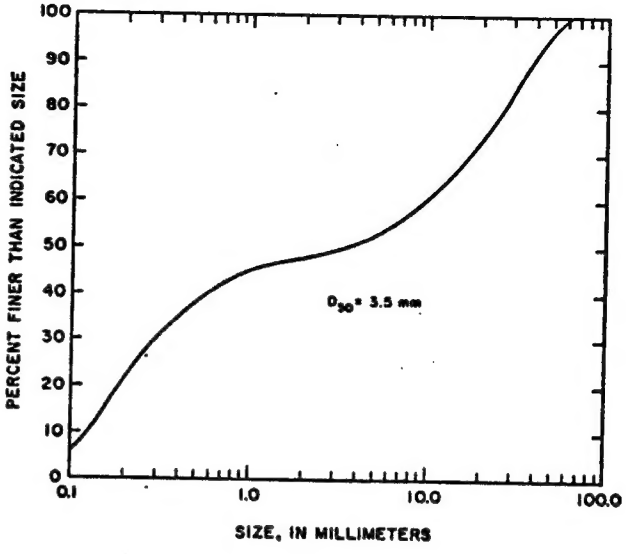

Figure A-25 - Composite Grain-Size Distribution for all Sections, from Survey in July, 1980